Characterization of Metabolic Differences in Benign, Slow Developing and Tumor-initiating Ovarian Cancers

Angela Suzanne Anderson

Dissertation submitted to the faculty of Virginia Polytechnic Institute and State University in partial fulfillment of the requirements for the degree of

Doctor of Philosophy
In
Human Nutrition, Foods and Exercise

Matthew W. Hulver, Co-Chair
Eva M. Schmelz, Co-Chair
Madlyn I. Frisard
Paul C. Roberts

May 1st, 2013
Blacksburg, Virginia

Keywords: Ovarian cancer, metabolism, Warburg effect, cancer stem cells, mitochondria

Characterization of Metabolic Differences in Benign, Slow Developing and Tumor-initiating Ovarian Cancers

Angela Suzanne Anderson

ABSTRACT

Ovarian cancer is known as the "silent killer," due to its late diagnosis and frequent recurrence after initial treatment. Finding a new way to diagnose and treat ovarian cancer in conjunction with current therapies is paramount. By capitalizing on metabolic changes that occur during cancer progression, interventions can be developed. The Nobel laureate Otto Warburg is credited with discovering an altered metabolic state within cancer cells known as the Warburg effect. In the Warburg effect, cancer cells participate in an increased rate of aerobic glycolysis with an excess secretion of lactate, allowing for carbon flux into biosynthetic pathways. Exactly which metabolic pathways are altered in ovarian cancer and at which stage in the progression of ovarian cancer they are occurring was unknown. Therefore using the recently established mouse ovarian surface epithelial (MOSE) progression model, we were able to measure metabolic changes in varying states of disease and levels of aggressiveness. As cells progressed from a benign early stage (MOSE-E), through a transitional intermediate stage (MOSE-I), to an aggressive late stage (MOSE-L), the MOSE cells became more glycolytic and lipogenic, establishing the MOSE model as a valuable model for studying ovarian cancer metabolism. Treating the MOSE cells with the naturally occurring chemotherapeutic agent sphingosine decreased p-AKT protein levels in the cell, decreased the glycolytic rate and decreased

de novo cholesterol synthesis. Cancer stem cells are known to be resistant to chemotherapy treatments and targeting their metabolism may be promising for combinatorial treatments. Therefore, the metabolism of highly aggressive tumor-initiating cells (TIC), harvested from ascites of C57Bl/6 mice injected with MOSE-L cells were characterized. Although the basal metabolism of the TICs was similar to the MOSE-L cells, TICs were more resistant to cell death as a consequence of external stresses and substrate depletion. The TICs could also up-regulate oxygen consumption rate (OCR) when uncoupled and increase glycolysis when ATP Synthase was inhibited, highlighting their resiliency. Taken together, we have identified targets for treatment strategies that could suppress the growth of primary tumors and may be effective against TICs, thereby suppressing tumor recurrence and possibly prolonging the life of women with ovarian cancer.

ACKNOWLEDGEMENTS

Matt, thank you for seeing something in me from the day we met. Thank you for not being daunted by the fact that I was a pregnant flight attendant who had been out of academia for 11 years. By giving me a chance, you allowed me an incredible opportunity that I will forever be grateful for. I am so blessed by your mentorship and friendship. It has been a pleasure working for you in the lab and in the classroom. You are brilliant and I have learned so much from watching you. Your care and concern for me as a person and as a student are phenomenal and I am the PhD candidate that I am because of you.

Eva, thank you for always being brutally honest with me. From the day I met you and you looked at my 8-month pregnant belly and said, "You know it is going to be hard," you have always been honest with me. Thank you for helping me become a better writer and ushering me through my first paper submission. Your comments have always made me better and I have learned a lot from you. Thank you for giving me the freedom and for being confident that I could accomplish what was asked for in the lab. I wouldn't be where I am today without you.

Madlyn, your friendship has been and is an incredible blessing to me. I can't imagine going through pregnancy and toddler-hood without you. You have been a confidant and a mentor. You are a delightful sounding board on things mito-related and otherwise. I would not have made it without you.

Chris, you have an incredible mind. Thank you for your endless ideas and insight into my research. You challenge me with your questions and have taught me how to think through my experiments so that I effectively test my hypotheses.

Mom and Dad, thank you for believing in me. You have always said I can accomplish anything I set my mind to. I would have not believed I could earn a PhD without the confidence you instilled in me. Your support and prayers have meant so much to me. Thank you for coming twice to live with us to help make this PhD happen. But more than anything, thank you for the role model you are to me and the love you have for me.

Søren and Leif, the incredible boys in my life. Your mommy set upon this journey to become the person God made me to be. You have only known me as a PhD student and have been patient with me as I worked nights and weekends to make this PhD possible. The joy you give me each day is in explainable and I have become a better person and student every day because of you. Thank you for loving me and making each day worth it!

Jonathan, my partner and my friend, how can I thank you for allowing me this incredible opportunity? You never once asked me to do anything else and have been fiercely supportive of my career. Thank you for telecommuting these last 5 years so that I could be here. Your sacrifices in your job, allowing for me to be successful in my job, are beyond belief. You have been my cheerleader as I balanced career and motherhood, never once believing I couldn't do them both. You have believed in me when I didn't believe in myself. You are my rock, my safe place and my best friend. I would have never begun this journey if it weren't for your encouragement and your support. I love you with all my heart!

ATTRIBUTION

Several colleagues aided in the writing and research behind two of my chapters presented as part of this dissertation. A brief description of their contributions is included here.

Chapter 5: METABOLIC CHANGES DURING OVARIAN CANCER PROGRESSION AS TARGETS FOR SPHINGOSINE TREATMENT

Chapter 5 was submitted and accepted to Experimental Cell Research.

Paul C. Roberts, PhD is currently an assistant professor in the department of Biomedical Sciences and Pathobiology at the Virginia/Maryland Regional College of Veterinarian Medicine. Dr. Roberts was co-author on this paper, co-principal investigator for one of the grants supporting this research, and edited the document.

Madlyn I. Frisard, PhD is currently an assistant professor in the department of Human Nutrition, Foods and Exercise at Virginia Tech. Dr. Frisard was co-author on this paper, helped design the mitochondrial respiration experiments and edited the document.

Ryan P. McMillan, PhD is currently a research associate in the department of Human Nutrition, Foods and Exercise at Virginia Tech. Dr. McMillan was co-author on this paper and helped design the radioactive experiments and enzyme assays.

Timothy J. Brown, BS was an undergraduate of Virginia Tech. Mr. Brown was a co-author on this paper and designed and executed the cholesterol assays.

Michael H. Lawless, BS was an undergraduate of Virginia Tech. Mr. Lawless was co-author on this paper and ran some of the Fatty Acid Synthase westerns.

Matthew W. Hulver, PhD is currently an associate professor in the Human Nutrition, Foods and Exercise Department. Dr. Hulver was co-author on this paper, principal investigator for one of the grants supporting this research, contributed to the research design of this project and edited the document.

Eva M. Schmelz, PhD is currently an associate professor in the Human Nutrition, Foods and Exercise Department. Dr. Schmelz was co-author on this paper, co-principal investigator for one of the grants supporting this research, contributed to the research design of this project and edited the document.

Chapter 6: OVARIAN TUMOR-INITIATING CELLS (TICs) DISPLAY A MORE FLEXIBLE METABOLISM THAN THEIR PARENTAL CELL LINE

Chapter 6 is in preparation for submission

Paul C. Roberts, PhD is currently an associate professor in the department of Biomedical Sciences and Pathobiology at the Virginia/Maryland Regional College of Veterinarian Medicine. Dr. Roberts was co-author on this paper, co-principal investigator for one of the grants supporting this research, helped with the design of the alamarBlue and MTT assays, provided the TIC cell line, and edited the document.

Madlyn I. Frisard, PhD is currently an assistant professor in the department of Human Nutrition, Foods and Exercise at Virginia Tech. Dr. Frisard was co-author on this paper, helped design the mitochondrial respiration experiments and edited the document.

Matthew W. Hulver, PhD is currently an associate professor in the Human Nutrition, Foods and Exercise Department. Dr. Hulver was co-author on this paper, principal investigator for one of the grants supporting this research, contributed to the research design of this project and edited the document.

Eva M. Schmelz, PhD is currently an associate professor in the Human Nutrition, Foods and Exercise Department. Dr. Schmelz was co-author on this paper, co-principal investigator for one of the grants supporting this research, contributed to the research design of this project and edited the document.

TABLE OF CONTENTS

TABLE OF FIGURES

TABLE OF TABLES

Chapter 1: INTRODUCTION

Cancer is a disease of self-autonomous and un-restrained growth. To support this unlimited growth rate, cellular metabolism must be adjusted to supply the building blocks for growth. Carbons in the form of glucose, fatty acids and amino acids can all contribute to the anabolic growth needs of nucleotides, proteins and phospholipids for cell replication. Due to the self-autonomous characteristic of cancer, these cells import nutrients in abundance while excreting excess carbons as lactate. It was this high level of lactate that was observed by Otto Warburg in the 1920's and given the name the "Warburg Effect" in response to the highly glycolytic nature of cancer cells. Much work has been done since Warburg's time understanding the metabolic changes of cancer cells.

Ovarian cancer lacks early signs and symptoms and is therefore usually diagnosed in stage III or stage IV when prognosis is poor. Discovering early events in ovarian cancer as biomarkers for early detection is crucial to increasing the survival rate of women with ovarian cancer. Because of the known metabolic shifts that take place in cancer, determining the time line and characteristics of these metabolic changes could lead to the detection and treatment of ovarian cancer. In addition, with the recent discovery of cancer stem cells, characterization of the metabolism of these stem cells is needed. By understanding how their metabolism differs from differentiated cancer cells, effective treatments to prevent cancer reoccurrence can be designed.

To date, the time at which metabolic shifts are occurring in the progression of ovarian cancer is unknown. Furthermore, it is unknown as to how the metabolism of ovarian cancer stems cells differs from that of differentiated ovarian cancer cells. The hypothesis

of this project is that metabolic changes in ovarian cancer will occur at an early stage, leading towards an increase in aerobic glycolysis to support the increase in growth rate seen in late-stage cancer cells. In addition, it is hypothesized that the cancer stem cells will have a less rigid and more flexible metabolism that allows them to survive in an array of conditions due to their resistance to conventional chemotherapies.

Chapter 2: REVIEW OF LITERATURE

1. Background

Although annual cancer deaths are on the decline, one in four Americans die each year due to deadliness of cancer[1]. Ovarian cancer is estimated to account for 14,030 deaths in 2013[2]. Unlike breast cancer with an estimated 90% five-year survival rate, ovarian cancer's five-year cancer survival rate hovers around 45%[1]. Due to a lack of early symptoms, ovarian cancer is often diagnosed when cancer has progressed to an aggressive stage, where treatments can be ineffective. Consequently research into early diagnosis of ovarian cancer is of paramount importance.

Cancer has traditionally been characterized by six hallmarks including sustained growth signaling, avoiding cell death, unrestrained replication, resisting growth suppressors, ability to induce angiogenesis, and invasion and metastasis[3]. Ten years later, Hanahan and Weinberg revised their initial six hallmarks to add four more characteristics of cancer including the ability of cancer cells to evade the immune system, inflammation, genomic instability and changes in cellular metabolism[4]. Changes in cellular metabolism mark are an early event in cancer development triggered by the cell's need to meet the macromolecule synthesis demand of rapid division. Understanding these metabolic changes can lead to the development of targeted treatments of cellular metabolism, and to the identification of ovarian cancer biomarkers vital to early diagnosis of ovarian cancer.

Otto Warburg is credited with the discovery that cancer cells shift their metabolism towards fermentation and away from respiration[5, 6]. He determined that blood that had been passed through tumor-laden tissue had increased lactic acid concentration in

comparison with blood that had been passed through healthy tissue[5]. This observed shift, common among cancers, has been coined the "Warburg effect." Warburg was a pioneer in this discovery, but based his "origin of cancer cells" on "respiratory destruction" within tumor cells, that shifted their metabolism towards aerobic glycolysis[6]. Research has shown that this is not completely true. Tumor cells in most cancers make this glycolytic shift even with fully functional mitochondria[7].

Sidney Weinhouse, a contemporary of Warburg, criticized the notion of mitochondrial impairment. Seeing no observed decrease in oxygen consumption, he postulated that the glycolytic flux is too high for oxidative phosphorylation to keep up, producing the increase in excreted lactate that Warburg observed[8]. Evidence in support of Weinhouse's criticism continues to increase. HeLa cells, an aggressive cervical cancer, grown in a galactose medium where glutamine supplied the carbon skeleton for ATP synthesis through the tricarboxylic acid (TCA) cycle, remodeled their mitochondria to up-regulate oxidative phosphorylation[9]. Similarly, when mouse mammary cells had their lactate dehydrogenase enzyme (LDH-A) silenced, forcing pyruvate into the TCA cycle instead of being reduced to lactate, the cells were able to up-regulate oxidative phosphorylation to compensate for the increased flux[10]. Mitochondria in cancer cells seem to function normally when forced to increase their oxidative phosphorylation. This shift to aerobic glycolysis must be a crucial alteration for cancer cells in spite of functioning mitochondria.

So why is there an increase in glycolysis and lactate excretion if the more effective oxidative phosphorylation pathway is fully functioning? Several hypotheses have been advanced to answer this question; however, the underlying reason is within the very

nature of cancer cells themselves. Their unrestricted growth demands increased macromolecule (lipids, nucleotides and proteins) synthesis in addition to ATP synthesis needs. To meet this anabolic need, which gives cancer cells a growth advantage, metabolic systems in the cell must be adjusted. High levels of glucose and glutamine uptake meet this need by shuttling their carbon skeletons into nucleotides, fatty acids and proteins[11].

Glucose, which is catabolized to pyruvate through glycolysis, produces ATP for cellular processes. Pyruvate can then be converted to acetyl CoA, which enters the TCA cycle and is reduced for energy or the acetyl CoA can be converted to citrate and immediately shuttled out into the cytoplasm for *de novo* fatty acid and cholesterol synthesis. Pyruvate not entering the mitochondria can be reduced to lactate in both aerobic and anaerobic conditions in times of an increased glycolytic rate where the TCA cycle cannot keep up with the flux of carbons. Reduction of pyruvate to lactate results in the regeneration of NAD^+ for sustained glycolysis. Less appreciated is the conversion of pyruvate and glutamate to alanine and α-ketoglutarate via alanine aminotransferase[12]. Alanine can be used for protein synthesis or excreted as a byproduct. In addition, the α-ketoglutarate produced can be used for anaplerosis of TCA cycle intermediates. More recently a 4th fate for pyruvate has been revealed in some cancer cells via a reverse carboxylation of pyruvate to oxaloacetate via pyruvate carboxylase for anaplerosis in times of limited glutamine supply[13].

In addition to glycolysis, glucose can also be shunted to the pentose phosphate pathway, where the byproducts include ribose-5-phosphate (the precursor for nucleotide synthesis) and NADPH (the reducing equivalent needed for *de novo* fatty acid and cholesterol

synthesis, the regeneration of reduced glutathione for managing oxidative stress, and to generate proline). In addition, glucose can be shuttled to glycogen for storage to be used in times of energy demand[14]. Other carbons originating as glucose can exit glycolysis as 3-phosphoglycerate for serine/glycine biosynthesis. Serine is needed in the folate pathway in the synthesis of methylene-tetrahyrofolate from tetrahydrofolate (THF), which leads to purine synthesis and the production of NADPH (Rabinowitz J, personal communication). Glycine is needed as one of the three amino acids that make up glutathione (GSH)[15].

The other essential fuel in growing cancer cells is glutamine. Glutamine can be deamidated to glutamate when it enters the cell. Glutamate can be used to make GSH[15] and glutamate can be further transaminated to α-ketoglutarate, where it can enter the TCA cycle and be reduced for energy or used for anaplerosis, termed glutaminolysis. Glutamine can also be a precursor to the synthesis of non-essential amino acids for protein synthesis[11, 16]. Figure 1.1 highlights the metabolic pathways of both glucose and glutamine and the subsequent anabolism of proteins, nucleotides and lipids. Altered cancer cell metabolism, which is now recognized as one of the hallmarks of cancer, is an important intracellular modification in meeting the growing needs of cancer cells.

Under hypoxic conditions or during mitochondrial impairment, glutaminolysis becomes increasingly important to meet the carbon demands for growth. Decreases in acetyl CoA entering the TCA cycle allow for reductive carboxylation, or a reversal of the TCA cycle, converting α-ketoglutarate to isocitrate and then to citrate, which can leave the mitochondria for anabolic growth. The reductive carboxylation of glutamine occurs with the induction of hypoxia-inducible factor 1 (HIF1), as constitutively active HIF1

drives reductive carboxylation in normoxic conditions[17]. Cells that contain ETC (electron transport chain) complex I and III mutations, fumarate hydratase mutations, or in cells where the ETC has been inhibited pharmacologically, rely heavily on reductive carboxylation[18]. Under normal culture conditions, reductive carboxylation occurs minimally,[19] where glutamine catabolism has been shown to increase the secretion of lactate, alanine and ammonia[20]. In hypoxia, the contribution of glutamine to reductive carboxylation nearly triples[21], highlighting the cancer cell's ability to metabolically adapt to changing microenvironment conditions.

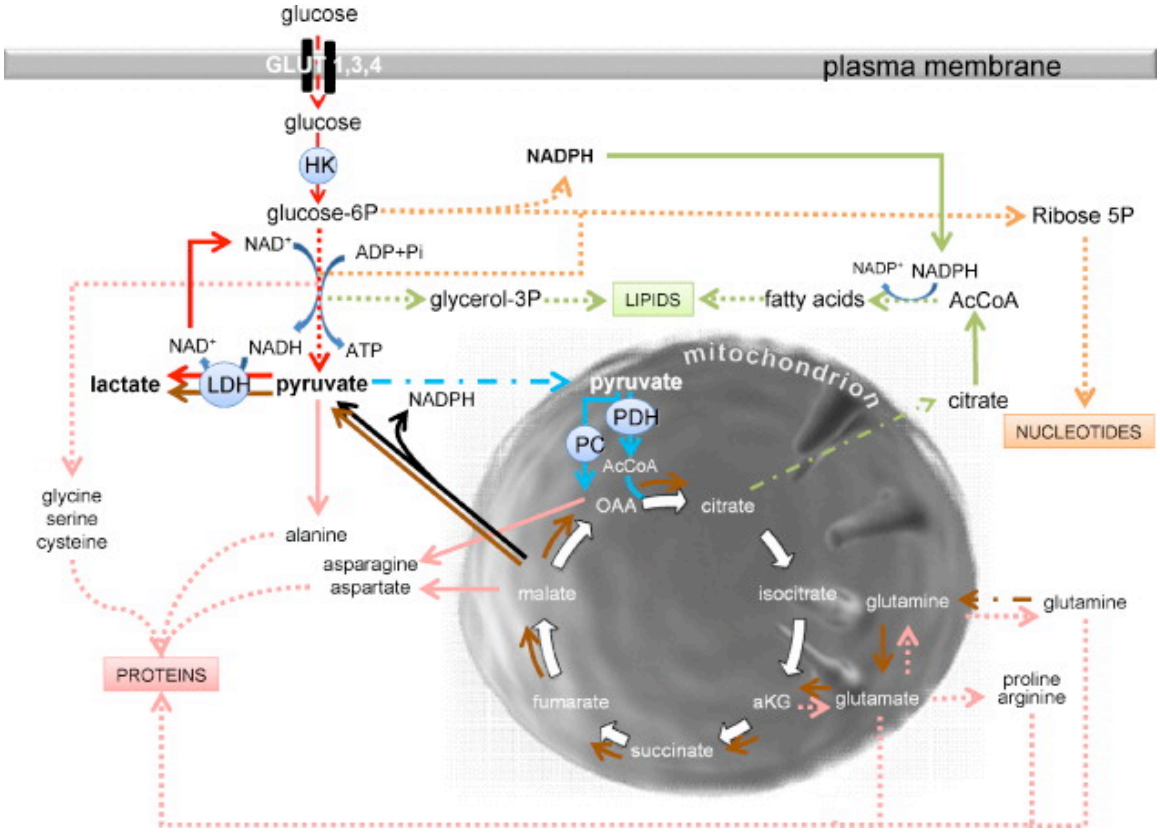

Figure 1.1 Metabolic re-programming to meet the growth needs of rapidly dividing cancer cells[11]. Red arrows identify the flux of glucose through glycolysis and the regeneration of NAD+ through the production of lactate. Orange arrows indicate the flux of carbons away from glycolysis to the pentose phosphate pathway (PPP) and the production of NADPH and nucleotides. Green arrows indicate the *de novo* fatty acid pathway with reducing equivalents from the PPP and carbons from citrate and glycolysis. Pink arrows indicate the synthesis of amino acids for protein synthesis. Brown arrows indicate the anaplerosis of TCA cycle intermediates from glutamine. The black arrow indicates the malic enzyme and subsequent production of NADPH that can be used for *de novo* fatty acid synthesis. The blue arrows

indicate the fate of pyruvate in the mitochondria, either into the TCA cycle or used in the regeneration of oxaloacetate.

2. Glucose and Fatty Acid Transport and Metabolism

Cell survival and growth is dependent on energy uptake and metabolism. Both fatty acids and glucose provide the needed acetyl CoA for subsequent generation of ATP, and carbon skeletons for macromolecule biosynthesis. Glucose is imported into the cell via sodium coupled glucose transporters (GLUTs) via facilitated diffusion along its concentration gradient[22]. GLUTs 1-5 are the most characterized GLUTs in mammalian cells with GLUT-1 and -4 as the major research focus[23]. GLUT-1 has a high affinity with a low K_m (~3mM) for glucose and is in most tissues responsible for basal glucose uptake[23]. GLUT-4 is found mainly in insulin-sensitive tissues where insulin will bind to its receptor, signaling GLUT-4 translocation to the plasma membrane to facilitate an increase in glucose transport by 10- to 40-fold. GLUT-4 is reported to have a K_m in the range of 2-10mM[23]. Expression of GLUT-1 has been correlated with tumor proliferation in epithelial ovarian cancers[24] and an increase of GLUT-1 was seen in ovarian cancer tissue over normal ovarian tissue[25, 26]. The expression of GLUT-4 is somewhat controversial; while GLUT-4 was not expressed in either healthy or cancerous ovarian tissue[25], another research group showed GLUT-4 expression in 71% of epithelial ovarian cancer tissue samples[27]. Other gynecological cancers have shown an increase in GLUT-4. Tissue from endometrial cancer patients showed an increase in both GLUT-1 and GLUT-4 protein[28].

Fatty acids are imported into the cell via several transporters including fatty acid translocase (FAT/CD36), plasma membrane fatty acid binding protein (FABPpm), and

fatty acid transport proteins 1-6 (FATPs)[29]. Although free fatty acids can be incorporated into phospholipids, the majority of fatty acids found in phospholipids are derived from *de novo* fatty acid synthesis. Consequently, the fatty acids that are taken into the cell more commonly are used for triglyceride synthesis and esterification of cholesterol, acylation of proteins and beta-oxidation for ATP synthesis[29]. Ovarian cancer is commonly marked by metastasis to the omentum where omental adipocytes reside. Ovarian cancer tissue harvested from the omentum had an increase in FABP4 protein[30]. In primary ovarian tumors FABP4 protein was low compared to the metastasized ovarian cancer in the omentum and expression was located only on the ovarian cancer cell/adipocyte boundary[30]. The relative expression of FAT/CD36 and FABPpm in ovarian cancer compared to normal ovary tissue is unknown. However FAT/CD36 protein is expressed in breast cancer cell lines[31] and endometrial cancer tissue albeit lower than normal endometrial tissue[28]. Interestingly, FABPpm protein expression was significantly increased in endometrial cancer tissue versus healthy tissue[28]. As seen with the omental metastases of ovarian cancer, fatty acid transport expression may be dependent upon the environment in which the cancer is found. An adipocyte rich environment such as the omentum may lead to an up-regulation in transporters not seen in primary ovarian cancer. Specific microenvironmental versus genetic cues remain to be investigated.

Glucose, glutamine and fatty acids make up the primary substrates for ATP synthesis through glycolysis and oxidative phosphorylation. The contribution of each fuel to ATP generation is unknown in ovarian cancer. However, in MCF-7 breast cancer cells, oxidative phosphorylation accounts for 80% of ATP generation with glucose and glutamine combining for 40% of the ATP generation through glycolysis and oxidative

phosphorylation[32]. The remainder of ATP generation is from fatty acids and unidentified sources, which may include lactate and ketones[32]. Cancer cells remain dependent on oxidative phosphorylation from multiple substrates for ATP generation.

3. Lactate and Monocarboxylate transporters (MCTs)

High lactate production has been a characteristic of cancer cells since Warburg's time in the 1920's. However, the explanation for this phenomenon is only recently coming to light. For the majority of the last century it has been hypothesized that cancer cells were highly glycolytic with lactate as the byproduct for ATP generation through glycolysis. We now know that cancer cells produce more ATP through oxidative phosphorylation and only approximately 7% of glucose carbons are used for macromolecule synthesis[20]. So why is there such a high rate of lactate production? Several reasons occur including disposing of high levels of pyruvate that are unable to be utilized by Pyruvate Dehydrogenase (PDH), maintaining available carbon pools for exponential growth unaffected by changes in external nutrient availability, and the regeneration of NAD^+ from NADH via Lactate Dehydrogenase (LDH)[12]. NAD^+ regeneration is needed to sustain the high rate of glycolytic flux, maintain redox status, and is used for amino acid and nucleotide synthesis[12].

Lactate is transported in and out of the cell through monocarboxylate transporters. There are four isoforms MCT1, MCT2, MCT3 and MCT4 that are proton-dependent and specifically transport lactate and pyruvate. MCT1 is ubiquitously expressed, but is especially found in heart and red muscle over other tissues[33]. MCT1 is up-regulated in

response to increased muscle contraction, suggesting it can function in the bidirectional transport of lactate[33]. In contrast, MCT4 is most evident in white muscle and other cells with a high glycolytic rate like cancer cells, suggesting it exports lactate. The combination of expression of MCT1 and MCT4 in cancer cells allow a symbiotic relationship within the tumor (Figure 3.1). MCT2 is found in cells where rapid uptake at low lactate concentrations may be required such as the proximal kidney tubules, neurons and sperm tails. MCT3 is found specifically in the retinal pigment epithelium[33]. The high level of lactate excretion from glycolytic cancer cells through MCTs leads to a unique acidic microenvironment, where malignant progression is favored[34].

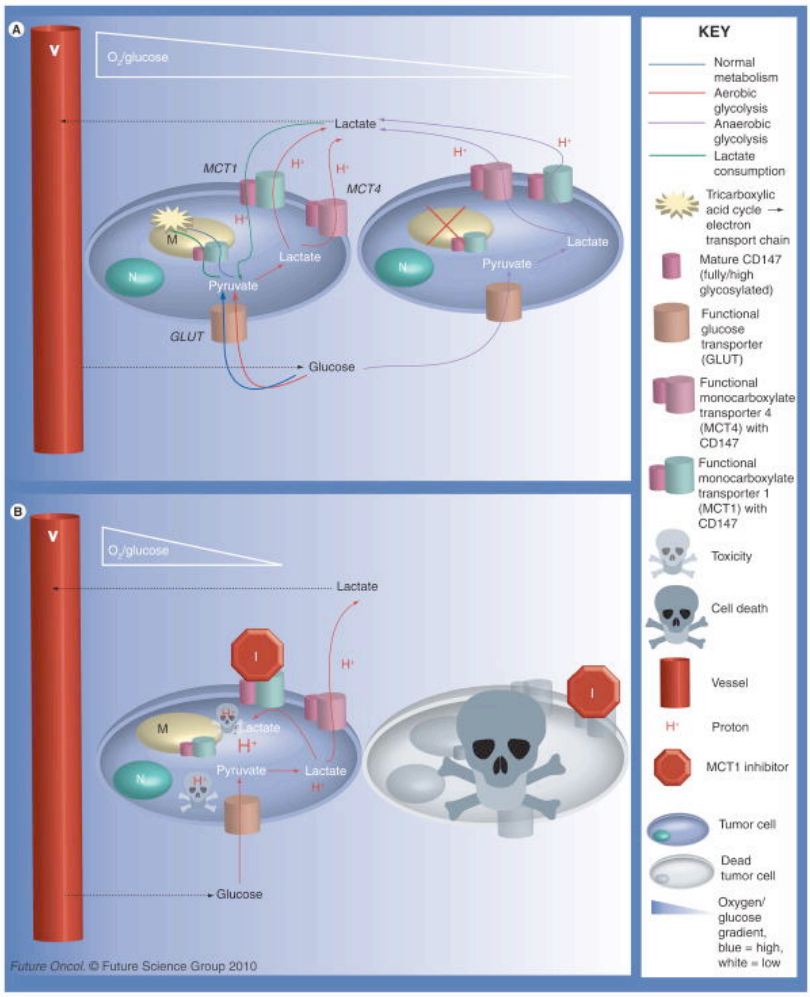

Figure 3.1 Cells close to blood vessels will have the advantage of high/adequate concentrations of oxygen and nutrients, such as glucose. Cells farther from vessels will experience varying degrees of hypoxia and starvation. (**A**) The metabolic pathways possible between cancer cells without MCT1 inhibition when the aerobic cells are able to consume/utilize lactate. Shown here is the Pasteur effect (anaerobic glycolysis) in the hypoxic cells farther from vessels. The well-oxygenated cells close to vessels may undergo healthy oxidative phosphorylation, possibly the Warburg effect (aerobic glycolysis), or lactate utilization. (**B**) Illustrates the consequences of MCT1 inhibition on cell-to-cell metabolism and intracellular pH. MCT4, having a high K_m, is unlikely to take up lactate unless there is a very high extracellular concentration of lactate. Excluded from this diagram are pH regulators other than MCTs, such as Na^+/H^+ exchanger (NHE1), which would serve to remove some of the H^+ from the cell. MCT1 inhibition can lead to cell death by two different means: the hypoxic cells are starved since cells close to vessels are forced to only take up glucose since the ability of lactate consumption is blocked, as seen by comparing (**A**) to (**B**) or the decrease in intracellular pH leads to toxicity, indicated by the protons represented in the diagram[35].
**Reproduced from Future Oncology, January 2010, Vol. 6, No. 1, Pages 127-148 with permission of Future Medicine Ltd.

4. *de novo* Fatty Acid Synthesis and Fatty Acid Synthase (FASN)

Due to the proliferation demands of growing cancer cells, the synthesis of fatty acids is a necessity. *de novo* fatty acid synthesis occurs via the condensation of acetyl CoA and malonyl CoA through several enzymatic steps by the enzyme fatty acid synthase (FASN) using ATP and the reducing equivalent NADPH. Acetyl CoA is produced in the mitochondria through either pyruvate dehydrogenase or through beta-oxidation, although with high levels of glucose uptake characteristic of cancer cells, most of the acetyl CoA entering the TCA cycle is derived from glucose[36]. Acetyl CoA is not permeable to the mitochondrial membrane and therefore enters the TCA cycle or is exported as acetyl-carnitine[37]. In times of high ATP and NADH ratios, citrate, the first intermediate produced in the TCA cycle, is shuttled out of the mitochondria via the Citrate Shuttle. In the cytoplasm citrate is then converted back to acetyl CoA via the enzyme ATP-citrate lyase (ACL). With citrate leaving the cell, TCA cycle intermediates must be replaced. Glutamine uptake is a necessity for growing cancer cells where it is converted to α-ketoglutarate and eventually to oxaloacetate combining with acetyl CoA to replenish the citrate leaving the TCA cycle[36]. Oxaloacetate replenishment is also crucial due to oxaloacetate itself leaving the mitochondria to produce pyruvate and the needed reducing equivalent for fatty acid synthesis, NADPH via the Malic Enzyme[11]. The excess pyruvate can then be excreted as lactate. The contribution of glucose and glutamine to *de novo* fatty acid synthesis are both crucial.

Targeting *de novo* fatty acid synthesis through FASN is another metabolic target in the treatment of ovarian cancer. Examination of immunohistochemical localization of FASN in ovarian cancer patients resulted in 71% of patients with positive staining for FASN.

FASN staining was absent in ovarian adenomas and tumors of low malignant potential. In addition, short-term survival was significantly increased in patients whose tumors showed no or locally concentrated expression of FASN versus diffuse staining[38]. The inhibition of FASN results in decreased growth, decreased invasion, and increased apoptosis, which may occur through multiple signaling pathways[39]. Although already shown to decrease AKT and downstream PI3K pathway targets, the loss of *de novo* fatty acid synthesis may lead to other alterations within the cell promoting growth arrest and apoptosis. These include cell starvation, loss of *de novo* phospholipids for membrane repair, toxic accumulation of malonyl CoA, inhibition of anti-apoptotic proteins, inhibition of DNA replication and increased metabolic stress (Figure 4.1)[39].

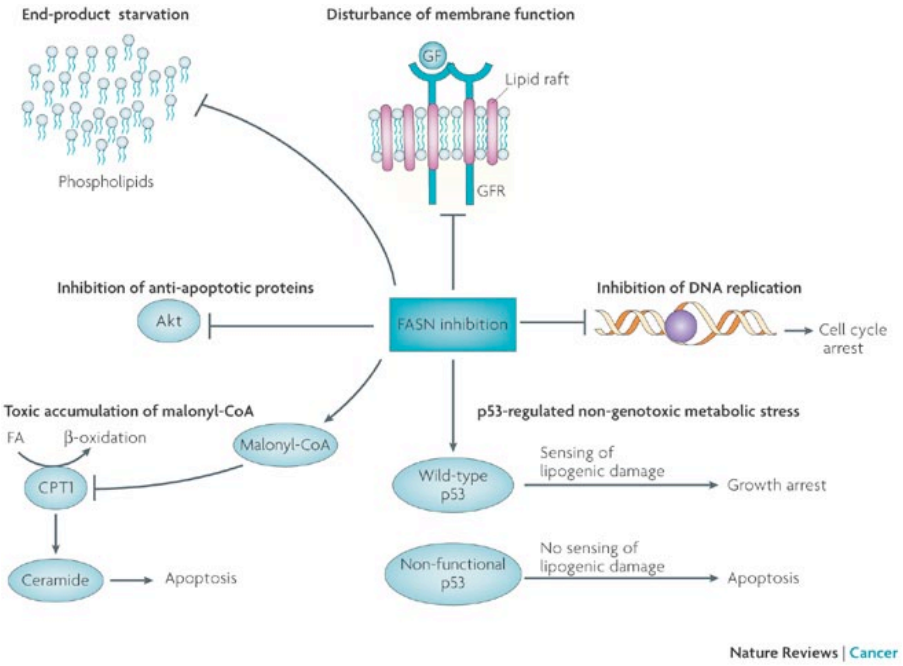

Figure 4.1 Several mechanisms have been proposed to explain the tumoricidal effects that occur after fatty acid synthase (FASN) blockade. *End-product starvation.* FASN has a major role in the synthesis of phospholipids required for the newly synthesized cellular membrane in highly proliferating tumor cells. The tumoricidal effects that occur after FASN inhibition may relate to the cellular starvation of phosphatidylcholine, the most abundant lipid affected by the modulation of FASN activity. *Disturbance of membrane function.* FASN inhibition, by inducing changes in the synthesis of membrane phospholipids and assembling of lipid rafts, may impair the correct localization and/or functioning of tyrosine kinase receptors (such as epidermal growth factor receptor (EGFR) and ERBB2) at the cellular membrane of tumor cells. *Inhibition of DNA replication.* Phospholipid biosynthesis is greatest during G1 and S phases in preparation

for cell division. FASN blockade produces rapid, potent inhibition of DNA replication, leading to a block in the cell cycle before G1. *p53-regulated non-genotoxic metabolic stress.* The decision between apoptosis and growth arrest following FASN inhibition is greatly influenced by p53 status. FASN inhibitors are more effective at initiating apoptosis in tumor cells with non-functioning p53, whereas cells with intact p53 function tend to exhibit cytostatic responses. *Toxic accumulation of malonyl-coenzyme A (CoA).* FASN inhibition causes accumulation of its substrate malonyl-CoA, which in turn inhibits carnitine palmitoyltransferase 1 (CPT1)-regulated fatty acid (FA) β-oxidation, thus promoting the accumulation of the sphingolipid ceramide followed by the induction of the pro-apoptotic genes involved in the ceramide-mediated apoptotic pathway (BNIP3, TRAIL and DAPK2). *Inhibition of anti-apoptotic proteins.* Inhibition of FASN results in the downregulation of AKT, which precedes the induction of tumor cell apoptosis in vitro and in vivo, suggesting a potential mechanism for FASN inhibition-related cell death[39]
**Reproduced from Nature Reviews Cancer, October 2007, Vol. 7, No. 10, Pages 763-777 with permission of Nature Publishing Group.

5. Adenosine Monophosphate–activated Protein Kinase (AMPK)

Adenosine monophosphate–activated protein kinase (AMPK) is an energy-sensing enzyme containing α-, β- and γ-subunits, each of which has at least two isoforms. An increase in the AMP:ATP ratio due to changes in energy demand produce conformational changes in AMPK enzyme, making it susceptible to phosphorylation and therefore activation by an AMPK kinase. AMPK works by inhibiting several enzymes including mammalian target of rapamycin (mTOR), acetyl-CoA carboxylase (ACC), fatty acid synthase (FAS), and glycerol phosphate acyltransferase (GPAT), which are key regulators of protein, fatty acid and glycerophospholipid synthesis[40]. Activated AMPK shifts metabolism from energy-consuming pathways to energy-producing pathways[41]. Activation of AMPK may work to decrease cancer growth through reduction in expression of SREBP-1C, which in turn inhibits *de novo* fatty acid synthesis and cholesterol synthesis[40] (see Figure 5.1) leading to cytoxicity in ovarian cancer cells[42].

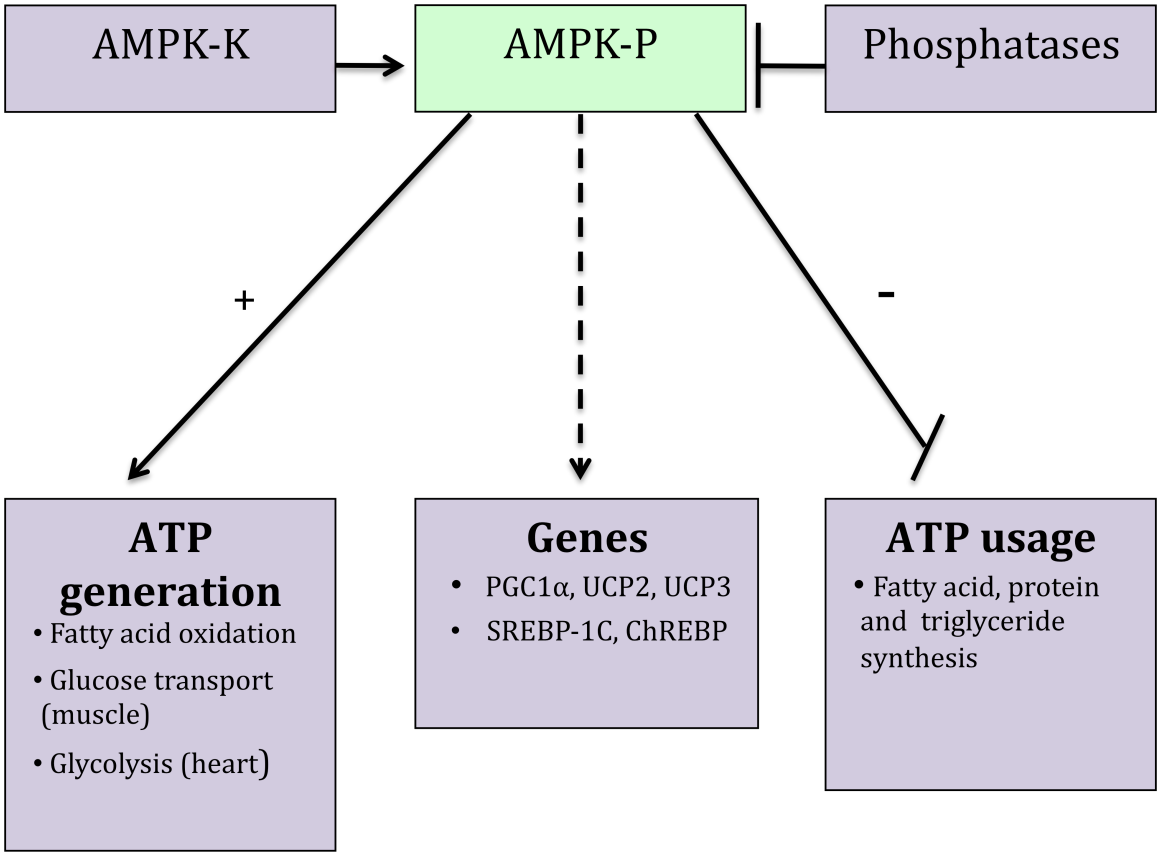

Figure 5.1. AMPK activation and cellular energy state. AMPK activation has been attributed to ATP depletion, which leads to changes in the AMP:ATP ratio. Recent studies indicate that binding of AMP to the γ-subunit of AMPK makes it more susceptible to phosphorylation and activation by an AMPK kinase (AMPKK) and less susceptible to dephosphorylation by phosphatases. Activation of AMPK also leads to an increase in cellular processes that generate ATP and a decrease in processes that use ATP but are not necessary immediate for cell survival. AMPK mediates these effects by either direct actions on enzymes or indirect regulation of gene expression (e.g. increasing the transcription of *Ppargc1a* [the gene encoding peroxisome proliferator-activated receptor γ coactivator 1α (PGC1α)], *Ucp2* and *Ucp3* (the genes encoding uncoupling proteins 2 and 3, respectively), and inhibiting the transcription factors SREBP-1C and CHREBP to suppress lipogenesis). + and − indicate upregulation and inhibition, respectively (Redrawn from reference [40]).
**Reproduced from Trends in Pharmacological Science, February 2005, Vol. 26, No. 2, Pages 69-76 with permission of Elsevier Publishing.

Another possible mechanism for AMPK-induced cytoxicity is through the FoxO3A transcription factor. Ovarian cancer cells, in response to decreased glycolysis, can activate the forkhead-box (Fox) gene family of transcription factors. In humans, 43 members of the Fox gene family have been identified and cataloged into subfamilies, each indicated by a corresponding letter and number, for example FoxA1, FoxA2, FoxB1

etc. The FoxO subfamily, which regulates expression of key elements in cellular metabolism, is composed of FoxO1, FoxO3A, FoxO4, and FoxO6[41, 43]. FoxO3A is ubiquitously expressed and in response to decreased glycolysis leads to the transcription of genes promoting autophagy and cell cycle arrest in order to increase ATP levels[41]. The AMPK pathway, activated when the ratio of AMP to ATP increases, is required for FoxO3A nuclear accumulation and for the subsequent transcription of target genes involved in autophagy and cell death[41].

AMPK's ability to induce cell death has led to the use of AMPK activators in the treatment of cancer. Metformin, one such drug designed for the treatment of type II diabetes, works by activating AMPK through the tumor suppressor kinase LKB1, which phosphorylates AMPK making it active[44]. AMPK then decreases gluconeogenesis in the liver thereby lowering blood glucose levels, among other physiological effects[45]. With a decrease in blood glucose, it is hypothesized that ovarian cancer cells will not have the needed nutrients to sustain growth and autophagy will ensue[45]. Ovarian cancer cells treated with Metformin showed inhibited proliferation and activation of AMPK[46, 47]. Metformin-treated mice transplanted with ovarian cancer showed activation of AMPK and inhibition of both angiogenesis and metastasis[48].

Another proposed mechanism is that Metformin may block complex I of the electron transport chain, which would result in low oxygen consumption by cells and elevation of the NADH:NAD^+ ratio. Because NAD^+ is a needed cofactor for β-oxidation and the TCA cycle, an increased NADH:NAD^+ ratio would decrease β-oxidation and TCA cycle flux, which then raises the AMP:ATP ratio and results in AMPK activation[49]. A recent meta-analysis showed a 31% reduction in cancer incidence in those patients who were

taking Metformin for treatment of diabetes[50]. Clinical trials are under way investigating the use of Metformin in the treatment of breast, prostate, pancreatic and other cancers; however there are no clinical trials at this time in the treatment of ovarian cancer (www.clinicaltrials.gov).

In addition to Metformin, 5-aminoimidazole-4-carboxamide-1-β-D-ribufuranoside (AICAR) is another drug targeting AMPK and works as an AMPK agonist. Activation of AMPK through either Metformin or AICAR decreases AKT phosphorylation[46] and inhibits the mTOR pathway through the tuberous sclerosis complex (TSC) inducing ovarian cancer cell death[51] (Figure 5.2). AKT has been shown to be constitutively active in ovarian cancer cells, sustaining high levels of glycolysis, and giving cancer cells the glycolytic phenotype observed by Warburg in metastatic cancer cells[51].

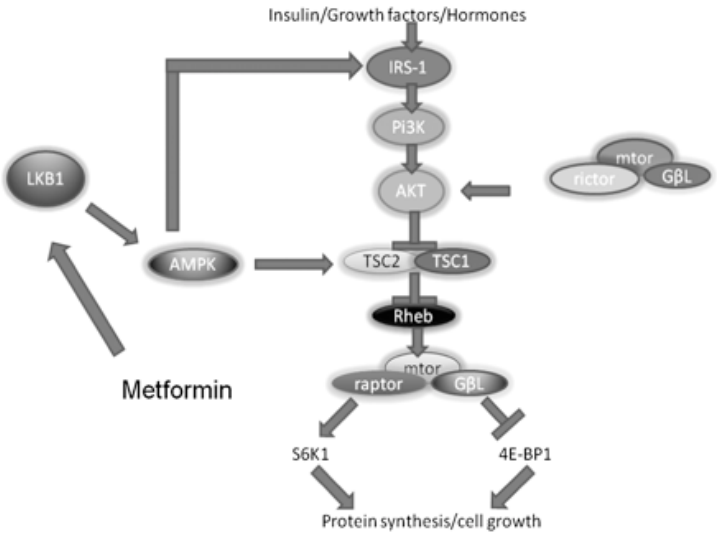

Figure 5.2 Effect of metformin on AMPK and mTOR pathway. Metformin activates the AMPK pathway through LKB1, eventually causing inhibition of the mTOR pathway and thus a reduction in protein synthesis and cellular proliferation. Metformin also appears to indirectly reduce AKT activation, through AMPK-mediated phosphorylation of IRS-1, causing inhibition of mTOR pathway. 4E-BP1, 4E-binding protein 1; AKT, v-AKT murine thymoma viral oncogene homologue; AMPK, AMP-activated protein kinase; GBL, G-protein b-subunit-like protein; IRS-1, insulin receptor substrate-1; LKB1, liver kinase B1; mTOR, mammalian target of rapamycin; PI3K, phosphoinositide 3-kinase; raptor, regulatory-associated protein of mTOR; Rheb, Ras homologue enriched in brain; rictor, rapamycin-insensitive companion of mTOR; S6K1, S6 kinase1; TSC1, tuberous sclerosis protein 1; TSC2, tuberous sclerosis protein 2[52].

6. Ovarian Cancer Mitochondria

Unlike Warburg's initial hypothesis, ovarian cancer mitochondria are TCA cycle and ETC competent. As much as 90% of ATP needs are generated by oxidative phosphorylation when ovarian cancer tissue was perfused and oxygen consumption and lactate were measured[53, 54]. The specific activities of malate dehydrogenase, succinate dehydrogenase, and glutamate dehydrogenase in isolated mitochondria from human ovarian cancer tissues were comparable to values found in skeletal muscle, heart and liver[55]. In addition, mitochondrial membrane potential, ATP biosynthesis and oxygen consumption rate were all found to be similar to isolated mitochondria from mouse livers.

However, there are differences in mitochondria of ovarian cancer cells versus normal cells. mtDNA mutations are 20% higher and a decrease in mtDNA or mitochondrial numbers are seen in ovarian cancer compared to their normal counterparts[53]. In breast cancer cells, reductions in mtDNA are associated with poor prognosis and tumor progression[56]. The mtDNA genome encodes for two rRNAs, 22 tRNAs and 13 polypeptides including seven subunits of complex I, one subunit of complex III, three subunits of complex IV, and two subunits of complex V[57]. Therefore any mtDNA mutation or decrease in mtDNA copy number altering the expression of these genes could cause an impairment of oxidative phosphorylation and enhanced production of reactive oxygen species (ROS)[58]. Although the isolated mitochondria of ovarian cancer cells are functionally competent, an overall decrease in mtDNA or mitochondrial number could impact the overall bioenergetics of the cell. 90% of ATP needs may be met by the

mitochondria through oxidative phophorylation, but 10% is still coming from the up-regulated carbon flux through glycolysis and this could be a result of reduced mtDNA or mitochondrial number. It is unknown what the ATP contributions from oxidative phosphorylation are in normal ovarian tissue.

In addition to a change in mtDNA, a cisplatin-resistant ovarian cancer cell line showed an altered mitochondrial cristae morphology, which included thicker and more irregular cristae, and in many mitochondria the cristae were absent[59]. It has been shown that in the absence of proper cristae formation, as a result of mitofilin siRNA-treatment, there is an increase in ROS, membrane potential, and metabolic flux through β-oxidation[60]. However, this was not matched with increased oxygen consumption, pointing to possible dysfunctions in the ETC with decreased or absent cristae formation. Although oxidative phosphorylation is active in cancer mitochondria, the mitochondria themselves may be altered internally to meet the altered metabolic needs of growing cancer cells.

When surveying single nucleotide polymorphisms (SNPs) of patients with ovarian cancer, genes involved in mitochondrial biogenesis were the most strongly associated with ovarian cancer risk. These genes include the transcription factor NRF1, the mitochondrial transcription termination factor MTERF, the co-factor PGC1-α, the ERR-α producing gene ESSRRA, and the kinase CAMK2D[61]. In light of this data, alterations in mitochondrial biogenesis may lead to ovarian cancer risk.

Mitochondria are the major source of reactive oxygen species (ROS) within cells. In normal cells, approximately 90% of oxygen that is taken into the cell is used by the ETC and 1-4% of this oxygen forms ROS[43]. Complexes I and III are thought to be the major

sources of ROS generation[62]. When the rate of ETC is slow (high proton motive force/ high membrane potential ($\Delta\psi_m$)), there is an increase generation of ROS. When ETC speeds up, in times of increased ATP need or due to uncoupling, the $\Delta\psi_m$ decreases, which results in a decrease in ROS production[62]. High $\Delta\psi_m$, which leads to an increase in ROS accumulation, has been shown to potentiate ovarian cancer progression[63]. In ovarian cancer cells, ROS can lead to the degradation of MAP kinase phosphatase 3 (MKP3) leading to constitutively active ERK 1/2 signaling, which is known to support tumor progression in ovarian cancer[63]. Other research has shown that H_2O_2 can activate the AKT pathway and VEGF expression through the activation of epidermal growth factor (EGF) in ovarian cancer cells[64]. When the H_2O_2 was quenched with catalase, there was a decrease in AKT activation, VEGF expression and a decrease in angiogenesis. H_2O_2 has also been shown to increase the expression of Ets-1. Ets-1 is a member of the Ets family of transcription factors and is often over-expressed in ovarian cancer[65]. Expression of Ets-1 has been found to be significantly associated with clinical stage, histological grade, and clinical outcome of patients with ovarian cancer[66]. When Ets-1 is over-expressed in ovarian cancer cells, glycolysis and fatty acid metabolism are up-regulated, while the TCA cycle, ETC and mitochondrial proteins are down-regulated. Increased expression of Ets-1 also causes a decrease in oxygen consumption and caused the cells to become more sensitive to glycolytic inhibitors[67]. The induction of Ets-1 expression due to increased H_2O_2, may be one mechanism to which cancer cells alter their metabolism to a more glycolytic phenotype. In summary, high $\Delta\psi_m$ increases cellular ROS levels, driving a more aggressive and glycolytic phenotype in ovarian

cancer. Therefore, examination of mitochondrial structure, function and ROS production should be considered as treatment targets in ovarian cancer.

7. Ovarian Cancer Stem Cells

Stem cells are a small group of cells able to phenotypically self-renew and produce differentiated progenitor daughter cells that have limited capacity for replication[68]. Tissue specific stem cells can produce differentiated cells for damaged tissue regeneration or for general tissue homeostasis[69]. These include cells such as hematopoietic stem cells (HSCs) for blood cells, satellite cells in muscle, keratinocytes in skin, and neural stem cells (NSCs) in the brain[69]. Emerging evidence points to tissue-specific stem cells also being capable of generating cells of other tissue types when transplanted in a second location[69]. Stem cells exist in niches, where a unique microenvironment is maintained, allowing for activation or repression of stem cells by external signals[68].

This long-lived stem cell population in cancer has been referred to as tumor-initiating cells (TICs) or cancer stem cells (CSCs)[70]. The cancer stem cells within a tissue have a unique genotype from their normal tissue counterparts[71]. Bapat et al. in 2005 were the first to identify an ovarian cancer stem cell population isolated from a human ascities[72]. These cells had the ability for self-renewal and anchorage-independent growth *in vitro* and tumorigenicity mimicking the original tumor *in vivo*. Cancer stem cells may originate from multiple sources and may change due to their microenvironment into several types of cancer stem cells (Figure 7.1)[73]. Not illustrated in Figure 7.1 (A), is that

there is evidence that the microenvironment may induce progenitor and/or stem cell populations from differentiated daughter cells. In human mammary epithelial cells cultured in 2D for 12 days, the percentage of cells expressing stem cell markers increased from 0.3% to 6%[74]. This increase was from the basal mammary epithelial cells, but not the luminal cells, indicating that some cells may be more predisposed to this conversion than others. It is already been demonstrated that by gene expression of stemness factors Oct4, Sox2, Klf4 and c-Myc, fibroblasts can be reprogrammed into induced pluripotent stem cells (iPSCs)[75]. New evidence suggests that this reprogramming into iPSCs may be blocked when AMPK is active, indicating that bioenergetics within the cell may play a role in addition to changes in the microenvironment[76].

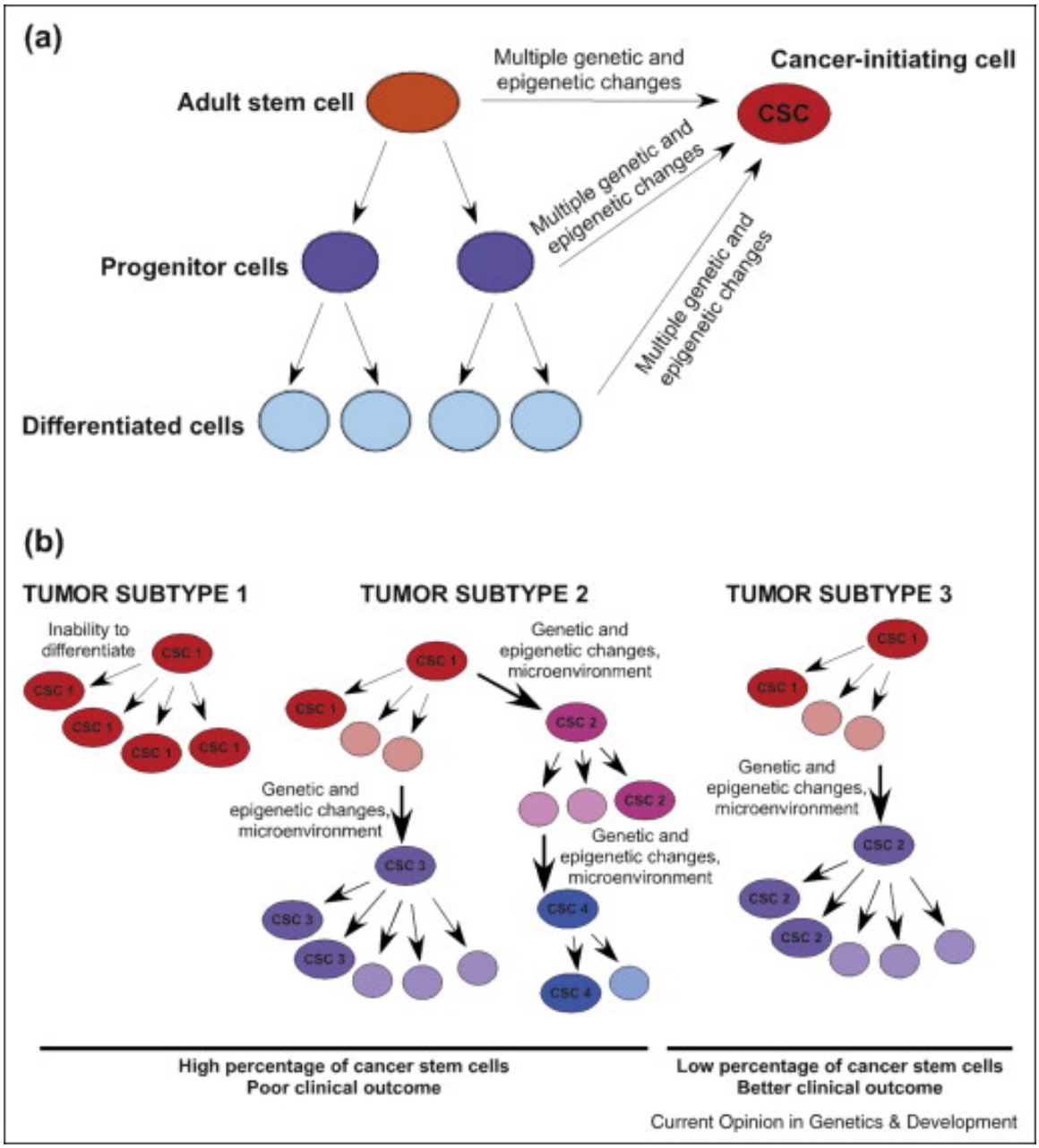

Figure 7.1. A current view of the cancer stem cells model, part 1. **(a)** Adult stem cells, progenitor cells, or differentiated cells may acquire the multiple genetic and epigenetic alterations required to become the cancer stem cell (CSC) involved in oncogenesis. This cancer-initiating cell may share some characteristics with the adult stem cells residing in the organ in which they are created, either because they originate from these cells or because they gain the properties of them. **(b)** During tumor growth, any cancer cell may develop new genetic or epigenetic alterations or be affected by the microenvironment, resulting in its change to a new type of cancer stem cell. The different cancer stem cells in a tumor will develop clonal cell populations of different sizes containing cancer stem cells and differentiated cells to varying degrees. The total percentage of a tumor that is made up of cancer stem cells may determine its subtype and associated clinical outcome[73].

**Reproduced from Current Opinion in Genetics and Development, February 2009, Vol. 19, No. 1, Pages 44-50 with permission of Elsevier Publishing.

Also referred to as a side population, ovarian cancer stem cells produce measureable tumors quicker than differentiated cancer cells and are more resistant to traditional chemotherapies[77, 78]. Once isolated, ovarian cancer stem cells can reproduce the original tumor within a mouse with as little as 100 cells[78]. Although not homozygous, many ovarian cancer stem cells express surface markers indicative of stem cells including CD44[78], c-kit/CD117[78], CD133[79-81]. In addition, others have shown ovarian cancer stem cells are TLR-4+/MyD88+, having constitutively active NFκB activity and producing increased levels of cytokines and chemokines[70]. Ovarian cancer stem cells have also been shown to express the protein ABCG2 (ATP-binding cassette sub-family G member 2) alternatively known as BCRP (breast cancer resistance protein), which works to export chemotherapeutic drugs out of the cell[82-84]. In addition, recently ovarian cancer stem cells have been shown to express EZH2, a specific histone-3-lysine-27 (H3K27) methyltransferase, which is important for epigenetic gene silencing and chromatin conformation[85]. Ovarian cancer stem cells also contain properties that allow them to proliferate in adverse conditions. When cultured in Matrigel, ovarian cancer stem cells can form vessel-like structures in 24 hours and acquire the endothelial markers CD34 and VE-cadherin within 7 days allowing for tumor vascularization[86].

The metabolic nature of ovarian cancer stem cells is still unknown. It has been shown that ovarian cancer stem cells over-express the enzyme aldehyde dehydrogenase isoform 1 (ALDH1), which oxidizes cytotoxic aldehydes to carboxylic acids producing NADPH[87, 88]. Although the metabolic significance of ALDH1 is relatively unknown, the production of NADPH is needed for increased fatty acid and cholesterol synthesis and the regeneration of reduced GSH. When ALDH+ ovarian cancer stem cells and mice

containing ALDH+ tumors were treated with the AMPK activator Metformin, there was a reduction in proliferation[89]. In breast cancer stem cells, Metformin not only reduced proliferation but induced apoptosis in glucose-deprived medium[90].

Recent evidence in breast cancer points to a dynamic equilibrium between cancer stem cells and non-stem cancer cells dependent on the inflammatory state or microenvironment, and that this equilibrium is mediated in part by miRNAs[91, 92]. miR-214 (p53), miR-199a (CD44), and miR-200a (ZEB2) have been implicated in the regulation of ovarian cancer stem cells[92]. Further evidence suggests that Metformin works directly in blocking the NF-κB pathway, as Metformin was not effective in reducing the cancer stem cell population in cells excreting low levels of IL-6, a downstream target of NF-κB[91].

In human glioma cancer cells, the cell surface marker CD44 (which is often used to characterize cancer stem cells) interacts with pyruvate kinase M2 (PKM2)[93, 94]. When PKM2 is phosphorylated and in its dimeric conformation, it is less favorable for cells to covert phosphoenolpyruvate to pyruvate, and instead carbons are shuttled out of glycolysis for anabolic synthesis including nucleotides, glycerol, NADPH, amino acids and sphingolipid synthesis[95]. When CD44 was reduced with siRNA in p53 knockout colorectal and glioma stem cells, there was an increase in carbon flux through pyruvate kinase for OXPHOS, resulting in an increase in ROS and an increase in sensitivity to chemotherapeutic drugs[93]. This points to the possibility of CD44 acting as a scaffold, allowing for tyrosine phosphorylation of PKM2[93]. In addition, metabolism in transformed mesenchymal stem cells from bone marrow show a reliance on oxidative phosphorylation and only when subjected to the tumor microenvironment do these stem

cells adapt by increasing glycolytic enzymes indicating metabolic flexibility[96]. It has also been shown that mammary cancer stem cells have reduced ROS levels and DNA damage along with an increased expression of glutamate-cysteine ligase (GCLM) and glutathione synthetase (GSS) to generate GSH to quench ROS[97]. This metabolic flexibility may explain the deadliness of metastatic cancer[98].

Although there is limited knowledge of metabolism in cancer stem cells, it is known that human embryonic stem cells (hESCs) and adult hematopoietic stem cells (HSCs) rely more heavily on glycolysis for ATP needs than on OxPhos[99]. HSCs have a decrease in mitochondrial number and a lower rate of OxPhos[100], while the hESCs have a lower $\Delta\psi_m$ than cardiomyocytes indicating lower mitochondrial function[101]. hESCs show an increased acidification of their medium compared to their differentiated counterparts[102]. This acidification may be crucial for the maintenance of stem cell niches or it may be an adaptation from the glycolytic nature of stem cells. Either way, when MCF7 breast cancer cells were cultured in ketones and lactate there was an increase in stem cell gene markers consistent with neural, embryonic, and hematopoietic stem cells and ketones and lactate increased the growth rate of ESCs[103]. In addition to being more glycolytic, neural stem and progenitor cells (NSPCs) rely heavily on FASN for lipid synthesis and impairment of FASN reduces neurogenesis[104]. Moreover, ESCs show a varied lipid composition with an increased level of unsaturated fatty acids, highlighting the differences in these unique cell populations[105]. Due to the known distinct metabolic phenotype of non-transformed stem cells, it is reasonable to hypothesize that cancer stem cells would also be phenotypically distinct from differentiated cancer cells.

In summary, adult stem cells and cancer stem cells can self-renew, produce differentiated progenitor daughter cells, and are reliant on external signals for activation. Adult stem cells are more glycolytic, more lipogenic and survive in a niche with increased acidification, similar to differentiated cancer cells. Transformed mesenchymal stem cells are basally more oxidative, but when challenged increase glycolysis. Additionally, MCF7 cells up-regulate stem cell markers when challenged with limited substrates. This evidence suggests that cancer stem cells may be able to adapt their metabolism to survive in varying conditions. In fact, chemotherapy may enrich the cancer stem cell population as it targets and kills differentiated cancer cells making subsequent chemotherapy treatments less effective[106]. Due to the limited knowledge of metabolism in cancer stem cells, it is evident that further investigation is needed augment current therapies and prevent cancer recurrence after chemotherapy.

8. Sphingosine

Sphingosine is a bioactive lipid known to regulate the cytoskeleton, the cell cycle and apoptosis[107]. It is part of the family of sphingolipids found naturally in most foods but is especially rich in dairy and soy products[108]. Sphingolipid metabolism is a complex dynamic and bidirectional flux from one metabolite to another, determining growth versus cell-cycle arrest and toxicity (Figure 8.1). Altering this rheostat between ceramide, sphingosine, and sphingosine-1-phosphate could influence whether cancer cells become apoptotic due to increases in ceramide and/or sphingosine, or continue to proliferate due to increases in sphingosine-1-phosphate[109].

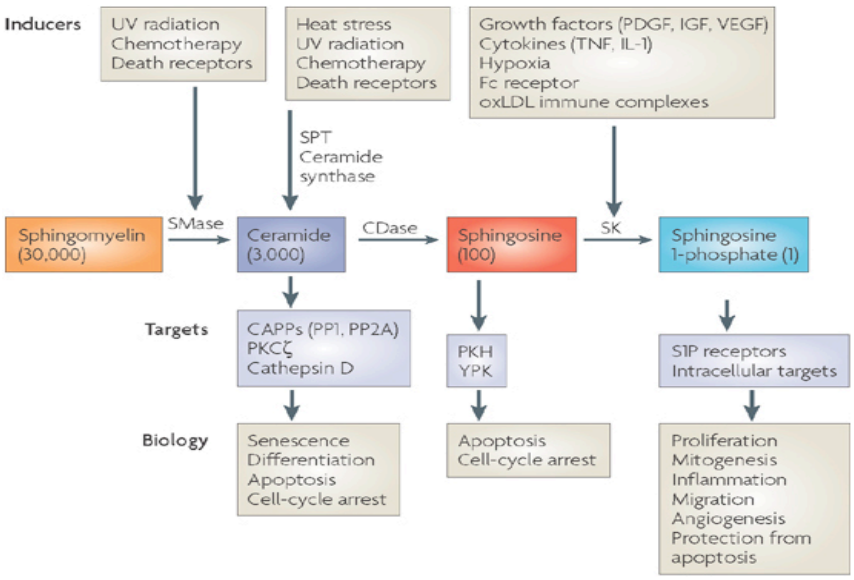

Figure 8.1 The scheme shows potential participation of the bioactive lipids ceramide, sphingosine and sphingosine-1-phosphate (S1P) in cell biological responses. Ceramide can be generated by the breakdown of sphingomyelin by sphingomyelinases (SMases) or synthesized de novo by serine palmitoyl transferase (SPT) and ceramide synthase. Both of these processes can be induced by diverse stimuli (beige boxes). Sphingosine and S1P can be generated by ceramidases (CDases) and sphingosine kinases (SKs). These interconnected metabolites interact with specific protein targets such as serine/threonine protein phosphatases, kinases and G protein-coupled receptors (S1P receptors), which in turn mediate the effects of these lipids and, at least in part, also mediate the effects of the inducers on specific cell responses. The numbers in brackets indicate the relative levels of these sphingolipids. CAPP, ceramide-activated Ser–Thr phosphatase; IGF; insulin-like growth factor; IL-1, interleukin-1; oxLDL, oxidized low-density lipoprotein; PDGF; platelet-derived growth factor; PKC, protein kinase C; PKH, PKB homologue; TNF-α, tumour necrosis factor-α; VEGF, vascular endothelial growth factor; YPK, yeast protein kinase[107].
**Reproduced from Nature Reviews Molecular Cell Biology, February 2008, Vol. 9, No. 2, Pages 139-150 with permission of Nature Publishing Group.

Sphingosine's role in cancer prevention is well documented in colon cancer, where sphingosine decreases aberrant colonic crypt formation and adenocarcinomas in mice without causing toxic side effects[110]. In colon cancer cell lines, the addition of sphingosine inhibited growth and induced cell death[111]. Dietary sphingomyelin has also been shown to delay the progression to late-stage malignant tumors in breast cancer[112]. Dietary sphingomyelin in ovarian cancer has shown to decrease growth and tumorigenic potential (Schmelz et al., manuscript in preparation) and to improve the cytoskeleton architecture towards that of benign cells (Creekmore et al., paper in review).

Sphingosine's ability to induce apoptosis and repair aberrant signaling, without toxic side effects or damage to healthy cells, allows it to be a promising chemotherapeutic agent. Dietary sphingomyelin is metabolized to its bioactive constituent sphingosine in the colon and absorbed; since more complex sphingolipids are not absorbed, the putative biological metabolite providing the anti-cancer effect is sphingosine [110].

Sphingosine's effect on cancer may be within the mitochondria. Increasing doses of sphingosine have been shown to decrease membrane potential with subsequent depolarization leading to the release of cytochrome C and apoptosis in Jurkat T-cells[113, 114]. The depolarization occurred before the induction of the mitochondrial dependent apoptotic pathway. Cardiac muscle mitochondria treated with 20μM sphingosine, showed a depolarization of the mitochondrial membrane and a decrease in state 3 respiration[115]. This was coupled with a subsequent increase in state 4 respiration and decreased ATP production. The effect of sphingosine on mitochondrial metabolic markers remains to be investigated in ovarian cancer.

Recent evidence suggests that increases in sphingosine and ceramide, due to inhibition of sphingosine kinase 1, can lead to an accumulation of glycolytic intermediates, a decrease in glucose uptake and an increase in proteolysis of c-myc in prostate cancer cells[116]. c-myc has been shown to upregulate expression of key glycolytic enzymes including Glut-1, phosphofructokinase, and enolase[117] and regulate LDH-a expression[12]. Although the mechanism is not completely clear, increases in sphingosine and ceramide dampen the Warburg effect.

Ceramide has also been shown to decrease insulin-mediated glucose uptake and decrease phosphorylation of AKT in C2C12 mouse myocytes[118]. AKT when phosphorylated, has as a myriad of targets contributing to the Warburg effect. AKT phosphorylates the Rab GTPases AS160 and TBC1D1 leading to Glut-4 translocation,[119] increases transcription of Glut-1 and stabilizes it in the membrane[12], and increases hexokinase stabilization by phosphorylating it and securing it to the mitochondrial membrane[12]. In addition via phosphorylation, AKT increases ATP-citrate lyase activity,[120] blocks the TSC1/TSC2 complex driving mTOR signaling,[52] and activates PFK-2 thereby increasing glycolysis[12]. With a decrease in AKT phosphorylation by ceramide, these pro-Warburg effect targets may be decreased. The anti-proliferative effects of sphingosine on ovarian cancer need to be further explored.

9. Conclusion

Ovarian cancer continues to be deadly to many women. Early diagnosis and effective treatments are critical to increasing survival rates. Metabolic changes are a hallmark in cancer development. By capitalizing on these metabolic changes, treatments can be designed alone or in conjunction with chemotherapy to decrease cancer growth and increase survival.

The Warburg effect still stands true today, despite some changes. Cancer cells do shift their metabolism towards aerobic glycolysis and away from oxidative phosphorylation. However, this shift is not a result of dysfunctional mitochondria, as Warburg first proposed. Instead, this shift in metabolism is necessary for cancer's exponential growth

rates. The increase in glucose uptake and the shuttling of carbons to the pentose phosphate pathway and through the TCA cycle to citrate, produce the needed building blocks and reducing equivalents for cancer growth. The other necessary substrate for metabolism not known to Warburg in his lifetime is glutamine. Glutamine converted to α-ketoglutarate replenishes the TCA cycle and is catabolized to supply glutamate to produce GSH. Mitochondria are central to the metabolism of the cell and are functional, though possibly altered, in ovarian cancer.

To support this altered metabolism and subsequent growth, substrate uptake and enzymatic pathways have been altered. Glucose, fatty acid and glutamine transporters are increased to support the increased influx of substrates. FASN is up-regulated producing *de novo* fatty acids. MCTs are up-regulated and important in the disposal of the excess lactate produced by one cancer cell and the transport of lactate back into another cancer cell to be utilized for energy.

Finding ways to reverse the metabolic changes seen in ovarian cancer will lead to more effective treatment regimens. The use of Metformin or AICAR in activating AMPK to increase catabolic processes and reduce anabolic processes shows promise in modulating metabolism to decrease cancer growth. In addition, the use of naturally occurring chemotherapeutic agents to synergistically complement existing treatments in the reversal of altered metabolism will increase the survival rate of this deadly cancer. However, treatments need to take into account the diversity of cancer cells including cancer stem cells. Because of the differential characteristics of these two distinct populations, effective treatments for differentiated tumor cells might be less effective for tumor stem

cells. A combinatorial treatment targeting both cell populations is crucial to eradicating ovarian cancer from women.

Although metabolic changes in many cancers are well documented, ovarian cancer metabolism research is still not well explored. Ovarian cancer may present a challenging model to study due to the heterogeneity of ovarian cancer with several subtypes include serous, clear cell, endometrioid, and mucinous tumors, each with a distinct molecular genotype[121, 122]. Additionally, new research indicates that ovarian cancer may be a secondary cancer that originated in other pelvic regions including the fallopian tubes[122]. Consequently, due to the complexity of ovarian cancer, other tissue models are more readily used to study cancer metabolism. However, the deadliness of ovarian cancer remains and with further investigation into the metabolic alterations, treatments and possible biomarkers will be established for both differentiated and stem cell populations. By modifying metabolism with agonists or naturally occurring chemotherapeutic agents, clinical trials can be established to complement current treatment regimens. Together the survival rate for women with ovarian cancer can be increased.

References

1. Siegel R, Ward E, Brawley O, Jemal A. Cancer statistics, 2011: the impact of eliminating socioeconomic and racial disparities on premature cancer deaths. *CA Cancer J Clin.* Jul-Aug 2011;61(4):212-236.
2. Siegel R, Naishadham D, Jemal A. Cancer statistics, 2013. *CA Cancer J Clin.* Jan 2013;63(1):11-30.
3. Hanahan D, Weinberg RA. The hallmarks of cancer. *Cell.* Jan 7 2000;100(1):57-70.
4. Hanahan D, Weinberg RA. Hallmarks of cancer: the next generation. *Cell.* Mar 4 2011;144(5):646-674.
5. Warburg O, Wind F, Negelein E. The Metabolism of Tumors in the Body. *J Gen Physiol.* Mar 7 1927;8(6):519-530.
6. Warburg O. On the origin of cancer cells. *Science.* Feb 24 1956;123(3191):309-314.
7. Zu XL, Guppy M. Cancer metabolism: facts, fantasy, and fiction. *Biochem Biophys Res Commun.* Jan 16 2004;313(3):459-465.
8. Weinhouse S. On respiratory impairment in cancer cells. *Science.* Aug 10 1956;124(3215):267-269.
9. Rossignol R, Gilkerson R, Aggeler R, Yamagata K, Remington SJ, Capaldi RA. Energy substrate modulates mitochondrial structure and oxidative capacity in cancer cells. *Cancer Res.* Feb 1 2004;64(3):985-993.
10. Fantin VR, St-Pierre J, Leder P. Attenuation of LDH-A expression uncovers a link between glycolysis, mitochondrial physiology, and tumor maintenance. *Cancer Cell.* Jun 2006;9(6):425-434.
11. Frezza C, Gottlieb E. Mitochondria in cancer: not just innocent bystanders. *Semin Cancer Biol.* Feb 2009;19(1):4-11.
12. Lunt SY, Vander Heiden MG. Aerobic glycolysis: meeting the metabolic requirements of cell proliferation. *Annu Rev Cell Dev Biol.* Nov 10 2011;27:441-464.
13. Cheng T, Sudderth J, Yang C, et al. Pyruvate carboxylase is required for glutamine-independent growth of tumor cells. *Proc Natl Acad Sci U S A.* May 24 2011;108(21):8674-8679.
14. Cheng KW, Agarwal R, Mitra S, et al. Rab25 increases cellular ATP and glycogen stores protecting cancer cells from bioenergetic stress. *EMBO Mol Med.* Feb 2012;4(2):125-141.
15. Franco R, Schoneveld OJ, Pappa A, Panayiotidis MI. The central role of glutathione in the pathophysiology of human diseases. *Arch Physiol Biochem.* Oct-Dec 2007;113(4-5):234-258.
16. Kroemer G, Pouyssegur J. Tumor cell metabolism: cancer's Achilles' heel. *Cancer Cell.* Jun 2008;13(6):472-482.
17. Wise DR, Ward PS, Shay JE, et al. Hypoxia promotes isocitrate dehydrogenase-dependent carboxylation of alpha-ketoglutarate to citrate to support cell growth and viability. *Proc Natl Acad Sci U S A.* Dec 6 2011;108(49):19611-19616.

18. Mullen AR, Wheaton WW, Jin ES, et al. Reductive carboxylation supports growth in tumour cells with defective mitochondria. *Nature.* Jan 19 2012;481(7381):385-388.
19. Metallo CM, Gameiro PA, Bell EL, et al. Reductive glutamine metabolism by IDH1 mediates lipogenesis under hypoxia. *Nature.* Jan 19 2012;481(7381):380-384.
20. DeBerardinis RJ, Mancuso A, Daikhin E, et al. Beyond aerobic glycolysis: transformed cells can engage in glutamine metabolism that exceeds the requirement for protein and nucleotide synthesis. *Proc Natl Acad Sci U S A.* Dec 4 2007;104(49):19345-19350.
21. Filipp FV, Scott DA, Ronai ZA, Osterman AL, Smith JW. Reverse TCA cycle flux through isocitrate dehydrogenases 1 and 2 is required for lipogenesis in hypoxic melanoma cells. *Pigment Cell Melanoma Res.* May 2012;25(3):375-383.
22. Joost HG, Thorens B. The extended GLUT-family of sugar/polyol transport facilitators: nomenclature, sequence characteristics, and potential function of its novel members (review). *Mol Membr Biol.* Oct-Dec 2001;18(4):247-256.
23. Frolova AI, Moley KH. Glucose transporters in the uterus: an analysis of tissue distribution and proposed physiological roles. *Reproduction.* Aug 2011;142(2):211-220.
24. Semaan A, Munkarah AR, Arabi H, et al. Expression of GLUT-1 in epithelial ovarian carcinoma: correlation with tumor cell proliferation, angiogenesis, survival and ability to predict optimal cytoreduction. *Gynecol Oncol.* Apr 2011;121(1):181-186.
25. Rudlowski C, Moser M, Becker AJ, et al. GLUT1 mRNA and protein expression in ovarian borderline tumors and cancer. *Oncology.* 2004;66(5):404-410.
26. Cantuaria G, Magalhaes A, Penalver M, et al. Expression of GLUT-1 glucose transporter in borderline and malignant epithelial tumors of the ovary. *Gynecol Oncol.* Oct 2000;79(1):33-37.
27. Shibata K, Kajiyama H, Mizokami Y, et al. Placental leucine aminopeptidase (P-LAP) and glucose transporter 4 (GLUT4) expression in benign, borderline, and malignant ovarian epithelia. *Gynecol Oncol.* Jul 2005;98(1):11-18.
28. Knapp P, Chabowski A, Harasiuk D, Gorski J. Reversed glucose and fatty acids transporter expression in human endometrial cancer. *Horm Metab Res.* Jun 2012;44(6):436-441.
29. Brusselmans K, Swinnen JV. The Lipogenic Switch in Cancer Mitochondria and Cancer: Springer New York; 2009:39-59.
30. Nieman KM, Kenny HA, Penicka CV, et al. Adipocytes promote ovarian cancer metastasis and provide energy for rapid tumor growth. *Nat Med.* 2011;17(11):1498-1503.
31. Kuemmerle NB, Rysman E, Lombardo PS, et al. Lipoprotein lipase links dietary fat to solid tumor cell proliferation. *Mol Cancer Ther.* Mar 2011;10(3):427-436.
32. Guppy M, Leedman P, Zu X, Russell V. Contribution by different fuels and metabolic pathways to the total ATP turnover of proliferating MCF-7 breast cancer cells. *Biochem J.* May 15 2002;364(Pt 1):309-315.

33. Halestrap AP, Price NT. The proton-linked monocarboxylate transporter (MCT) family: structure, function and regulation. *Biochem J.* Oct 15 1999;343 Pt 2:281-299.
34. Gatenby RA, Gillies RJ. Why do cancers have high aerobic glycolysis? *Nat Rev Cancer.* Nov 2004;4(11):891-899.
35. Kennedy KM, Dewhirst MW. Tumor metabolism of lactate: the influence and therapeutic potential for MCT and CD147 regulation. *Future Oncol.* Jan 2010;6(1):127-148.
36. Vander Heiden MG, Cantley LC, Thompson CB. Understanding the Warburg effect: the metabolic requirements of cell proliferation. *Science.* May 22 2009;324(5930):1029-1033.
37. Lligona-Trulla L, Arduini A, Aldaghlas TA, Calvani M, Kelleher JK. Acetyl-L-carnitine flux to lipids in cells estimated using isotopomer spectral analysis. *J Lipid Res.* Jul 1997;38(7):1454-1462.
38. Gansler TS, Hardman W, 3rd, Hunt DA, Schaffel S, Hennigar RA. Increased expression of fatty acid synthase (OA-519) in ovarian neoplasms predicts shorter survival. *Hum Pathol.* Jun 1997;28(6):686-692.
39. Menendez JA, Lupu R. Fatty acid synthase and the lipogenic phenotype in cancer pathogenesis. *Nat Rev Cancer.* Oct 2007;7(10):763-777.
40. Luo Z, Saha AK, Xiang X, Ruderman NB. AMPK, the metabolic syndrome and cancer. *Trends Pharmacol Sci.* Feb 2005;26(2):69-76.
41. Chiacchiera F, Simone C. The AMPK-FoxO3A axis as a target for cancer treatment. *Cell Cycle.* Mar 15 2010;9(6):1091-1096.
42. Zhou W, Han WF, Landree LE, et al. Fatty acid synthase inhibition activates AMP-activated protein kinase in SKOV3 human ovarian cancer cells. *Cancer Res.* Apr 1 2007;67(7):2964-2971.
43. Hagland H, Nikolaisen J, Hodneland LI, Gjertsen BT, Bruserud O, Tronstad KJ. Targeting mitochondria in the treatment of human cancer: a coordinated attack against cancer cell energy metabolism and signalling. *Expert Opin Ther Targets.* Aug 2007;11(8):1055-1069.
44. Shackelford DB, Shaw RJ. The LKB1-AMPK pathway: metabolism and growth control in tumour suppression. *Nat Rev Cancer.* Aug 2009;9(8):563-575.
45. Kellenberger LD, Bruin JE, Greenaway J, et al. The role of dysregulated glucose metabolism in epithelial ovarian cancer. *J Oncol.* 2010;2010:514310.
46. Rattan R, Giri S, Hartmann LC, Shridhar V. Metformin attenuates ovarian cancer cell growth in an AMP-kinase dispensable manner. *J Cell Mol Med.* Jan 2011;15(1):166-178.
47. Gotlieb WH, Saumet J, Beauchamp MC, et al. In vitro metformin anti-neoplastic activity in epithelial ovarian cancer. *Gynecol Oncol.* Aug 2008;110(2):246-250.
48. Rattan R, Graham RP, Maguire JL, Giri S, Shridhar V. Metformin suppresses ovarian cancer growth and metastasis with enhancement of cisplatin cytotoxicity in vivo. *Neoplasia.* May 2011;13(5):483-491.
49. Aljada A, Mousa SA. Metformin and neoplasia: implications and indications. *Pharmacol Ther.* Jan 2012;133(1):108-115.

50. Decensi A, Puntoni M, Goodwin P, et al. Metformin and cancer risk in diabetic patients: a systematic review and meta-analysis. *Cancer Prev Res (Phila).* Nov 2010;3(11):1451-1461.
51. Priebe A, Tan L, Wahl H, et al. Glucose deprivation activates AMPK and induces cell death through modulation of Akt in ovarian cancer cells. *Gynecol Oncol.* Aug 2011;122(2):389-395.
52. Clements A, Gao B, Yeap SH, Wong MK, Ali SS, Gurney H. Metformin in prostate cancer: two for the price of one. *Ann Oncol.* Dec 2011;22(12):2556-2560.
53. Moreno-Sanchez R, Rodriguez-Enriquez S, Saavedra E, Marin-Hernandez A, Gallardo-Perez JC. The bioenergetics of cancer: is glycolysis the main ATP supplier in all tumor cells? *Biofactors.* Mar-Apr 2009;35(2):209-225.
54. Kallinowski F, Schlenger KH, Runkel S, et al. Blood flow, metabolism, cellular microenvironment, and growth rate of human tumor xenografts. *Cancer Res.* Jul 15 1989;49(14):3759-3764.
55. Lim HY, Ho QS, Low J, Choolani M, Wong KP. Respiratory competent mitochondria in human ovarian and peritoneal cancer. *Mitochondrion.* May 2011;11(3):437-443.
56. Yu M, Zhou Y, Shi Y, et al. Reduced mitochondrial DNA copy number is correlated with tumor progression and prognosis in Chinese breast cancer patients. *IUBMB Life.* Jul 2007;59(7):450-457.
57. Modica-Napolitano JS, Singh KK. Mitochondria as targets for detection and treatment of cancer. *Expert Rev Mol Med.* Apr 2002;4(9):1-19.
58. Wu CW, Yin PH, Hung WY, et al. Mitochondrial DNA mutations and mitochondrial DNA depletion in gastric cancer. *Genes Chromosomes Cancer.* Sep 2005;44(1):19-28.
59. Andrews PA, Albright KD. Mitochondrial defects in cis-diamminedichloroplatinum(II)-resistant human ovarian carcinoma cells. *Cancer Res.* Apr 1 1992;52(7):1895-1901.
60. John GB, Shang Y, Li L, et al. The mitochondrial inner membrane protein mitofilin controls cristae morphology. *Mol Biol Cell.* Mar 2005;16(3):1543-1554.
61. Permuth-Wey J, Chen YA, Tsai YY, et al. Inherited variants in mitochondrial biogenesis genes may influence epithelial ovarian cancer risk. *Cancer Epidemiol Biomarkers Prev.* Jun 2011;20(6):1131-1145.
62. Finkel T. Signal transduction by mitochondrial oxidants. *J Biol Chem.* Feb 10 2012;287(7):4434-4440.
63. Chan DW, Liu VW, Tsao GS, et al. Loss of MKP3 mediated by oxidative stress enhances tumorigenicity and chemoresistance of ovarian cancer cells. *Carcinogenesis.* Sep 2008;29(9):1742-1750.
64. Liu LZ, Hu XW, Xia C, et al. Reactive oxygen species regulate epidermal growth factor-induced vascular endothelial growth factor and hypoxia-inducible factor-1alpha expression through activation of AKT and P70S6K1 in human ovarian cancer cells. *Free Radic Biol Med.* Nov 15 2006;41(10):1521-1533.
65. Wilson LA, Gemin A, Espiritu R, Singh G. ets-1 is transcriptionally up-regulated by H2O2 via an antioxidant response element. *FASEB J.* Dec 2005;19(14):2085-2087.

66. Takai N, Miyazaki T, Nishida M, Nasu K, Miyakawa I. c-Ets1 is a promising marker in epithelial ovarian cancer. *Int J Mol Med.* Mar 2002;9(3):287-292.
67. Verschoor ML, Wilson LA, Verschoor CP, Singh G. Ets-1 regulates energy metabolism in cancer cells. *PLoS One.* 2010;5(10):e13565.
68. Hsu YC, Fuchs E. A family business: stem cell progeny join the niche to regulate homeostasis. *Nat Rev Mol Cell Biol.* Feb 2012;13(2):103-114.
69. Blau HM, Brazelton TR, Weimann JM. The evolving concept of a stem cell: entity or function? *Cell.* Jun 29 2001;105(7):829-841.
70. Alvero AB, Chen R, Fu HH, et al. Molecular phenotyping of human ovarian cancer stem cells unravels the mechanisms for repair and chemoresistance. *Cell Cycle.* Jan 1 2009;8(1):158-166.
71. Wani AA, Sharma N, Shouche YS, Bapat SA. Nuclear-mitochondrial genomic profiling reveals a pattern of evolution in epithelial ovarian tumor stem cells. *Oncogene.* Oct 12 2006;25(47):6336-6344.
72. Bapat SA, Mali AM, Koppikar CB, Kurrey NK. Stem and progenitor-like cells contribute to the aggressive behavior of human epithelial ovarian cancer. *Cancer Res.* Apr 15 2005;65(8):3025-3029.
73. Marotta LL, Polyak K. Cancer stem cells: a model in the making. *Curr Opin Genet Dev.* Feb 2009;19(1):44-50.
74. Chaffer CL, Brueckmann I, Scheel C, et al. Normal and neoplastic nonstem cells can spontaneously convert to a stem-like state. *Proc Natl Acad Sci U S A.* May 10 2011;108(19):7950-7955.
75. Takahashi K, Yamanaka S. Induction of pluripotent stem cells from mouse embryonic and adult fibroblast cultures by defined factors. *Cell.* Aug 25 2006;126(4):663-676.
76. Vazquez-Martin A, Vellon L, Quiros PM, et al. Activation of AMP-activated protein kinase (AMPK) provides a metabolic barrier to reprogramming somatic cells into stem cells. *Cell Cycle.* Mar 1 2012;11(5):974-989.
77. Szotek PP, Pieretti-Vanmarcke R, Masiakos PT, et al. Ovarian cancer side population defines cells with stem cell-like characteristics and Mullerian Inhibiting Substance responsiveness. *Proc Natl Acad Sci U S A.* Jul 25 2006;103(30):11154-11159.
78. Zhang S, Balch C, Chan MW, et al. Identification and characterization of ovarian cancer-initiating cells from primary human tumors. *Cancer Res.* Jun 1 2008;68(11):4311-4320.
79. Baba T, Convery PA, Matsumura N, et al. Epigenetic regulation of CD133 and tumorigenicity of CD133+ ovarian cancer cells. *Oncogene.* Jan 15 2009;28(2):209-218.
80. Curley MD, Therrien VA, Cummings CL, et al. CD133 expression defines a tumor initiating cell population in primary human ovarian cancer. *Stem Cells.* Dec 2009;27(12):2875-2883.
81. Guo R, Wu Q, Liu F, Wang Y. Description of the CD133+ subpopulation of the human ovarian cancer cell line OVCAR3. *Oncol Rep.* Jan 2011;25(1):141-146.
82. Hu L, McArthur C, Jaffe RB. Ovarian cancer stem-like side-population cells are tumourigenic and chemoresistant. *Br J Cancer.* Apr 13 2010;102(8):1276-1283.

83. Dou J, Jiang C, Wang J, et al. Using ABCG2-molecule-expressing side population cells to identify cancer stem-like cells in a human ovarian cell line. *Cell Biol Int.* Mar 2011;35(3):227-234.
84. Ricci F, Bernasconi S, Perego P, et al. Ovarian carcinoma tumor-initiating cells have a mesenchymal phenotype. *Cell Cycle.* May 15 2012;11(10):1966-1976.
85. Rizzo S, Hersey JM, Mellor P, et al. Ovarian cancer stem cell-like side populations are enriched following chemotherapy and overexpress EZH2. *Mol Cancer Ther.* Feb 2011;10(2):325-335.
86. Alvero AB, Fu HH, Holmberg J, et al. Stem-like ovarian cancer cells can serve as tumor vascular progenitors. *Stem Cells.* Oct 2009;27(10):2405-2413.
87. Deng S, Yang X, Lassus H, et al. Distinct expression levels and patterns of stem cell marker, aldehyde dehydrogenase isoform 1 (ALDH1), in human epithelial cancers. *PLoS One.* 2010;5(4):e10277.
88. Landen CN, Jr., Goodman B, Katre AA, et al. Targeting aldehyde dehydrogenase cancer stem cells in ovarian cancer. *Mol Cancer Ther.* Dec 2010;9(12):3186-3199.
89. Shank JJ, Yang K, Ghannam J, et al. Metformin targets ovarian cancer stem cells in vitro and in vivo. *Gynecol Oncol.* Nov 2012;127(2):390-397.
90. Menendez JA, Oliveras-Ferraros C, Cufi S, et al. Metformin is synthetically lethal with glucose withdrawal in cancer cells. *Cell Cycle.* Aug 1 2012;11(15):2782-2792.
91. Hirsch HA, Iliopoulos D, Struhl K. Metformin inhibits the inflammatory response associated with cellular transformation and cancer stem cell growth. *Proc Natl Acad Sci U S A.* Jan 15 2013;110(3):972-977.
92. Kwon MJ, Shin YK. Regulation of ovarian cancer stem cells or tumor-initiating cells. *Int J Mol Sci.* 2013;14(4):6624-6648.
93. Tamada M, Nagano O, Tateyama S, et al. Modulation of glucose metabolism by CD44 contributes to antioxidant status and drug resistance in cancer cells. *Cancer Res.* Mar 15 2012;72(6):1438-1448.
94. Tamada M, Suematsu M, Saya H. Pyruvate kinase m2: multiple faces for conferring benefits on cancer cells. *Clin Cancer Res.* Oct 15 2012;18(20):5554-5561.
95. Mazurek S. Pyruvate kinase type M2: a key regulator within the tumour metabolome and a tool for metabolic profiling of tumours. *Ernst Schering Found Symp Proc.* 2007(4):99-124.
96. Funes JM, Quintero M, Henderson S, et al. Transformation of human mesenchymal stem cells increases their dependency on oxidative phosphorylation for energy production. *Proc Natl Acad Sci U S A.* Apr 10 2007;104(15):6223-6228.
97. Diehn M, Cho RW, Lobo NA, et al. Association of reactive oxygen species levels and radioresistance in cancer stem cells. *Nature.* Apr 9 2009;458(7239):780-783.
98. Berridge MV, Herst PM, Tan AS. Metabolic flexibility and cell hierarchy in metastatic cancer. *Mitochondrion.* Nov 2010;10(6):584-588.
99. Rafalski VA, Mancini E, Brunet A. Energy metabolism and energy-sensing pathways in mammalian embryonic and adult stem cell fate. *J Cell Sci.* Dec 1 2012;125(Pt 23):5597-5608.

100. Piccoli C, Ria R, Scrima R, et al. Characterization of mitochondrial and extra-mitochondrial oxygen consuming reactions in human hematopoietic stem cells. Novel evidence of the occurrence of NAD(P)H oxidase activity. *J Biol Chem.* Jul 15 2005;280(28):26467-26476.
101. St John JC, Ramalho-Santos J, Gray HL, et al. The expression of mitochondrial DNA transcription factors during early cardiomyocyte in vitro differentiation from human embryonic stem cells. *Cloning Stem Cells.* 2005;7(3):141-153.
102. Vacanti NM, Metallo CM. Exploring metabolic pathways that contribute to the stem cell phenotype. *Biochim Biophys Acta.* Feb 2013;1830(2):2361-2369.
103. Martinez-Outschoorn UE, Prisco M, Ertel A, et al. Ketones and lactate increase cancer cell "stemness," driving recurrence, metastasis and poor clinical outcome in breast cancer: achieving personalized medicine via Metabolo-Genomics. *Cell Cycle.* Apr 15 2011;10(8):1271-1286.
104. Knobloch M, Braun SM, Zurkirchen L, et al. Metabolic control of adult neural stem cell activity by Fasn-dependent lipogenesis. *Nature.* Jan 10 2013;493(7431):226-230.
105. Panopoulos AD, Yanes O, Ruiz S, et al. The metabolome of induced pluripotent stem cells reveals metabolic changes occurring in somatic cell reprogramming. *Cell Res.* Jan 2012;22(1):168-177.
106. Zhan Q, Wang C, Ngai S. Ovarian cancer stem cells: a new target for cancer therapy. *Biomed Res Int.* 2013;2013:916819.
107. Hannun YA, Obeid LM. Principles of bioactive lipid signalling: lessons from sphingolipids. *Nat Rev Mol Cell Biol.* Feb 2008;9(2):139-150.
108. Vesper H, Schmelz EM, Nikolova-Karakashian MN, Dillehay DL, Lynch DV, Merrill AH, Jr. Sphingolipids in food and the emerging importance of sphingolipids to nutrition. *J Nutr.* Jul 1999;129(7):1239-1250.
109. Pyne NJ, Pyne S. Sphingosine 1-phosphate and cancer. *Nat Rev Cancer.* Jul 2010;10(7):489-503.
110. Schmelz EM, Dillehay DL, Webb SK, Reiter A, Adams J, Merrill AH, Jr. Sphingomyelin consumption suppresses aberrant colonic crypt foci and increases the proportion of adenomas versus adenocarcinomas in CF1 mice treated with 1,2-dimethylhydrazine: implications for dietary sphingolipids and colon carcinogenesis. *Cancer Res.* Nov 1 1996;56(21):4936-4941.
111. Schmelz EM, Roberts PC, Kustin EM, et al. Modulation of intracellular beta-catenin localization and intestinal tumorigenesis in vivo and in vitro by sphingolipids. *Cancer Res.* Sep 15 2001;61(18):6723-6729.
112. Simon KW, Tait L, Miller F, et al. Suppression of breast xenograft growth and progression in nude mice: implications for the use of orally administered sphingolipids as chemopreventive agents against breast cancer. . *Food & Function.* 2010;1(1):90-98.
113. Cuvillier O, Edsall L, Spiegel S. Involvement of sphingosine in mitochondria-dependent Fas-induced apoptosis of type II Jurkat T cells. *J Biol Chem.* May 26 2000;275(21):15691-15700.
114. Dangel GR, Lang F, Lepple-Wienhues A. Effect of sphingosine on Ca2+ entry and mitochondrial potential of Jurkat T cells--interaction with Bcl2. *Cell Physiol Biochem.* 2005;16(1-3):9-14.

115. Hassoun SM, Lancel S, Petillot P, et al. Sphingosine impairs mitochondrial function by opening permeability transition pore. *Mitochondrion.* Jun 2006;6(3):149-154.
116. Watson DG, Tonelli F, Alossaimi M, et al. The roles of sphingosine kinases 1 and 2 in regulating the Warburg effect in prostate cancer cells. *Cell Signal.* Apr 2013;25(4):1011-1017.
117. Osthus RC, Shim H, Kim S, et al. Deregulation of glucose transporter 1 and glycolytic gene expression by c-Myc. *J Biol Chem.* Jul 21 2000;275(29):21797-21800.
118. Chavez JA, Holland WL, Bar J, Sandhoff K, Summers SA. Acid ceramidase overexpression prevents the inhibitory effects of saturated fatty acids on insulin signaling. *J Biol Chem.* May 20 2005;280(20):20148-20153.
119. Sakamoto K, Holman GD. Emerging role for AS160/TBC1D4 and TBC1D1 in the regulation of GLUT4 traffic. *Am J Physiol Endocrinol Metab.* Jul 2008;295(1):E29-37.
120. Migita T, Narita T, Nomura K, et al. ATP citrate lyase: activation and therapeutic implications in non-small cell lung cancer. *Cancer Res.* Oct 15 2008;68(20):8547-8554.
121. Roberts PC, Mottillo EP, Baxa AC, et al. Sequential molecular and cellular events during neoplastic progression: a mouse syngeneic ovarian cancer model. *Neoplasia.* Oct 2005;7(10):944-956.
122. Kurman RJ, Shih Ie M. The origin and pathogenesis of epithelial ovarian cancer: a proposed unifying theory. *Am J Surg Pathol.* Mar 2010;34(3):433-443.

Chapter 3: SPECIFIC AIMS

Ovarian cancer is the leading cause of gynecological cancer deaths and the fifth leading cause of cancer deaths in women. With early diagnosis, there is a 92% rate of survival[1]. However, detection most commonly occurs when the cancer has progressed to stage III or IV. Understanding the etiology of ovarian cancer and identifying early biomarkers of ovarian cancer is critical to increase the survival rates of women afflicted with this disease.

Since Warburg's first communication on the glycolytic nature of cancer cell metabolism, there has been a debate as to whether this hypothesis encompasses all changes pertaining to cancer cell metabolism. It is now clear that mitochondrial dysfunction is not apparent in all cancer cells[2]. The glycolytic shift now is understood as a survival mechanism to produce the macromolecules and reducing equivalents required to meet the cancer cells need of proteins, nucleic acids and lipids to support rapid cell growth. This confers a distinct growth advantage even in normoxic conditions with functional mitochondria[3]. Since these glycolytic cells mostly have a more aggressive and metastatic phenotype[4], it has been suggested that aerobic glycolysis is a hallmark for invasive cancers[5]. Therefore, chemopreventive and chemotherapeutic strategies that modify these metabolic pathways could successfully remove the cancer cells' growth advantage and prevent cancer growth.

For these studies we use a recently developed and characterized a mouse ovarian surface epithelial (MOSE) cell model of progressive ovarian cancer[6, 7] to identify and delineate events involved in ovarian cancer progression. Serial passaging of primary MOSE cells induced spontaneous immortalization and transformation and allowed for the capturing of genetically and phenotypically distinct early, intermediate and late stages of ovarian cancer, representing the

stages from a benign to a highly aggressive and invasive disease. This model is unique in its ability to compare syngeneic stages of cancer progression, a model that does not exist for the human disease. As cells progress, they increase their growth rate, acquire the ability to grow as spheroids, invade collagen and form tumors *in vivo*[6]. The progression of MOSE cells is accompanied by changes in their gene expression levels and a successive dysregulation of their cellular architecture[7].

In addition to the progression component of this model, late-stage MOSE cells injected intraperitoneally into C57BL/6 mice and harvested from the ascites were enriched for a population containing cancer stem cells or tumor-initiating cells (TICs). Characterization of this cell type indicates that these cells are self-renewing, express the surface marker CD44 at high levels, form spheroids in serum-free medium, and can form tumors *in vivo* with as little as 100 cells (Roberts et al., in preparation). This comprehensive model is ideal to determine metabolic alterations in the progression of ovarian cancer and how these metabolic changes are dissimilar in the TICs.

THE SPECIFIC AIMS OF THIS DISSERTATION PROJECT ARE:

SPECIFIC AIM 1: To determine changes in cellular metabolism as ovarian surface epithelial cells progress from a benign early-stage (MOSE-E) to an aggressive late-stage ovarian cancer (MOSE-L).

Hypothesis: Metabolic changes that convey the "Warburg Effect" are present as the MOSE cells progress from MOSE-E to MOSE-L to meet the growing needs of the cell;

treatment with non-toxic concentrations of sphingosine will reverse metabolic changes seen in the MOSE-L cells.

Objective 1: Determination of metabolic changes that are taking place during MOSE progression, and identification of the stage at which these metabolic changes are occurring.

Objective 2: Determination of how non-toxic concentrations of sphingosine can reverse the metabolic changes seen with cancer progression.

SPECIFIC AIM 2: Determine changes in the metabolism of ovarian tumor-initiating cells (TICs).

Hypothesis: The TICs have a more flexible metabolism interchanging between oxidative phosphorylation and glycolysis while utilizing different fuels for energy depending on their microenvironment, to support their higher tumorigenicity and metastatic potential over the MOSE-L cells.

Objective 1: Determine how the TIC's metabolism differs from the MOSE-E and MOSE-L cells, including response to treatment with an AMPK agonist.

Objective 2: Determine the metabolism of the TICs *in vivo* in varying microenvironment conditions using TICs harvested from ascites or solid tumors found in C57BL/6 mice.

References

1. *Facts and Figures 2008.* Atlanta: American Cancer Society;2008.
2. Zu XL, Guppy M. Cancer metabolism: facts, fantasy, and fiction. *Biochem Biophys Res Commun.* Jan 16 2004;313(3):459-465.
3. Yuneva M, Zamboni N, Oefner P, Sachidanandam R, Lazebnik Y. Deficiency in glutamine but not glucose induces MYC-dependent apoptosis in human cells. *J Cell Biol.* Jul 2 2007;178(1):93-105.
4. Postovit LM, Adams MA, Lash GE, Heaton JP, Graham CH. Oxygen-mediated regulation of tumor cell invasiveness. Involvement of a nitric oxide signaling pathway. *J Biol Chem.* Sep 20 2002;277(38):35730-35737.
5. Gatenby RA, Gillies RJ. Why do cancers have high aerobic glycolysis? *Nat Rev Cancer.* Nov 2004;4(11):891-899.
6. Roberts PC, Mottillo EP, Baxa AC, et al. Sequential molecular and cellular events during neoplastic progression: a mouse syngeneic ovarian cancer model. *Neoplasia.* Oct 2005;7(10):944-956.
7. Creekmore AL, Silkworth WT, Cimini D, Jensen RV, Roberts PC, Schmelz EM. Changes in gene expression and cellular architecture in an ovarian cancer progression model. *PLoS One.* 2011;6(3):e17676.

Chapter 4: RESEARCH DESIGN

SPECIFIC AIM 1: To determine changes in cellular metabolism as ovarian surface epithelial cells progress from a benign early-stage (MOSE-E) to an aggressive late-stage ovarian cancer (MOSE-L).

Hypothesis: Metabolic changes that convey the "Warburg Effect" are present as the MOSE cells progress from MOSE-E to MOSE-L to meet the growing needs of the cell; and treatment with non-toxic concentrations of sphingosine will reverse metabolic changes seen in the MOSE-L cells.

Objective 1: Determination of metabolic changes that are taking place during MOSE progression, and identification of the stage at which these metabolic changes are occurring.

Objective 2: Determination of how non-toxic concentrations of sphingosine can reverse the metabolic changes seen with cancer progression.

Research Model:

Cell Culture: Mouse ovarian surface epithelial (MOSE) cells at different stages of tumorgenic potential (early, intermediate, late) will be used to determine metabolic changes during ovarian cancer progression. The MOSE cell model was established[1] and is used in the Schmelz and Roberts labs at Virginia Tech. Its uniqueness as a progression model will allow for determining when in the progression of ovarian cancer metabolic changes are taking place and whether these metabolic changes model the Warburg theory. It also allows for screening of chemotherapeutic agents like sphingosine, to determine their differential effectiveness.

Experimental Strategy: MOSE-E, MOSE-I and MOSE-L cells will be cultured along with their 1.5μM sphingosine-treated counterparts for three passages in high glucose DMEM supplemented with 4% fetal bovine serum (FBS), mimicking a continuous dietary treatment. The 1.5μM sphingosine-treatment is non-toxic to the cells with little to no cell death (Brayfield et al., in preparation). Measurements of substrate metabolism, macromolecule synthesis, metabolic enzyme activity, mitochondrial function, mRNA levels and protein levels of key metabolic enzymes will be assessed (Table 1).

Table 1: Metabolic Endpoint Measurements for Specific Aim 1 Cell Culture Studies

• Glucose and Fatty Acid oxidation
• Glucose uptake
• Fatty Acid synthesis
• Pyruvate Dehydrogenase activity and Pyruvate oxidation
• Enzyme activities of Citrate Synthase and β-HAD
• Lactate excretion
• Mitochondrial Respiration and Glycolysis Rate
• Gene expression of key Glucose and Fatty Acid metabolic genes
• Protein levels of FASN, PDK1 and p-AKT

Note:

- β-HAD is β-hydroxyacyl-CoA Dehydrogenase, the third enzyme in the beta oxidation of fatty acids
- FASN is the catalytic enzyme, fatty acid synthase, which produces saturated fatty acids from malonyl CoA and acetyl CoA

- p-AKT is the phosphorylated serine/threonine-specific protein kinase, which when active through phosphorylation, activates intracellular signaling cascades and is known to be active in ovarian cancer[2]
- A full list of quantitative real-time RT-PCR (qPCR) results for the key glucose and fatty acid metabolic genes can be found in Appendix A

SPECIFIC AIM 2: Determine changes in the metabolism of ovarian tumor-initiating cells (TICs).

Hypothesis: The TICs have a more flexible metabolism interchanging between oxidative phosphorylation and glycolysis while utilizing different fuels for energy depending on their microenvironment, to support their higher tumor growth rate and metastatic potential over the MOSE-L cells.

Objective 1: Determine how the TIC's metabolism differs from the MOSE-E and MOSE-L cells, including response to treatment with an AMPK agonist.

Research Model:

Cell Culture: The highly tumorigenic and metastatic ovarian cancer cell line, the TICs (Tumor-initiating Cells), are a derivative of MOSE-L cells injected into a C57BL/6 mouse and harvested from the ascites and maintained in tissue culture. The TICs have increased tumorigenicity *in vitro* and *in vivo* (Roberts et al., in preparation). *In vitro* the TICs are more invasive in collagen and matrigel than the MOSE-L. This highly invasive phenotype is enhanced in serum-free medium where the TICs express a higher percentage of stem cell markers compared to the MOSE- L cells. Additionally, the TICs are more efficient at forming colonies, where in serum-free medium they can recapitulate a tumor colony from one cell. *In vivo*, they have higher

proliferation rates that exacerbate peritoneal disease by producing the same disease state as the MOSE-L cells, with 1000-fold less cells. Due to the highly aggressive phenotype of the TICs and the evidence that cancer stem cells are chemo-resistant, using the TICs as a model to determine metabolic targets to augment current therapy is vital for increasing survival rates of women with ovarian cancer.

Experimental Strategy for Objective 1: MOSE-E, MOSE-L and TICs will be cultured in high glucose DMEM with 4% FBS. In addition, TICs will be cultured with puromycin to retain only the cells that express the firefly plasmid. In addition to the measurements of cell metabolism as outlined under Specific Aim 1, outcome measurements will include substrate metabolism, response to the cancer inhibiting drug AICAR, survivability in varying substrate mediums and gene expression (Table 2).

Table 2: Metabolic Endpoint Measurements for Specific Aim 2 Cell Culture Studies

• Glucose and Fatty Acid oxidation
• *de novo* fatty acid synthesis
• Lactate levels
• Mitochondrial Respiration and Glycolysis rate
• Gene expression of Glucose and Fatty Acid transporters, as well as other Glucose and Fatty Acid metabolic genes
• alamarBlue determining ability to survive with varying substrate availability
• MTT assay determining cytotoxicity of AICAR

Note:

- A full list of qPCR results for the Glucose and Fatty acid transporters as well as other key glucose and fatty acid metabolic genes can be found in Appendix B

Objective 2: Determine the metabolism of the TICs *in vivo* in varying microenvironment conditions using TICs harvested from ascites or solid tumors found in C57BL/6 mice.

Research Model:

Cell Culture: The highly tumorigenic and metastatic ovarian cancer cell line TIC is passaged through a C57BL/6 mouse and re-harvested from ascites and solid tumor. These cells will be grown out for three passages using puromycin to assure a pure population of TICs.

Experimental Strategy for Objective 2: Outcome measurements will include mitochondrial function through mitochondrial respiration and glycolysis rate.

References

1. Facts and Figures 2008. Atlanta: American Cancer Society;2008.
2. Zu XL, Guppy M. Cancer metabolism: facts, fantasy, and fiction. Biochem Biophys Res Commun. Jan 16 2004;313(3):459-465.
3. Yuneva M, Zamboni N, Oefner P, Sachidanandam R, Lazebnik Y. Deficiency in glutamine but not glucose induces MYC-dependent apoptosis in human cells. J Cell Biol. Jul 2 2007;178(1):93-105.

4. Postovit LM, Adams MA, Lash GE, Heaton JP, Graham CH. Oxygen-mediated regulation of tumor cell invasiveness. Involvement of a nitric oxide signaling pathway. J Biol Chem. Sep 20 2002;277(38):35730-35737.
5. Gatenby RA, Gillies RJ. Why do cancers have high aerobic glycolysis? Nat Rev Cancer. Nov 2004;4(11):891-899.
6. Roberts PC, Mottillo EP, Baxa AC, et al. Sequential molecular and cellular events during neoplastic progression: a mouse syngeneic ovarian cancer model. Neoplasia. Oct 2005;7(10):944-956.
7. Creekmore AL, Silkworth WT, Cimini D, Jensen RV, Roberts PC, Schmelz EM. Changes in gene expression and cellular architecture in an ovarian cancer progression model. PLoS One. 2011;6(3):e17676.
8. Fresno Vara JA, Casado E, de Castro J, Cejas P, Belda-Iniesta C, Gonzalez-Baron M. PI3K/Akt signalling pathway and cancer. Cancer Treat Rev. Apr 2004;30(2):193-204.

Chapter 5: METABOLIC CHANGES DURING OVARIAN CANCER PROGRESSION AS TARGETS FOR SPHINGOSINE TREATMENT

Angela S. Anderson[a], Paul C. Roberts[b], Madlyn I. Frisard[a], Ryan P. McMillan[a], Timothy J. Brown[a], Michael H. Lawless[a], Matthew W. Hulver[a*] and Eva M. Schmelz[a*]

[a] Department of Human Nutrition, Foods and Exercise, Virginia Tech, Blacksburg, VA

[b] Biomedical Science and Pathobiology, Virginia Tech, Blacksburg, VA

*to whom correspondence should be addressed:

Dr. Eva M. Schmelz (eschmelz@vt.edu)

Virginia Tech, 1981 Kraft Drive [0913], ILSB 1011, Blacksburg, VA24060

Tel: 001-540-231-3649

FAX: 001-540-231-5522

and

Dr. Matthew W. Hulver (hulvermw@vt.edu)

Virginia Tech, 1981 Kraft Drive [0913], Blacksburg, VA24060

Accepted for publication in Experimental Cell Research DOI: 10.1016/j.yexcr.2013.02.017

Abstract

Tumor cells often exhibit an altered metabolic phenotype. However, it is unclear as to when this switch takes place in ovarian cancer, and the potential for these changes to serve as therapeutic targets in clinical prevention and intervention trials. We used our recently developed and characterized mouse ovarian surface epithelial (MOSE) cancer progression model to study metabolic changes in distinct disease stages. As ovarian cancer progresses, complete oxidation of glucose and fatty acids were significantly decreased, concurrent with increases in lactate excretion and ^{3}H-deoxyglucose uptake by the late-stage cancer cells, shifting the cells towards a more glycolytic phenotype. These changes were accompanied by decreases in TCA flux but an increase in citrate synthase activity, providing substrates for *de novo* fatty acid and cholesterol synthesis. Also, uncoupled maximal respiration rates in mitochondria decreased as cancer progressed. Treatment of the MOSE cells with 1.5μM sphingosine, a bioactive sphingolipid metabolite, decreased citrate synthase activity, increased TCA flux, decreased cholesterol synthesis and glycolysis. Together, our data confirm metabolic changes during ovarian cancer progression, indicate a stage specificity of these changes, and suggest that multiple events in cellular metabolism are targeted by exogenous sphingosine which may be critical for future prevention trials.

Keywords: metabolism, cancer progression, sphingosine, substrate flux, citrate synthase, cholesterol

Introduction

Ovarian cancer is the leading cause of gynecological cancer deaths and the fifth leading cause of cancer deaths in women. While the origins of ovarian cancer are still debated, most ovarian cancers are thought to originate in the layer of epithelial cells surrounding the ovary or the fimbriae of the fallopian tubes. While early diagnosis leads to a 92% rate of survival[3], the cancer is most commonly diagnosed when has progressed to stage III or IV, drastically reducing the chance of survival. Understanding the etiology of ovarian cancer and identifying early events in ovarian cancer for diagnostic and prevention purposes is critical to increase the survival rates of women afflicted with this disease.[1]

The observation that cancer cells have an altered metabolic phenotype, allowing them to adapt to and survive dynamic microenvironmental conditions, was first made by Otto Warburg and has been subsequently been labeled the "Warburg Effect"[4, 5]. Warburg observed a higher uptake of glucose and elevated lactate production and secretion, and concluded that cancer cells primarily use aerobic glycolysis rather than oxidative phosphorylation as the primary source for ATP synthesis, due to impaired mitochondria. Although this glycolytic shift takes place under normoxic conditions, anaerobic metabolism is also critical for tumor development where the hypoxic core of growing tumors limits access to oxygen. To avoid acid-induced apoptosis, monocarboxylate transporters must export excess lactic acid[6, 7]. The resulting acidic microenvironment generated by the secreted lactate, carbon dioxide production, bicarbonate depletion and other mechanisms has been shown to promote progression and metastasis[8, 9].

[1] Abbreviations: So, sphingosine; TCA, tricarboxylic acid cycle; FASN, fatty acid synthase; ß-HAD, ß-hydroxyl-CoA dehydrogenase; PDH, pyruvate dehydrogenase; OCR, oxygen consumption rate; ECAR, extracellular acidification rate;

Since Warburg's first communication of the glycolytic nature of cancer cell metabolism, there has been a debate as to whether this hypothesis encompasses all changes pertaining to cancer cell metabolism. It is now clear that mitochondrial dysfunction is not apparent in all cancer cells[10], and that the aberrant metabolic phenotype is the consequence of mutations or epigenetic silencing modulating the expression of metabolic enzymes or their regulators such as *p53*, *MYC*, *AMP-activated kinase (AMPK)* or *Hypoxia-inducible factor 1 alpha (HIF1α)*[11] rather than their cause. The glycolytic shift now is understood as a survival mechanism to produce the macromolecules and reducing equivalents required to meet the cancer cell's need of proteins, nucleic acids and lipids to support rapid cell growth. This confers a distinct growth advantage even in normoxic conditions with functional mitochondria[12]. Since these glycolytic cells mostly have a more aggressive and metastatic phenotype[13], it has been suggested that aerobic glycolysis is a hallmark for invasive cancers[14]. Therefore, chemopreventive and chemotherapeutic strategies that modify these metabolic pathways could successfully remove the cancer cells' growth advantage and prevent cancer growth.

Sphingolipids are a class of structurally diverse bioactive lipids involved in a variety of cellular processes including the regulation of growth, apoptosis, autophagy, motility and many more in a metabolite-specific manner[15, 16]. Sphingolipid metabolites are also involved in cellular metabolism, inhibiting (sphingosine, So) or activating (sphingosine-1-posphate, S1P) glucose uptake, inhibiting (So) or activating (S1P) insulin signaling pathways and mediating AKT (protein kinase B) inhibition (So) or activation (S1P). The endogenous sphingolipid metabolites S1P and ceramide have been implicated in reduced pancreatic ß-cell function, insulin resistance, atherosclerotic plaque formation, and other factors associated with obesity and metabolic syndrome (see recent comprehensive review[17]). In contrast, our previous studies have shown

that the administration of complex sphingolipids via the diet suppressed carcinogen-induced[18-21], mutant *Adenomatous Polyposis Coli*-mediated[22, 23] or inflammation-driven colon cancer[24], and suppressed breast xenograft progression[25] in mice without any apparent side effects. The sphingolipid bases that are generated from the dietary complex sphingolipids are likely the effective metabolites in the observed suppression of tumor growth and progression[22, 26]. The effects of exogenous sphingolipid metabolites on the altered metabolism in ovarian cancer cells and their impact on tumor growth and progression are not known.

We have recently developed and characterized a mouse ovarian surface epithelial (MOSE) cell model of progressive ovarian cancer[1, 27] to identify and delineate events involved in ovarian cancer progression. Serial passaging of primary MOSE cells induced spontaneous immortalization and transformation and allowed for the capturing of genetically and phenotypically distinct early (benign), intermediate and late (highly aggressive and invasive) stages of ovarian cancer. This model is unique in its ability to compare syngeneic stages of cancer progression, a model that does not exist for the human disease. As cells progress, they increase their growth rate, acquire the ability to grow as spheroids, invade collagen and form tumors *in vivo*[1]. The progression of MOSE cells is accompanied by changes in their gene expression levels and a successive dysregulation of their cellular architecture also reported in the human disease[27]. In the present studies, this ovarian cancer model was used to determine when during cancer progression metabolic changes are taking place and identify potential targets for exogenous So in the prevention of ovarian cancer. We investigated shifts in cellular metabolism and substrate utilization during ovarian cancer cells progression, determined changes in mitochondrial function, and investigated how exogenous So affects the observed changes.

Together, our results suggest that alterations in the metabolic phenotype of the progressive MOSE cells are targets for a cancer prevention regimen with exogenous So.

Methods and Materials

Cell Culture. MOSE cells were cultured in DMEM (Sigma) supplemented with 4% FBS (Atlanta Biologicals) and 100ug/ml each of penicillin and streptomycin (Gibco). Classification into early-benign (MOSE-E), intermediate (MOSE-I), and late–aggressive (MOSE-L) phenotypes was established as previously described[1]. So-treated cells were cultured in medium containing 1.5 μmol/L So (Avanti Lipids) as BSA complex (60 μM fatty acid-free fraction V, Calbiochem) for at least 3 passages to mimic long-term exposure to diet-derived sphingolipid metabolites. This treatment regimen has been shown to be necessary to induce significant changes in gene and protein expression level and cytoskeleton organization (data not shown). This concentration was not toxic for any cell line. Cells were cultured at 37°C in a humidified incubator with 5% CO_2.

Real-time PCR (qPCR). Cells were seeded in 100mm culture dishes and harvested 24 hours later. Total RNA was extracted using the RNeasy Mini Kit (Qiagen). cDNA synthesis was performed on 500ng of RNA using the ImProm-II Reverse Transcription System (Promega). qPCR was performed using 50ng of cDNA with SensiMix Plus SYBR Mastermix (Quantace) in the ABI 7900HT (Applied Biosystems) with the following parameters: 42 cycles at 95°C for 10 minutes, 95°C for 15 seconds, 58°C for 30 seconds and 72°C for 15 seconds, followed by a dissociation curve segment. Data was quantified using the ΔΔCT method and expressed relative

to RPL19 as the housekeeping gene[27]. Primer pairs were designed with the Beacon Design software and were as followed: pyruvate dehydrogenase (PDHb) Fwd: CAT TCG GCA GCT AGT AGA G; PDHb Rev: CTT CAC GAA CTG TCA ACT G; pyruvate dehydrogenase kinase 1 (PDK1) Fwd: CTG GGC GAG GAG GAT CTG ACT G; PDK1 Rev: ACA GCA CGG GAC GTT TCA ACA C; ribosomal protein L19 (RPL19) Fwd: GCA AGC CTG TGA CTG TCC ATT CC; RPL19 Rev: GCA TTG GCA GTA CCC TTC CTC TTC. Data expressed are the mean of two independent experiments performed in duplicate with three biological replicates. Data are presented as Mean ± SEM.

Western Blotting. Cells were treated as indicated, harvested by scraping into Ripa lysis buffer[27], supplemented with Complete Mini Protease Inhibitor Cocktail (Roche), homogenized with a 22-gauge needle, and centrifuged at 15,000*g* for 15 min. Equal amounts of proteins were separated using 8g/100g or 12g/100g gels, transferred to PVDF membrane (Bio-Rad), and blocked with blocking buffer (Rockland). Blots were probed with primary antibodies against FASN, p-AKT, pyruvate dehydrogenase kinase 1 (PDK1) (Cell Signaling) or α-Tubulin (Abcam), followed by incubation with the appropriate secondary antibodies. Proteins were visualized and quantitated using the Odyssey Infrared Imaging System (Licor). Data presented are the mean infrared units ± SEM from at least two independent experiments performed on six biological replicates (FASN and PDK1), normalized to α–tubulin.

Glucose and Fatty Acid Oxidation. MOSE cells were seeded at 2.5 x 10^5 cells/ well in 6-well cell culture plates, incubated for 3 h, and washed with PBS. Following 2 h of incubation in serum-free medium, glucose and fatty acid oxidation were assessed via co-incubation with U-^{14}C

glucose and ^{3}H-palmitic acid. Glucose oxidation was measured via $^{14}CO_2$ production as previously described[28]. Incorporation of $^{14}CO_2$ derived from U-^{14}C glucose into NaOH was measured using a LS 6500 scintillation counter (Beckman Coulter). Concomitantly, fatty acid oxidation was assessed by measuring $^{3}H_2O$ from ^{3}H-palmitate (Perkin Elmer) as previously described[29]. Data presented as the mean from two independent experiments performed in replicates of six, corrected for protein content. Data are presented as mean ± SEM.

Lactate Assay. MOSE cells were seeded at a density of 2.5 x 10^5 cells/well in 6-well cell culture plates. After 3 h, cells were washed with PBS and incubated in phenol red-free, serum-free DMEM (Gibco). The medium was collected after 8 h and assayed for lactate concentration using a colorimetric kit according to the manufacturer's instructions (BRSC, University of Buffalo). Data presented are the mean from three independent experiments performed in replicates of six biological replicates, corrected for cell number. Data are presented as mean ± SEM.

Glucose Uptake. MOSE cells were seeded at 2.5 x 10^5 cells/well in 6-well cell culture plates. After 3 h, cells were washed with PBS and incubated in serum-free medium for 2 h. Glucose uptake was assessed by measuring ^{3}H-2-Deoxy-glucose as previously described[30]. Data presented are the mean from two independent experiments performed in replicates of six biological replicates, normalized to protein content. Data are presented as mean ± SEM.

Enzyme Activity Assays. MOSE cells were seeded at a density of 5 x 10^5 cells/well in 6-well cell culture plates. After 3 h, cells were washed with PBS and scraped in 200µl of PK buffer

(0.1M di-potassium phosphate). Citrate synthase, and ß-HAD activities were determined spectrophotometrically as previously described[31]. Data presented are the mean from two independent experiments performed in replicates of six biological replicates, corrected for protein content. Data are presented as mean ± SEM.

2-Carbon Labeled Pyruvate Metabolism for Pyruvate Dehydrogenase (PDH) Activity and TCA flux determination. The ^{14}C-label on the number 1 carbon of pyruvate will result in ^{14}C-labeled CO_2 produced through the PDH reaction, where [1-^{14}C]-pyruvate indicates PDH activity. The ^{14}C-label on the number 2 carbon of pyruvate will result in ^{14}C-labeled acetyl-CoA production as a result of pyruvate oxidation by PDH. As such, any production of $^{14}CO_2$ using [2-^{14}C]-pyruvate as a substrate is a result of oxidation of acetyl-CoA in the TCA cycle. MOSE cells were seeded at a density of 5 x 10^5 cells/well in 6-well cell culture plates. After 3 h, cells were washed with PBS and serum-free medium was added for two hours. Oxidation was assessed by measuring $^{14}CO_2$ production as described above, substituting labeled pyruvate for U-^{14}C glucose. Data presented are the mean from two independent experiments performed in replicates of six, corrected for protein content. Data are presented as mean ± SEM.

De Novo Fatty Acid Synthesis. MOSE cells were seeded at a density of 5 x 10^5 cells/well in 6-well cell culture plates. After 3 h, cells were washed with PBS and serum-free medium was added for two hours. *De Novo* fatty acid synthesis was assessed by measuring the quantity of ^{14}C-2-pyruvate (Perkin Elmer) partitioned into fatty acids as previously described[31, 32]. Data presented are the mean from replicates of six, corrected for protein content. Data are presented as mean ± SEM.

Cholesterol Biosynthesis. MOSE cells were grown for 48 h, harvested in 1ml ice-cold PBS, and lipids were extracted with methanol:chloroform (2:1) and centrifuged at 4000 rpm for 5 min. To the supernatant, 1ml of citric acid, 2ml of water and 1ml chloroform were added. After centrifugation, the chloroform layer was transferred to a glass tube and evaporated with nitrogen gas. The cholesterol assay was performed according to manufacturer's instructions using the Amplex Red Cholesterol Assay Kit (Invitrogen). Data expressed are the mean of four independent experiments performed in duplicate, corrected for cell number and presented as mean ± SEM. An increase in fold change was calculated as treated cells/ control cells. For a fold decrease, the negative inverse of the fold change was calculated; statistical significance was calculated from the original data.

Mitochondrial Respiration. Mitochondrial respiration of MOSE cells was determined using an XF24 extracellular flux analyzer (Seahorse Bioscience) as described by Gerencser et al. with some modifications[33]. Cells were seeded into XF24 V7 cell culture microplates at a density of 35,000 cells per well for MOSE-I and MOSE-L and 50,000 cells per well for MOSE-E and incubated for 48 h in replicates of five. Then the medium was changed and the experiments were conducted in serum-free, bicarbonate-free medium after 1 h incubation. Cells were loaded into the XF24 and experiments consisted of 3-minute mixing, 2-minute wait, and 3-minute measurement cycle. Oxygen consumption was measured under basal conditions in the presence of the mitochondrial inhibitors 0.5μmol/L oligomycin (Calbiochem) or 0.25μmol/L rotenone (Sigma), or in the presence of the mitochondrial uncoupler, 0.3μmol/L carbonylcyanide-p-trifluoromethoxyphenylhydrazone FCCP (Sigma) to assess maximal oxidative capacity. All

experiments were performed at 37°C. Oxygen consumption rate (OCR), ATP synthesis rate and extracellular acidification rate (ECAR) were calculated by the oligomycin or FCCP-induced change compared with the basal rates. Data presented are the mean from three independent experiments performed in replicates of five and corrected for protein. Data are presented as Mean ± SEM.

Statistics. Data are presented as mean ± SEM. When comparing more than one cell type, results were analyzed with a one-way ANOVA followed by Tukey's post ad hoc test. When comparing treated versus non-treated cells of the same cancer stage, data were analyzed using a student's two-tailed *t-test*. Results were considered significant at $p<0.05$.

Results

The MOSE ovarian cancer progression model presents a unique opportunity to study cellular and molecular changes as cancer progresses. Our previous studies have shown that among other functional categories, genes involved in cellular metabolism are changing during the progression of the MOSE cells[27]. These included genes involved in mitochondrial morphology and energy production, and glucose and fatty acid metabolism. Thus, we assessed whether the MOSE cells develop a glycolytic phenotype indicative of an aggressive cancer phenotype by assaying quantitative changes in the cellular metabolism during ovarian cancer progression.

Glucose and fatty acid oxidation in MOSE cells. As shown in Figure 1A-B, glucose oxidation is higher than fatty acid oxidation in all cell types, demonstrating a choice of all MOSE

cells for glucose over fatty acids as the preferred substrate. As cells progress, there was a significant decrease in glucose oxidation in both the MOSE-I ($p<0.01$) and MOSE-L cells ($p<0.001$), indicating a successive loss of glucose oxidation through the TCA cycle (Figure 1A). A significant decrease in fatty acid oxidation was detected in the MOSE-L cells ($p<0.001$); however, the level of fatty oxidation was already modest in the MOSE-E (Figure 1B). In comparison, glucose oxidation in MOSE-E cells is higher (~12nmol/mg-protein/h) and fatty acid oxidation is lower than average C2C12 skeletal muscle metabolism (~14nmol/mg-protein/h)[30], confirming the MOSE cells utilization of glucose as energy source.

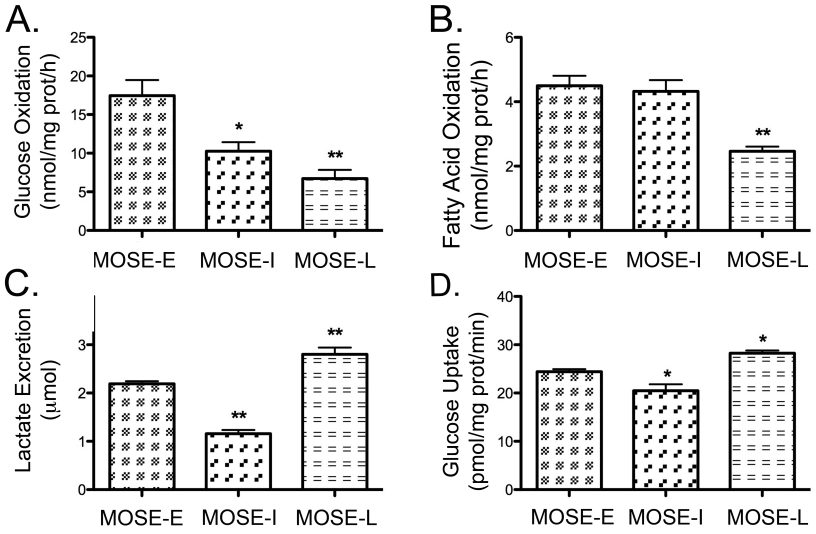

Figure 1. MOSE cancer cell progression results in a glycolytic phenotype. Cells were incubated in serum-free medium for 2h, the appropriate substrates added and changes in (A) glucose oxidation at 3 h, (B) fatty acid oxidation at 3 h, (C) lactate secretion at 8 h and (D) glucose uptake at 10 min in early (MOSE-E) intermediate (MOSE-I) and late (MOSE-L) stages of ovarian cancer were measured as described under methods. Data are presented as mean ± SEM. Different from MOSE-E, *$p\leq0.01$, **$p\leq0.001$.

Lactate secretion and glucose uptake. Warburg observed that cancer cells preferably convert glucose to lactate even under normoxic conditions[4, 5]. To further investigate this glycolytic shift during progression of the MOSE cells, we assayed cellular glucose uptake and

lactate secretion. As expected, glucose uptake was moderately, but significantly elevated in the MOSE-L cells compared to the MOSE-E ($p<0.05$) and the MOSE-I ($p<0.001$) (Figure 1C). In addition to an increase in glucose uptake, lactate secretion was elevated compared to MOSE-E ($p<0.001$) and MOSE-I cells ($p<0.001$) (Figure 1D). Interestingly, MOSE-I cells representing an intermediate pheno- and genotype showed a significant decrease in both lactate secretion ($p<0.001$) and glucose uptake compared to MOSE-E ($p<0.05$) and MOSE-L cells ($p<0.001$), suggesting that transitional stages during cancer progression may have differing energy requirements and substrate utilization.

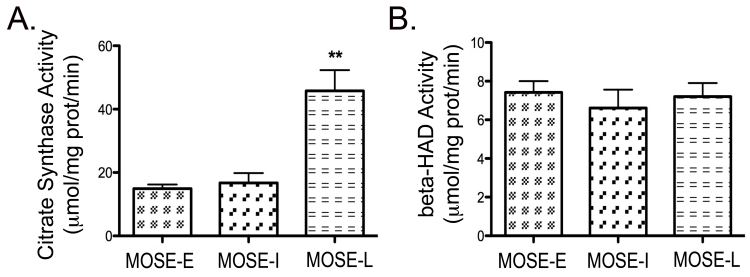

Figure 2. Changes in enzymatic activity during MOSE progression. (A) Citrate synthase and (B) β-hydroxyacyl-CoA dehydrogenase (ßHAD) activity in MOSE cells measured at baseline and for 6 min after substrate administration. Data are presented as mean ± SEM. **different from MOSE-E, $p \leq 0.001$.

Changes in citrate synthase activity and TCA flux. Given the increasingly glycolytic phenotype and the decrease of carbon flux away from oxidative phosphorylation of the MOSE cells, we next sought to further define the metabolic changes during MOSE cell progression. By measuring enzymatic changes in the TCA cycle, we determined changes in carbon flux through the TCA. We measured citrate synthase activity (Figure 2A), indicative of TCA activity and β-HAD activity, indicative of beta-oxidation activity. Citrate synthase activity did not change in MOSE-I but showed a significant increase in the MOSE-L cells ($p<0.001$) over MOSE-E (Figure 2A), which was somewhat surprising given the decrease in total oxidation. However, there was

no difference in β-HAD activity (Figure 2B), suggesting that acetyl CoA does not fully complete oxidation in the TCA cycle but may be shuttled out of the mitochondria as citrate, accounting for the decrease in fatty acid oxidation but no change in β-HAD activity. Therefore, we further investigated the activity of the TCA cycle by determining the flux of carbon skeletons from pyruvate through the TCA cycle using carbon-1 and carbon-2 labeled radioisotopes, respectively. Carbon-1 labeled pyruvate is cleaved in the PDH reaction producing radiolabeled CO_2 and acetyl CoA while carbon-2 labeled pyruvate is an indication of a complete carbon flux through the TCA cycle, producing radiolabeled CO_2. As shown in Figure 3A, there were no significant differences in PDH activity but the TCA flux with the carbon-2 labeled pyruvate was significantly decreased in the MOSE-L cells ($p<0.001$) (Figure 3B), confirming the decrease in total oxidation. qPCR data show a decrease in expression of PDHb ($p<0.05$), one of the key enzymes in the PDH complex (Figure 3C). In addition, mRNA and protein levels show an increase in pyruvate dehydrogenase kinase 1 (PDK1) ($p<0.05$ mRNA and $p<0.001$ protein), the kinase that negatively regulates PDH activity (Figure 3D, E, and F).

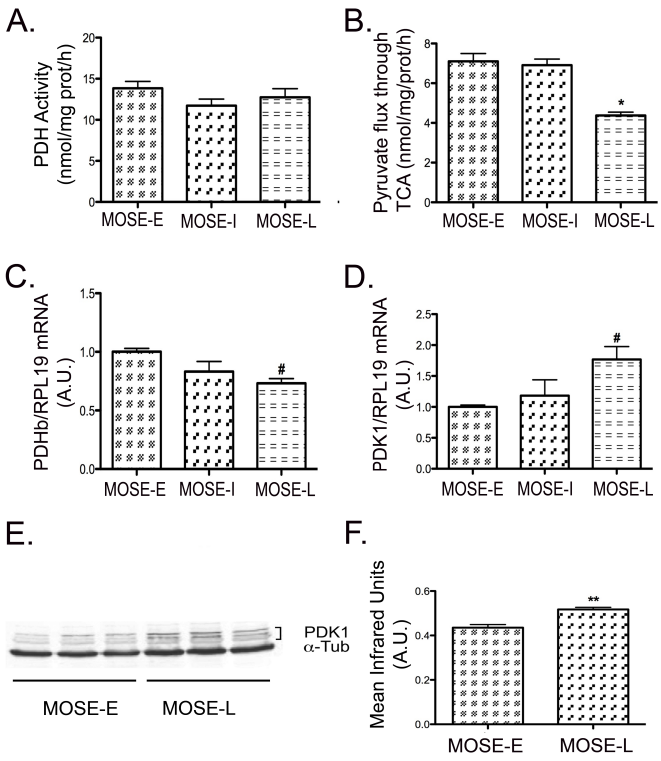

Figure 3. MOSE cell progression leads to a decrease in substrate flux through the TCA. (A) Pyruvate dehydrogenase (PDH) activity after 3 h incubation with the substrate (B) and substrate flux through TCA in MOSE cells representing progressive ovarian cancer at 3 h. (C) qPCR determination of PDHb and (D) qPCR determination of pyruvate dehydrogenase kinase 1 (PDK1), a negative regulator of PDH. (E-F) Protein levels of PDK1. Data are presented as mean ± SEM. Different from MOSE-E, $^{\#}p\leq0.05$, $*p\leq0.01$, $**p\leq0.001$.

de novo fatty acid and cholesterol synthesis. Next, we investigated if citrate leaves the TCA cycle and serves as substrate for fatty acid and cholesterol biosynthesis. Rather than determining the many potential key enzymes in these processes, we determined two key endpoints: de novo synthesis of fatty acids and cholesterol. As shown in Figure 4A, *de novo* fatty acid synthesis is significantly elevated in MOSE-L cells ($p<0.001$). This was associated with a significant increase in FASN protein levels of ($p<0.001$) (Figure 4B, C). In addition, cholesterol levels were also significantly increased in MOSE-L cells ($p<0.001$), (Figure 4D), suggesting that citrate generated by increased citrate synthase activity is utilized for lipid synthesis. Whether other

pathways such as nucleotide synthesis are also fueled by this substrate will be investigated in future studies.

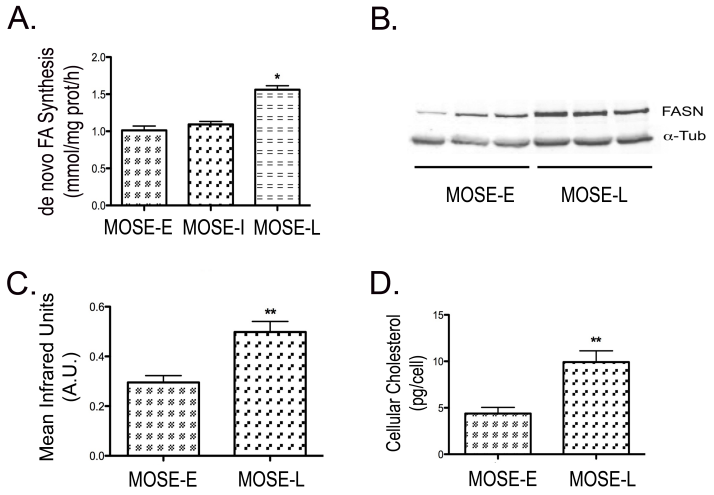

Figure 4. Lipid de novo synthesis is increased during MOSE cell progression. (A) *De novo* fatty acid synthesis at 3 h; (B-C) Western Blot analysis of fatty acid synthase (FASN) protein levels in MOSE cells; (D) Increased cellular cholesterol levels in MOSE-L cells at basal conditions. Data are presented as mean ± SEM. Different from MOSE-E, *p≤0.01, **p≤0.001.

Mitochondrial oxygen consumption rate. To further explore the mechanisms driving this glycolytic shift in the presence of ample oxygen, we assessed changes in mitochondrial capacity during MOSE cell progression. A decrease in mitochondrial capacity could allow for citrate to be shuttled out of the mitochondria, which would correspond to the observed decrease in TCA cycle flux. As cancer progresses towards a more aggressive phenotype, we observed a significant decline in the respiration, expressed as basal OCR from MOSE-E (14.0 ± 1.01 pmoles/min) to MOSE-I (10.44 ± 0.6 pmoles/min; $p<0.05$) to MOSE-L (6.20 ± 1.1 pmoles/min; $p<0.001$ vs MOSE-E; $p<0.01$ vs MOSE-I), indicating a reduction in oxidative metabolism. The increased FCCP-stimulated maximal oxygen consumption over basal OCR also declines as cancer progresses (Figure 5A). MOSE-E cells strongly responded to FCCP stimulation with an increase OCR; this response significantly declined from MOSE-I to MOSE-L ($p<0.001$) (Figure 5B).

MOSE-L cells also showed a significantly reduced ATP synthesis rate as compared to MOSE-E ($p<0.001$) and MOSE-I ($p<0.05$) (Figure 5C), indirectly measured by reduced OCR when ATP synthase was inhibited, indicating a reliance on oxidative metabolism for ATP production.

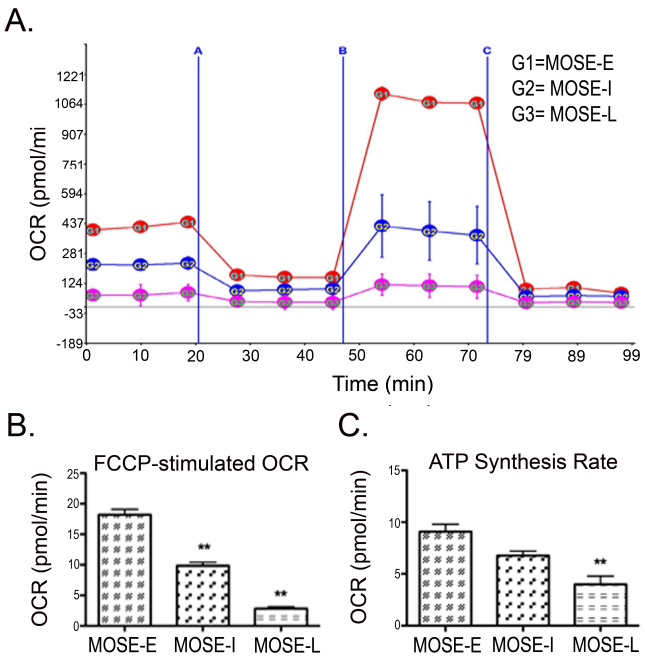

Figure 5. Oxidative Capacity Rate is reduced in a step-wise manner during MOSE cell progression. Oxidative capacity rate (OCR) was measured during an uncoupling challenge. Cellular respiration was modified by oligomycin, an ATP synthase blocker, carbonylcyanide-p-trifluoromethoxyphenyl hydrazone (FCCP), an electron transport chain uncoupler followed by rotenone, a complex one inhibitor of the electron transport chain. (A) Image of representative experiment where A is oligomycin treatment, B is FCCP treatment and C is rotenone treatment, measured over 2 h; (B) Change over base-line in OCR after FCCP treatment; (C) ATP synthesis rate as calculated by the difference between basal OCR and oligomycin blocked OCR. Data are presented as mean ± SEM. Different from MOSE-E, **$p\leq0.001$.

Glycolysis rate. To confirm that the increase in glucose uptake in the MOSE-L cells correspond with an increased rate of glycolysis, we measured the extracellular acidification rate (ECAR), a marker for glycolysis. Cells with an increase in anaerobic glycolysis have an increase in proton production leading to an increase in acidification of the medium or ECAR. As shown in Figure 6C, the basal ECAR significantly increased in MOSE-L cells when compared to

MOSE-E ($p<0.05$), indicating that the more aggressive cells are indeed more glycolytic. This appears to be close to the maximum rate for these cells since the ECAR change after oligomycin treatment increased significantly less than MOSE-E and MOSE-I cells ($p<0.01$) (Figure 6A-B). This suggests that glycolysis in the MOSE-L cells has been activated to a maximum rate that cannot be increased when ATP synthesis from oxidative metabolism is inhibited.

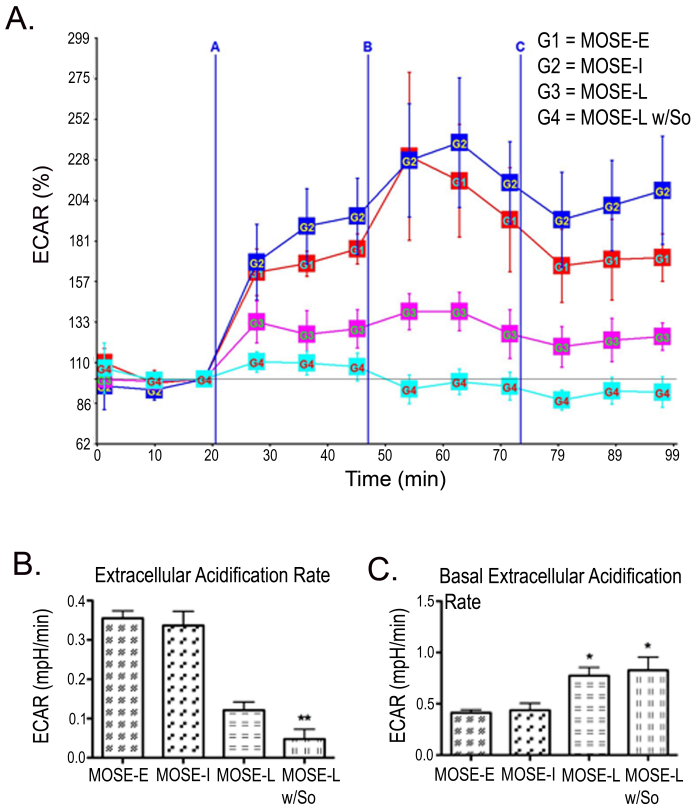

Figure 6. Extracellular Acidification Rate (ECAR) shows an increase in glycolysis during MOSE cell progression. Extracellular acidification rate (ECAR), an indication of the rate of glycolysis was modified by oligomycin, carbonylcyanide-p-trifluoromethoxyphenyl hydrazone (FCCP), and rotenone (see Fig.5). (A) Image of representative experiment where A is oligomycin treatment, B is FCCP treatment and C is rotenone treatment, measured over 2 h; (B) Change in ECAR over baseline after olygomycin treatment, where So treatment for 3 passages decreased glycolysis rate; (C) Basal ECAR levels in MOSE cells, where MOSE-L and MOSE-L w/ So treatment have an increased rate of glycolysis at basal conditions. Data are presented as mean ± SEM. Different from MOSE-E *$p\leq0.01$, **$p\leq0.001$.

Metabolic changes during MOSE progression as targets for chemopreventive efforts with exogenous sphingosine. After establishing the altered cellular metabolism during MOSE cell progression, we next determined if So treatment could reverse the glycolytic phenotype. Our previous studies show that So is generated in the intestinal tract from complex sphingolipids in the diet and resulted in a significant suppression of colon and breast cancer growth and progression in vivo. Importantly, this effect is not a result of induction of apoptosis but a reduction of proliferation[20, 21, 25]. Therefore, for the present studies, exogenous So concentrations were used that reduced cell growth and reduced the tumorigenic potential of the MOSE-L cells (data not shown).

There was no statistically significant decrease of So treatment on glucose uptake (28.2 ± 0.58 pmol/mg prot/min vs 25.0 ± 1.83 pmol/mg prot/min in So-treated MOSE-L) ($p=0.098$) or lactate secretion in the MOSE-L cells (2.80 ± 0.14 μM v. 2.57 ± 0.17 μM in So-treated MOSE-L) ($p=0.307$). However, So decreased ECAR in MOSE-L cells from 0.12 mPH/min in the MOSE-L to 0.05 mPH/min in MOSE-L cells ($p<0.05$), a -2.53-fold reduction compared to untreated cells (Figure 7A) while it did not affect their basal ECAR (Figure 6C). This indicates that So further reduced the capacity of the MOSE-L cells to respond to the increased demand on glycolysis for ATP production.

So significantly decreased citrate synthase activity in MOSE-L cells from 45.8 μmol/mg protein/min in the MOSE-L to 25.2 μmol/mg protein/min ($p<0.001$), a -1.82-fold decrease while there was no significant change in MOSE-E or –I cells (Figure 7B). So treatment did not alter ß-HAD activity but the reduction of citrate synthase activity coincides with a significantly increased TCA flux of pyruvate carbons in all MOSE cells (Figure 7C). This effect was modest in the MOSE-E (from 7.1 nmol/mg protein/h to 9.4 nmol/mg protein/h, $p<0.01$, a 1.33 fold

increase), but more robust in the MOSE-I (from 6.9 nmol/mg protein/h to 10.6 nmol/mg protein/h, $p<0.01$, a 1.53-fold increase) and MOSE-L cells (from 4.4 nmol/mg protein/h to 6.5 nmol/mg protein/h, $p<0.001$, a 1.49-fold increase) compared to their untreated counterparts (see also Figure 3B). We also observed a significant decrease in PDH activity (Figure 7D) in MOSE-L cells treated with So (from 12.75 nmol/mg protein/h to 9.82 nmol/mg protein/hr, a -1.3-fold decrease, $p< 0.05$); there was no difference in MOSE-E or MOSE-I. While we did not detect a reversal of the elevated fatty acid synthesis or the expression of FASN in the MOSE-L cells after treatment with So (not shown), cellular cholesterol levels were significantly reduced in So-treated cells (from 4.4 pg cholesterol/cell to 2.6 pg cholesterol/cell) ($p<0.05$), by -1.70-fold in MOSE-E cells, and by -1.41-fold in MOSE-L cells (from 9.9 pg cholesterol/cell to 7.0 pg cholesterol/cell) ($p=0.055$) (Figure 7E). Finally, to direct our future mechanistic studies we determined the impact of So on activity of AKT that is critically involved in the regulation of metabolism. As shown in Figure 7 (F, G), AKT phosphorylation was significantly decreased after So treatment by -1.62-fold ($p<0.05$).

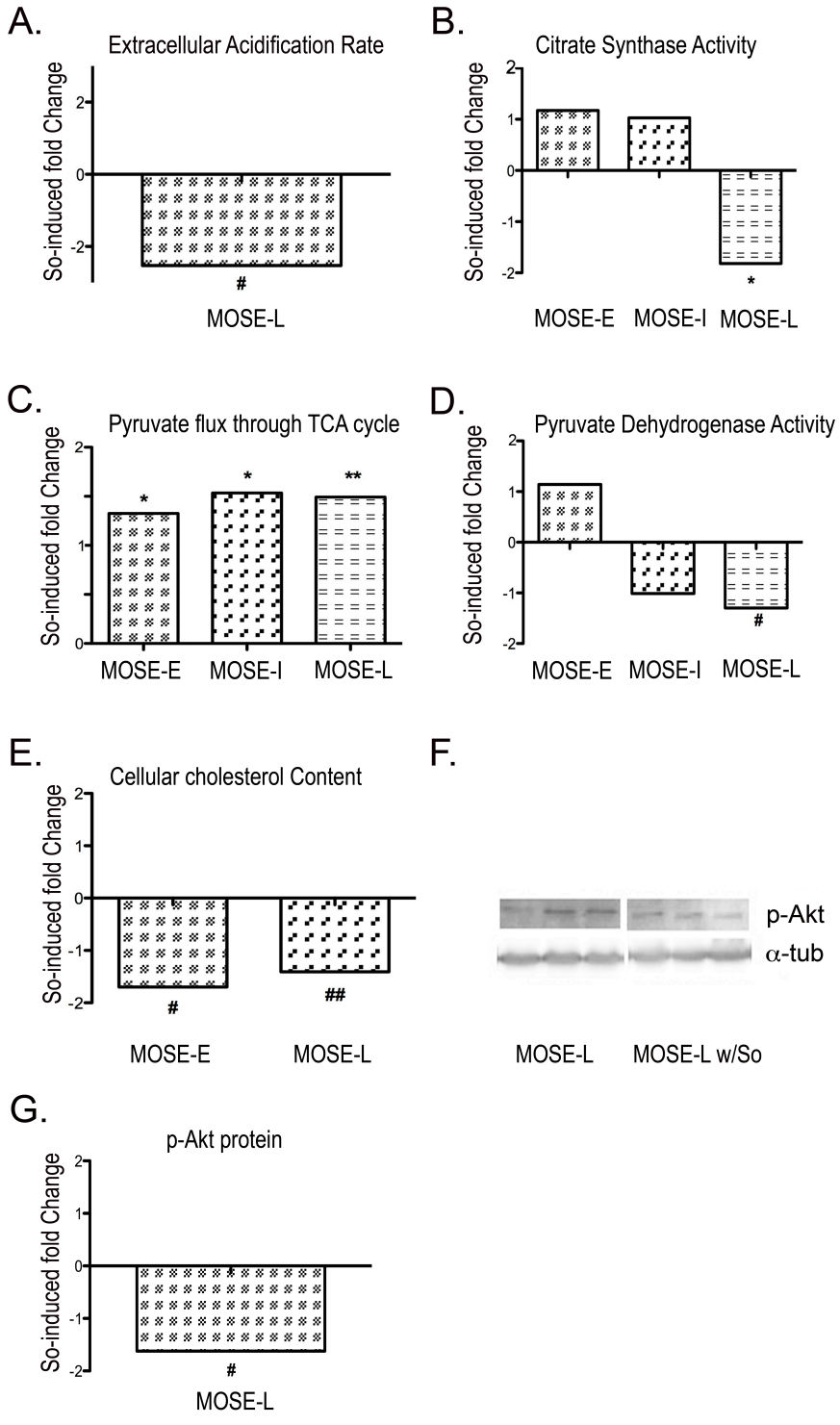

Figure 7. Sphingosine-induced changes restore a more oxidative phenotype. Changes in (A), extracellular acidification rate (ECAR), (B) citrate synthase activity, (C) pyruvate flux through TCA, (D) pyruvate dehydrogenase activity, (E) cholesterol content, (F, G) p-AKT protein content upon sphingosine (So) treatment in three replicates of MOXE-L (first three

bands) MOSE-L cells treated with sphingosine (So) (last three bands). Data are presented as fold-differences from untreated controls. Different from untreated controls $^{\#}p \leq 0.05$, $*p \leq 0.01$, $**p \leq 0.001$, ##p=0.055.

Discussion

The early detection of ovarian cancer significantly increases the survival of women with ovarian cancer. Since an aberrant metabolism has been described in many cancers, our present studies investigated the time course of the metabolic switch and the altered use of intermediate substrates in a mouse cell model for progressive ovarian cancer and identified targets for sphingosine, the bioactive sphingolipid metabolite critically involved in the suppression of colon and breast cancer. Here we demonstrate the increasingly glycolytic nature of MOSE cells as an early event during progression, and significant changes in ECAR, glucose uptake and lactate secretion that occur only in late stages. Furthermore, we show an aberrant TCA cycle flux that results in substrates leaving the TCA cycle, associated with an elevated fatty acid and cholesterol biosynthesis in the more aggressive MOSE-L. Treatment with exogenous So in concentrations that did not induce cell death but decreased the tumorigenic potential of the MOSE-L cells did not alter glucose uptake and lactate secretion at any stage of the disease. However, the rate of glycolysis, citrate synthase activity, and the carbon flux through the TCA cycle were shifted towards levels seen in the benign MOSE-E, which was accompanied by a significant reduction of cholesterol levels. These results demonstrate that So –while not inducing cell death- can partially reverse metabolic changes that occur even during late stages of ovarian cancer.

Although the MOSE cells are cultured in an oxygen abundant environment, they make the same glycolytic shift observed with *in vivo* ovarian cancers, characterized by decrease in glucose and fatty acid oxidation, an increase in glucose uptake and lactate production and secretion,

confirming the events that constitute the Warburg effect. This is in contrast to the hypothesis that the glycolytic shift occurs only as response to hypoxia[10], but confirms that detectable changes of glucose uptake are a late event in carcinogenesis, coinciding with the progression from a pre-malignant to an invasive phenotype as has been described in colon cancer[34] and aligns with the increased demand for macromolecule synthesis, necessary for the fast growing MOSE-L cells[1]. Consequently, increased glucose uptake is not indicative of early stages of ovarian cancer.

The secretion of lactate by tumor cells has been shown to generate a microenvironment permissive for progression of cancers and metastasis[8, 9, 35]. Secreted lactate can be taken up by tumor and other neighboring cells and recycled to pyruvate as an energy source[36] while the lactate-induced low pH favors the expansion of transformed cells; normal cells are more sensitive to the acidic environment. Furthermore, lactate contributes to an immune suppressive microenvironment by modulation of monocyte proliferation, differentiation and activation (see recent review[37]). This identifies lactate production and secretion as a promising target for prevention efforts; lactate secretion is, however, not a target of exogenous So in cells growing under normoxic conditions.

Although there was no difference in PDH activity during the progression of the MOSE cells, it is possible that with the increase in glucose uptake, MOSE-L cells actually have reduced PDH activity, but an increase in flux compared to MOSE-E, leading to no statistical difference. The increase in PDK mRNA and protein support this hypothesis with the concomitant decrease in PDH mRNA and protein. The progression of the MOSE cells was also accompanied by a decrease in carbon flux through the TCA cycle, but an increase in citrate synthase activity. With a decrease in carbon flux, but an increase in citrate synthase activity in the MOSE-L cells, we

hypothesized that not only is pyruvate being converted to lactate and secreted by the cells, but a significant portion is being converted to acetyl CoA and entering the TCA cycle. Instead of completing the TCA cycle, the acetyl CoA is converted to citrate and is shuttled out of the mitochondria as citrate. In the cytoplasm the citrate is converted to acetyl CoA and used as a precursor for *de novo* fatty acid and cholesterol biosynthesis. Both are elevated in MOSE-L cells that proliferate twice as fast as MOSE-E cells[1]; to support their increased growth rate, an increase in phospholipid, fatty acid and cholesterol synthesis would be crucial. Thus, increasing TCA flux by So may reduce the available substrate for cholesterol biosynthesis, impairing membrane assembly, and, potentially, cell growth. If this is independent of modulating the expression or activity of critical enzymes in cholesterol biosynthesis, or affecting fatty acid synthesis in cells grown in fatty acid-depleted medium, this needs to be investigated in more detail. This is especially important since the reduction of cholesterol has been associated with a decrease in cancer incidence in patients using statins[38], potentially via modulating processes involving membranes such as migration[39].

The changes in cellular metabolism and the increasingly glycolytic nature were accompanied by a reduction in oxidative capacity of the mitochondria. FCCP uncouples mitochondrial respiration from ATP synthesis thus requiring the mitochondria to drastically increase oxygen consumption to keep up with the flow of protons back into the matrix. This reflects the capacity of a cell to meet an increased ATP demand. Our data indicate a decrease in FCCP-stimulated respiration in the MOSE-L cells in conjunction with a decreased ATP synthesis rate and a lower basal OCR (Figure 6A), suggesting that during neoplastic progression, MOSE cells have lost the capacity to up-regulate their oxygen consumption upon energy demand. The reduced FCCP-stimulated respiration could result either from dysfunction in the electron transport chain,

decreased number of mitochondria or mitochondria that are already uncoupled and therefore cannot respond to further uncoupling. Similar results have been reported for highly aggressive lung cancer cells, compared to a less aggressive lung cancer cell line and it was concluded that the aggressive cells have a decreased capacity of switching from glycolysis to mitochondrial respiration[40].

Ovarian cancer cells are exfoliated and disseminate throughout the peritoneal cavity rather than the blood or lymphatic systems. Up to 2uM S1P in ascites of ovarian cancer patients have been reported[41, 42] that can support tumor growth and progression. The concentrations of So in ascites are not known. Our *in vivo* studies have shown that the induction of apoptosis is not involved as a mechanism of tumor suppression by orally administered sphingolipids but rather a reduction of proliferation of the tumor cells[20, 22]. Thus, here we use non-toxic concentrations of So over time to identify potential targets of So that reduced cancer cell growth but not their viability (data not shown). So treatment completely inhibited the modest upregulation of glycolysis to meet ATP needs after FCCP treatment of MOSE-L cells. This has also been observed by other anti-cancer treatments and is thought to be associated with a toxic effect on cancer but not non-transformed cells[43]. This may be tissue specific since the suppression of respiration protects against apoptosis in muscle[44]. While So treatment does not induce cell death, one could speculate that this lack of response to energy demand puts the cell into a disadvantage and may be associated with a suppression of tumor growth; this needs to be investigated in more detail.

Figure 8 illustrates possible mechanisms for the So-induced changes observed. So has been shown to decrease phosphorylated AKT (p-AKT), thereby decreasing its activity[45], which was confirmed in our experiments (Figure 7G, H). Activated AKT is known to increase glycolysis

through phosphorylation of hexokinase, securing it to the mitochondrial membrane and through the phosphorylation of phosphofructokinase-2 producing 2,6-bisphosphate, which allosterically increases the activity of phosphofructokinase-1 thereby increasing the flux of glycolysis[46, 47]. It is also known to phosphorylate ATP-citrate lyase, an integral enzyme in *de novo* fatty acid synthesis, enhancing the activity of the enzyme[48, 49]. However, a direct effect of So on key enzymes of the TCA cycle, glycolysis or cholesterol biosynthesis are also possible. Furthermore, So treatment over time could affect the sphingolipid metabolite profile in the MOSE cells, which could be involved in the observed effects; detailed analyses are currently conducted in our laboratories.

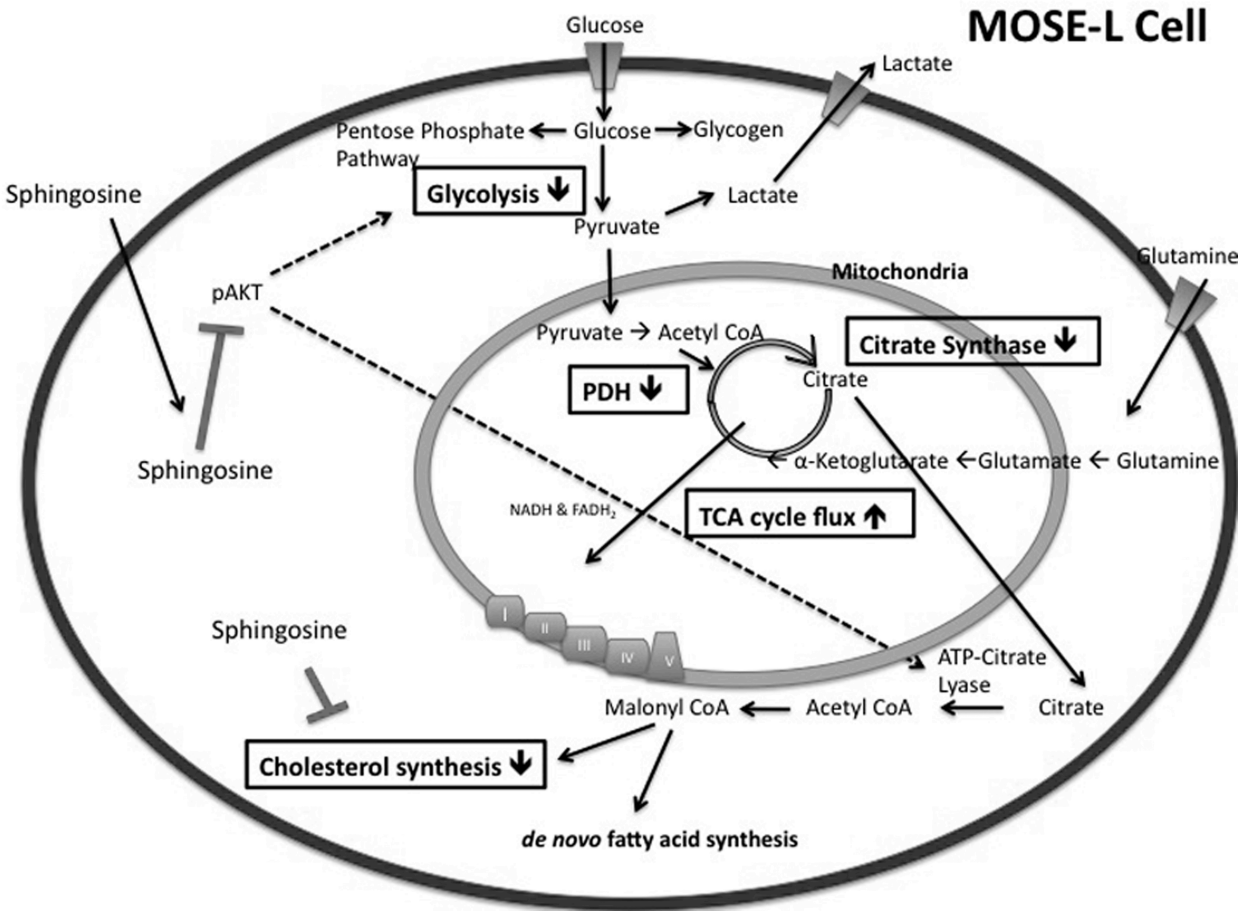

Figure 8. Metabolic changes in aggressive MOSE-L cells, and targets for intervention with So. MOSE-L cells demonstrate an increased uptake of glucose, glycolysis, and lactate secretion

in addition to an altered TCA flux and citrate synthase activity, generating intermediates for fatty acid and cholesterol synthesis. Boxes indicate So-induced changes in metabolic parameters in MOSE-L cells. Activated AKT (p-AKT) stimulates glycolysis, and activates ATP-citrate lyase, elevating lipid synthesis. In addition to a direct effect of So on cholesterol biosynthesis, TCA cycle, and glycolysis, the inactivation of AKT by So could decrease the activity of ATP-citrate lyase and indirectly lead to a decrease in cholesterol synthesis.

Conclusion

We demonstrate the development of an increasingly glycolytic and lipogenic phenotype, and changes in the mitochondria respiration capacity during ovarian cancer progression synthesis. These changes occur mostly in the tumorigenic MOSE-L cells and are therefore not a marker for early stage ovarian cancer. Treatment with non-toxic concentrations of So modulates cellular metabolism via several targets; while not detrimental to the cancer cells, the observed changes in citrate synthase activity, TCA flux, mitochondrial respiration and cholesterol biosynthesis by So treatment may be a disadvantage to the tumor cells and impair tumor growth. The MOSE model has proven to reflect metabolic changes that have been associated with tumorigenesis and progression and is used to further explore the beneficial effect of dietary sphingolipids in the prevention and treatment of ovarian cancer.

ACKNOWLEDGEMENTS

We would like to thank Dr. Yaru Wu for her assistance in using the Seahorse XF24 extracellular flux analyzer.

FUNDING

These studies were supported in part by NIH R01 CA118846 and AICR grant 04B071 (EMS, PCR), and funds provided by the Fralin Life Sciences Institute at Virginia Tech (MWH). The funding agencies had no role in the design, performance and analyses of experiments, and writing this report.

DISCLOSURE STATEMENT

The authors have no conflict of interest to disclose.

References

1. Roberts PC, Mottillo EP, Baxa AC, et al. Sequential molecular and cellular events during neoplastic progression: a mouse syngeneic ovarian cancer model. *Neoplasia.* Oct 2005;7(10):944-956.
2. Fresno Vara JA, Casado E, de Castro J, Cejas P, Belda-Iniesta C, Gonzalez-Baron M. PI3K/Akt signalling pathway and cancer. *Cancer Treat Rev.* Apr 2004;30(2):193-204.
3. *Facts and Figures 2008.* Atlanta: American Cancer Society;2008.
4. Warburg O. On the origin of cancer cells. *Science.* Feb 24 1956;123(3191):309-314.
5. Warburg O, Wind F, Negelein E. The Metabolism of Tumors in the Body. *J Gen Physiol.* Mar 7 1927;8(6):519-530.
6. Pinheiro C, Reis RM, Ricardo S, Longatto-Filho A, Schmitt F, Baltazar F. Expression of monocarboxylate transporters 1, 2, and 4 in human tumours and their association with CD147 and CD44. *J Biomed Biotechnol.*2010:427694.
7. Ganapathy V, Thangaraju M, Prasad PD. Nutrient transporters in cancer: relevance to Warburg hypothesis and beyond. *Pharmacol Ther.* Jan 2009;121(1):29-40.
8. Cuvier C, Jang A, Hill RP. Exposure to hypoxia, glucose starvation and acidosis: effect on invasive capacity of murine tumor cells and correlation with cathepsin (L + B) secretion. *Clin Exp Metastasis.* Jan 1997;15(1):19-25.
9. Rofstad EK, Mathiesen B, Kindem K, Galappathi K. Acidic extracellular pH promotes experimental metastasis of human melanoma cells in athymic nude mice. *Cancer Res.* Jul 1 2006;66(13):6699-6707.
10. Zu XL, Guppy M. Cancer metabolism: facts, fantasy, and fiction. *Biochem Biophys Res Commun.* Jan 16 2004;313(3):459-465.
11. Cairns RA, Harris IS, Mak TW. Regulation of cancer cell metabolism. *Nat Rev Cancer.* Feb 2011;11(2):85-95.
12. Yuneva M, Zamboni N, Oefner P, Sachidanandam R, Lazebnik Y. Deficiency in glutamine but not glucose induces MYC-dependent apoptosis in human cells. *J Cell Biol.* Jul 2 2007;178(1):93-105.
13. Postovit LM, Adams MA, Lash GE, Heaton JP, Graham CH. Oxygen-mediated regulation of tumor cell invasiveness. Involvement of a nitric oxide signaling pathway. *J Biol Chem.* Sep 20 2002;277(38):35730-35737.
14. Gatenby RA, Gillies RJ. Why do cancers have high aerobic glycolysis? *Nat Rev Cancer.* Nov 2004;4(11):891-899.
15. Gault CR, Obeid LM, Hannun YA. An overview of sphingolipid metabolism: from synthesis to breakdown. *Adv Exp Med Biol.* 2010;688:1-23.
16. Gangoiti P, Camacho L, Arana L, et al. Control of metabolism and signaling of simple bioactive sphingolipids: Implications in disease. *Prog Lipid Res.* Oct 2010;49(4):316-334.
17. Holland WL, Summers SA. Sphingolipids, insulin resistance, and metabolic disease: new insights from in vivo manipulation of sphingolipid metabolism. *Endocr Rev.* Jun 2008;29(4):381-402.
18. Schmelz EM, Dillehay DL, Webb SK, Reiter A, Adams J, Merrill AH, Jr. Sphingomyelin consumption suppresses aberrant colonic crypt foci and increases the proportion of adenomas versus adenocarcinomas in CF1 mice treated with 1,2-dimethylhydrazine:

implications for dietary sphingolipids and colon carcinogenesis. *Cancer Res.* Nov 1 1996;56(21):4936-4941.
19. Schmelz EM, Bushnev AS, Dillehay DL, Sullards MC, Liotta DC, Merrill AH, Jr. Ceramide-beta-D-glucuronide: synthesis, digestion, and suppression of early markers of colon carcinogenesis. *Cancer Res.* Nov 15 1999;59(22):5768-5772.
20. Schmelz EM, Sullards MC, Dillehay DL, Merrill AH, Jr. Colonic cell proliferation and aberrant crypt foci formation are inhibited by dairy glycosphingolipids in 1, 2-dimethylhydrazine-treated CF1 mice. *J Nutr.* Mar 2000;130(3):522-527.
21. Lemonnier LA, Dillehay DL, Vespremi MJ, Abrams J, Brody E, Schmelz EM. Sphingomyelin in the suppression of colon tumors: prevention versus intervention. *Arch Biochem Biophys.* Nov 15 2003;419(2):129-138.
22. Schmelz EM, Bushnev AS, Dillehay DL, Liotta DC, Merrill AH, Jr. Suppression of aberrant colonic crypt foci by synthetic sphingomyelins with saturated or unsaturated sphingoid base backbones. *Nutr Cancer.* 1997;28(1):81-85.
23. Symolon H, Schmelz EM, Dillehay DL, Merrill AH, Jr. Dietary soy sphingolipids suppress tumorigenesis and gene expression in 1,2-dimethylhydrazine-treated CF1 mice and ApcMin/+ mice. *J Nutr.* May 2004;134(5):1157-1161.
24. Mazzei JC, Zhou H, Brayfield BP, Hontecillas R, Bassaganya-Riera J, Schmelz EM. Suppression of intestinal inflammation and inflammation-driven colon cancer in mice by dietary sphingomyelin: importance of peroxisome proliferator-activated receptor gamma expression. *J Nutr Biochem.* Dec 2011;22(12):1160-1171.
25. Simon KW, Tait L, Miller F, et al. Suppression of breast xenograft growth and progression in nude mice: implications for the use of orally administered sphingolipids as chemopreventive agents against breast cancer. . *Food & Function.* 2010;1(1):90-98.
26. Schmelz EM, Crall KJ, Larocque R, Dillehay DL, Merrill AH, Jr. Uptake and metabolism of sphingolipids in isolated intestinal loops of mice. *J Nutr.* May 1994;124(5):702-712.
27. Creekmore AL, Silkworth WT, Cimini D, Jensen RV, Roberts PC, Schmelz EM. Changes in gene expression and cellular architecture in an ovarian cancer progression model. *Plos One.* 2011;6(3):e17676.
28. Cortright RN, Sandhoff KM, Basilio JL, et al. Skeletal muscle fat oxidation is increased in African-American and white women after 10 days of endurance exercise training. *Obesity (Silver Spring).* Jul 2006;14(7):1201-1210.
29. Dyck DJ, Peters SJ, Glatz J, et al. Functional differences in lipid metabolism in resting skeletal muscle of various fiber types. *Am J Physiol.* Mar 1997;272(3 Pt 1):E340-351.
30. Frisard MI, McMillan RP, Marchand J, et al. Toll-like receptor 4 modulates skeletal muscle substrate metabolism. *Am J Physiol Endocrinol Metab.* May 2010;298(5):E988-998.
31. Heilbronn LK, Civitarese AE, Bogacka I, Smith SR, Hulver M, Ravussin E. Glucose tolerance and skeletal muscle gene expression in response to alternate day fasting. *Obes Res.* Mar 2005;13(3):574-581.
32. Hulver MW, Berggren JR, Cortright RN, et al. Skeletal muscle lipid metabolism with obesity. *Am J Physiol Endocrinol Metab.* Apr 2003;284(4):E741-747.
33. Gerencser AA, Neilson A, Choi SW, et al. Quantitative microplate-based respirometry with correction for oxygen diffusion. *Anal Chem.* Aug 15 2009;81(16):6868-6878.

34. Younes M, Lechago LV, Lechago J. Overexpression of the human erythrocyte glucose transporter occurs as a late event in human colorectal carcinogenesis and is associated with an increased incidence of lymph node metastases. *Clin Cancer Res.* Jul 1996;2(7):1151-1154.
35. Walenta S, Schroeder T, Mueller-Klieser W. Lactate in solid malignant tumors: potential basis of a metabolic classification in clinical oncology. *Curr Med Chem.* Aug 2004;11(16):2195-2204.
36. Sonveaux P, Vegran F, Schroeder T, et al. Targeting lactate-fueled respiration selectively kills hypoxic tumor cells in mice. *J Clin Invest.* Dec 2008;118(12):3930-3942.
37. Singer K, Gottfried E, Kreutz M, Mackensen A. Suppression of T-cell responses by tumor metabolites. *Cancer Immunol Immunother.* Mar 2011;60(3):425-431.
38. Farwell WR, Scranton RE, Lawler EV, et al. The association between statins and cancer incidence in a veterans population. *J Natl Cancer Inst.* Jan 16 2008;100(2):134-139.
39. Murai T, Maruyama Y, Mio K, Nishiyama H, Suga M, Sato C. Low cholesterol triggers membrane microdomain-dependent CD44 shedding and suppresses tumor cell migration. *J Biol Chem.* Jan 21 2011;286(3):1999-2007.
40. Wu M, Neilson A, Swift AL, et al. Multiparameter metabolic analysis reveals a close link between attenuated mitochondrial bioenergetic function and enhanced glycolysis dependency in human tumor cells. *Am J Physiol Cell Physiol.* Jan 2007;292(1):C125-136.
41. Hong G, Baudhuin LM, Xu Y. Sphingosine-1-phosphate modulates growth and adhesion of ovarian cancer cells. *FEBS Lett.* Nov 5 1999;460(3):513-518.
42. Wang D, Zhao Z, Caperell-Grant A, et al. S1P differentially regulates migration of human ovarian cancer and human ovarian surface epithelial cells. *Mol Cancer Ther.* Jul 2008;7(7):1993-2002.
43. Chen V, Staub RE, Fong S, Tagliaferri M, Cohen I, Shtivelman E. Bezielle selectively targets mitochondria of cancer cells to inhibit glycolysis and OXPHOS. *PLoS One.* 2012;7(2):e30300.
44. Lesnefsky EJ, Chen Q, Moghaddas S, Hassan MO, Tandler B, Hoppel CL. Blockade of electron transport during ischemia protects cardiac mitochondria. *J Biol Chem.* Nov 12 2004;279(46):47961-47967.
45. Chang HC, Tsai LH, Chuang LY, Hung WC. Role of AKT kinase in sphingosine-induced apoptosis in human hepatoma cells. *J Cell Physiol.* Aug 2001;188(2):188-193.
46. Vander Heiden MG, Cantley LC, Thompson CB. Understanding the Warburg effect: the metabolic requirements of cell proliferation. *Science.* May 22 2009;324(5930):1029-1033.
47. Lunt SY, Vander Heiden MG. Aerobic glycolysis: meeting the metabolic requirements of cell proliferation. *Annu Rev Cell Dev Biol.* Nov 10 2011;27:441-464.
48. Berwick DC, Hers I, Heesom KJ, Moule SK, Tavare JM. The identification of ATP-citrate lyase as a protein kinase B (Akt) substrate in primary adipocytes. *J Biol Chem.* Sep 13 2002;277(37):33895-33900.
49. Migita T, Narita T, Nomura K, et al. ATP citrate lyase: activation and therapeutic implications in non-small cell lung cancer. *Cancer Res.* Oct 15 2008;68(20):8547-8554.

Chapter 6: OVARIAN TUMOR-INITIATING CELLS (TICs) DISPLAY A MORE FLEXIBLE METABOLISM THAN THEIR PARENTAL CELL LINE

Angela S. Anderson[a], Paul C. Roberts[b], Madlyn I. Frisard[a], Matthew W. Hulver[a*] and Eva M. Schmelz[a*]

[a] Department of Human Nutrition, Foods and Exercise, Virginia Tech, Blacksburg, VA

[b] Biomedical Science and Pathobiology, Virginia Tech, Blacksburg, VA

*to whom correspondence should be addressed:

Dr. Eva M. Schmelz (eschmelz@vt.edu)

Virginia Tech, 1981 Kraft Drive [0913], ILSB 1011, Blacksburg, VA 24060

Tel: 001-540-231-3649

FAX: 001-540-231-5522

and

Dr. Matthew W. Hulver (hulvermw@vt.edu)

Virginia Tech, 1981 Kraft Drive [0913], TLSB 1012, Blacksburg, VA 24060

Tel: 001-540-231-7354

In preparation for submission

Abstract

An altered metabolism during ovarian cancer progression allows for increased macromolecular synthesis and unrestrained growth in late-stage aggressive mouse ovarian epithelial cancer cells (MOSE-L) compared to early-stage benign cells (MOSE-E). Within this population of MOSE-L cells are tumor-initiating cells (TICs). These small populations of TICs are highly aggressive and metastatic, and are able to recapitulate the original tumor with as little as 100 cells. However, their metabolic phenotype has not been characterized. We compared the benign MOSE-E cells and slow developing MOSE-L cells to the TICs, allowing for characterization of distinct metabolic stages. TICs exhibit a decrease in glucose and fatty acid oxidation with a concomitant increase in lactate secretion. When challenged with external cellular modulators, the TICs are more resistant to change. TICs have an increased survival rate in depleted medium containing fatty acids and glutamine as the substrates for energy, as well as an increased survival rate when treated with AICAR, an AMPK agonist compared to MOSE-E and MOSE-L cells. When stimulated with oligomycin, the TICs ramp up glycolysis to overcome the inhibition of ATP Synthase, whereas the MOSE-E and MOSE-L cells have a reduced ability to increase glycolysis. When uncoupled with FCCP, the TICs can increase oxygen consumption rate (OCR) to maintain mitochondrial membrane potential similar to the MOSE-E cells, whereas the MOSE-L cells have a reduced capacity for increased OCR. Together, our data show that TICs located within a tumor have a distinct metabolic profile that may render them resistant to conventional treatments. By better understanding their metabolic phenotype and external environmental conditions that support their survival, treatment interventions can be designed to augment current therapy regimens.

Keywords: metabolism, cancer progression, cancer stem cell, tumor-initiating cell, ovarian cancer

Introduction

Ovarian cancer remains the 4th leading cause of cancer death among women[1]. Recent studies indicate that 75% of ovarian cancer cases are diagnosed in stage III or stage IV[2]. Standard treatment for advanced ovarian cancer includes cytoreductive surgery followed by platinum-based chemotherapy with a 50% to 70% relapse of disease within 18 months[3]. More recently, it has been reported that these platinum-resistant ovarian tumors are enriched in cancer stem cells, suggesting that these cells may be crucial in recurrent disease[4]. In fact, chemotherapy may enrich the cancer stem cell population as it targets and kills differentiated cancer cells making subsequent chemotherapy treatments less effective[5].

Stem cells are a small group of cells able to phenotypically self-renew and produce differentiated daughter cells that have limited capacity for replication. In cancer, this long-lived stem cell population has been referred to as tumor-initiating cells (TICs) or cancer stem cells (CSCs)[6]. TICs within a tissue have a unique phenotype, distinctly different from their normal tissue counterparts[7]. Ovarian cancer TIC populations that were isolated from a human ascites[8] had the ability for self-renewal; anchorage-independent growth *in vitro*; and tumorigenicity mimicking the original tumor *in vivo*[8]. It is unknown whether this distinct cancer cell population confers the same metabolic profile as other cancer cells exhibiting the well-documented Warburg effect[9, 10]. It is known that human embryonic stem cells (hESCs), adult hematopoietic stem cells (HSCs) and induced pluripotent stem cells (iPSCs) exhibit a decrease in oxygen consumption, producing more ATP through glycolysis than through oxidative phosphorylation (OxPhos)[11, 12]. They also exhibit increased lactate secretion with a concomitant increase in acidification of their medium compared to their differentiated counterparts[11]. However, the metabolic phenotype of ovarian cancer TICs is not well described.

Metabolic changes are necessary to sustain unrestricted growth in cancer cells. As cancer cells rapidly divide, the need for macromolecular synthesis of lipids, nucleotides and proteins for cell division are vital. A high carbon flux through glycolysis not only allows for pyruvate and ATP production, but also allows for carbons to leave glycolysis for *de novo* macromolecule biosynthesis. This altered metabolism permits glucose-derived carbon intermediates to be used for macromolecular synthesis giving cancer cells the needed building blocks for sustained growth levels[13]. We have recently demonstrated that mouse ovarian surface epithelial (MOSE) cells, representing early (benign), intermediate, and late (aggressive and invasive) stages of ovarian cancer[14, 15] also exhibit an increasingly glycolytic phenotype[16]. As cells progress through distinct stages, they increase their growth rate, acquire the ability to grow as spheroids, invade collagen, and form tumors *in vivo*[14]. By passaging the late stage MOSE cells (MOSE-L) through mice, the MOSE-L cells were enriched for TICs that exhibit increased tumorgenicity (Cohen et al., in preparation). This is consistent with other investigators, that ovarian TICs produce measureable tumors quicker than regular cancer cells[17, 18]. In the present studies, we investigated the metabolism of these highly aggressive cells. We hypothesize that due to the increased growth rate and invasive nature of the ovarian TICs, their metabolism will also be phenotypically distinct. These metabolic changes may be important to drive the proliferation and tumorigenic potential of these tumor-initiating cells and therefore, may present a target for the prevention of outgrowths of platinum-resistant ovarian cancers.

Methods and Materials

Cell Culture. The MOSE cell model has been developed from C57BL/6 mice as described[14]. Classification into early-benign (MOSE-E), transitional intermediate and late–aggressive (MOSE-L) phenotypes was established based on their morphology, growth rate, anchorage-independent and spheroid growth capacity and tumorigenicity *in vivo*[14]. Highly aggressive tumor initiating cells (TICs) were isolated from the tumor ascites of *in vivo* passaged MOSE-L cells. Briefly, MOSE-L cells (1 x10^6 cells) were implanted into syngeneic C57BL/6 mice and ascites fluid was harvested after 8 weeks. Tumor cells from the ascites fluid were allowed to propagate in cell culture for 4 passages until all other cell types had died off. These *in vitro* passaged cells were subsequently transduced with firefly luciferase lentiviral particles (GeneCopeia) following the product protocol provided, to facilitate live imaging. A high luciferase expressing subclone was isolated and is subsequently referred to as MOSE-L^{FFL}-TICv. They are referred to as TICs throughout these studies and represent a highly aggressive, tumor initiating cell variant of the MOSE-L cell line. The characteristics of these cells will be reported elsewhere. MOSE cells were routinely cultured in DMEM (Sigma) supplemented with 4% FBS (Atlanta Biologicals) and 100 ug/ml each of penicillin and streptomycin (Gibco) at 37°C in a humidified incubator with 5% CO_2. TICs were additionally cultured with 4 ug/ml puromycin (Sigma) to maintain the firefly luciferase plasmid.

Animals. 6 month-old C57BL/6 mice (Harlan Laboratories) were housed in a 12 h light and 12 h dark cycle with free access to water and standard rodent chow. 1 x 10^4 TICs in 100µl sterile PBS were injected intraperitoneally. After 3 weeks, mice were euthanized by CO_2

asphyxiation and matched tumors from ascites fluid and diaphragm were harvested from individual mice, digested as described (Cohen et al., in preparation), and a single cell solution was plated into tissue culture dishes. Cells were cultured for 3 passages with puromycin to exclude other tumor-associated cells before performing mitochondrial stress tests to assess oxygen consumption rate and extracellular acidification rate, using the Seahorse Biosciences XF24 Analyzer (see below). All animal studies were approved by the Virginia Tech Institutional Animal Care and Usage Committee.

Real-time PCR (qPCR). MOSE cells and TICs were seeded in 100 mm culture dishes and harvested 72 hours later. Total RNA was extracted using the RNeasy Mini Kit (Qiagen). cDNA synthesis was performed on 500ng of RNA using the ImProm-II Reverse Transcription System (Promega). qPCR was performed using 50ng of cDNA with SensiMix Plus SYBR Mastermix (Quantace) in the ABI 7900HT (Applied Biosystems) with the following parameters: 42 cycles at 95°C for 10 minutes, 95°C for 15 seconds, 58°C for 30 seconds and 72°C for 15 seconds, followed by a dissociation curve segment. Data was quantified using the ΔΔCT method and expressed relative to RPL19 as the housekeeping gene[15]. Primer pairs were designed with the NCBI Primer Blast (http://www.ncbi.nlm.nih.gov/tools/primer-blast/) or Beacon Design software and were as followed: Glucose transporter 1 (Glut 1) Fwd: GCC AGC CAA AGT GAC AAG; Glut1 Rev: TTC GGA AGA GGT CTC ATC TAG; Glucose transporter 2 (Glut 2) Fwd: ATC AGG ACT GTA TTG TGG GC; Glut 2 Rev: TGA GGC CAG CAA TCT GAC TA; Glucose transporter 3 (Glut 3) Fwd: CTT CTG TAG GAC CCG AGG AA; Glut 3 Rev: GAG ATG GGG TCA CCT TCG TT; Glucose transporter 4 (Glut 4) Fwd: TGC CCG AAA GAG TCT AAA GC; Glut 4 Rev: GAC ATT GGA CGC TCT CTC TC; Fatty acid transport protein

isoform 1 (FATP1) Fwd: TAC CAC TCT GCA GGG AAC AT; FATP1 Rev: AGA ACT TCT TGC GCA GTA CC; Fatty acid binding protein isoform 4 (FABP4) Fwd: GGA TGG AAA GTC GAC CAC AA; FABP4 Rev: GCC TTT CAT AAC ACA TTC CAC C; Pyruvate dehydrogenase (PDHb) Fwd: CAT TCG GCA GCT AGT AGA G; PDHb Rev: CTT CAC GAA CTG TCA ACT G; pyruvate dehydrogenase kinase 1 (PDK1) Fwd: CTG GGC GAG GAG GAT CTG ACT G; PDK1 Rev: ACA GCA CGG GAC GTT TCA ACA C; Uncoupling protein 2 (UCP2) Fwd: GTC GTC GGG TCG CCA GCT TC; Rev: TTG TGT CCG GAC CGC AGG AGA; Ribosomal protein L19 (RPL19) Fwd: GCA AGC CTG TGA CTG TCC ATT CC; RPL19 Rev: GCA TTG GCA GTA CCC TTC CTC TTC. Data expressed are on three biological replicates performed in duplicate. Data are presented as Mean ± SEM.

Glucose and Fatty Acid Oxidation using Dual-Labeled ^{14}C-Glucose and ^{3}H-Palmitate to Assess Substrate Choice for Oxidation. MOSE cells and TICs were seeded at 5 x 10^5 cells/ well in 6-well cell culture plates, incubated for 3 h, and washed with PBS. Following 2 h of incubation in serum-free medium, glucose and fatty acid oxidation were assessed via co-incubation with U-^{14}C glucose and ^{3}H-palmitic acid. Glucose oxidation was measured via $^{14}CO_2$ production as previously described[19]. Incorporation of $^{14}CO_2$ derived from U-^{14}C glucose into NaOH was measured using a LS 6500 scintillation counter (Beckman Coulter). Concomitantly, fatty acid oxidation was assessed by measuring $^{3}H_2O$ generation from ^{3}H-palmitate (Perkin Elmer) as previously described[20]. Data presented as the mean from three independent experiments performed in replicates of six, corrected for protein content. Data are presented as mean ± SEM.

Glucose Oxidation. MOSE cells and TICs were seeded at 2.5 x 10^5 cells/ well in 6-well cell culture plates, incubated for 3 h, and washed with PBS. Following 2 h of incubation in serum-free medium, glucose oxidation was measured via $^{14}CO_2$ production essentially as previously described[19] except that glucose was substituted for BSA-bound palmitate. Incorporation of $^{14}CO_2$ derived from U-^{14}C glucose into NaOH was measured using a LS 6500 scintillation counter (Beckman Coulter). Data are presented as the mean ± SEM from three independent experiments performed in replicates of three or six, corrected for protein content.

Fatty Acid Oxidation. MOSE cells and TICs were seeded at 2.5 x 10^5 cells/ well in 6-well cell culture plates, incubated for 3 h, and washed with PBS. Following 2 h of incubation in serum-free medium, glucose and fatty acid oxidation were assessed via co-incubation with U-^{14}C palmitate. Fatty acid oxidation was measured via $^{14}CO_2$ production as previously described[19] and acid soluble metabolites were measured as the remaining label after acidification. Incorporation of $^{14}CO_2$ derived from U-^{14}C palmitate into NaOH was measured using a LS 6500 scintillation counter (Beckman Coulter). Data presented as the mean ± SEM from three independent experiments performed in replicates of three or six, corrected for protein content.

Lactate Assay. After the 3 h incubation with radioactive isotopes in the dual-labeled glucose and fatty acid experiments, 300µl of medium was collected and assayed for lactate concentration using a colorimetric kit according to the manufacturer's instructions (BRSC, University of Buffalo). Data presented are the mean ± SEM from three independent experiments performed in replicates of six biological replicates, corrected for protein.

De Novo Fatty Acid Synthesis. *de novo* fatty acid synthesis was assessed by measuring the quantity of ^{14}C-glucose (Perkin Elmer) from the dual-label glucose and fatty acid experiment that was partitioned into fatty acids as previously described[21, 22]. Data presented are the mean from three independent experiments performed in six biological replicates, corrected for protein content. Data are presented as mean ± SEM.

Mitochondrial Respiration. Mitochondrial respiration of the MOSE cells and TICs was determined using an XF24 extracellular flux analyzer (Seahorse Bioscience) as described[23] with some modifications. Cells were seeded into XF24 V7 cell culture microplates at a density of 50,000 cells per well and incubated for 48 h. The medium was changed and the experiments were conducted in serum-free, bicarbonate-free medium after 1 h incubation. Cells were loaded into the XF24 and experiments consisted of 3-minute mixing, 2-minute wait, and 3-minute measurement cycle. Oxygen consumption was measured under basal conditions in the presence of the mitochondrial inhibitors 0.5μmol/L oligomycin (Calbiochem) or 0.25μmol/L rotenone (Sigma), or in the presence of the mitochondrial uncoupler, 0.3μmol/L carbonylcyanide-p-trifluoromethoxyphenylhydrazone, FCCP (Sigma) to assess maximal oxidative capacity. All experiments were performed at 37°C. FCCP-stimulated oxygen consumption rate (OCR) and oligomycin-stimulated extracellular acidification rate (ECAR) were calculated by the oligomycin- or FCCP-induced change minus the basal rates. Data presented are the mean from six independent experiments performed in replicates of six or seven and corrected for protein. Data are presented as Mean ± SEM.

Determination of survival and proliferation. For the proliferation assay, MOSE cells and TICs were plated at 3 x 10^3 cells per well in 96-well plates and allowed to adhere overnight. Increasing concentrations of AICAR (Tocris Biosciences) were administered and cells were allowed to grow for 48 h. 50µl of MTT (3-(4,5-Dimethylthiazol-2-yl)-2,5-diphenyltetrazolium bromide) (Sigma) was added. After 1 h, the medium was removed, 100µl of cell lysis buffer (20% SDS, 40% dimethylformamide, 40% dH_2O) was added, and the plates were incubated overnight at 37°C. The reduction of tetrazolium bromide to formazan was determined spectrophotometrically at 570nm. Data presented are the mean from three independent experiments performed in replicates of six per AICAR concentration. Data are presented as Mean ± SEM.

For the survival assay, MOSE cells and TICs were plated 5 x 10^3 in 96-well plates and allowed to grow for 48 h at 37°C. Plates were washed with PBS and media with the indicated substrates were added for 24 h. At 24 h, 5µl of alamarBlue was added and plates were incubated for 3 h at 37°C. The levels of reduced alamarBlue were measured by a fluorescence plate reader using an excitation wavelength at 560nm and an emission wavelength of 590nm. Substrate media were as follows: Full medium (high glucose DMEM with 4% FBS + 60 µM fatty acid-free BSA fraction V, Calbiochem); Full substrate medium (high glucose DMEM with 200µM 2:1 oleate:palmitate (Sigma), reflecting in vivo fatty acid concentrations, in 60 µM BSA fraction V); glucose only (no glucose, no glutamine, no phenol red DMEM + 4.5mM glucose + 60 µM BSA fraction V; and fatty acid only (no glucose, no glutamine, no phenol red DMEM + 200µM 2:1 oleate:palmitate (Sigma) in 60 µM BSA fraction V). Data presented are the mean fluorescence units (reduced alamarBlue) ± SEM from three independent experiments performed in replicates of six.

Statistics. Data are presented as mean ± SEM. Results were analyzed with a one-way ANOVA followed by Tukey's post ad hoc test. When comparing different cell types grown on different mediums, results were analyzed with a two-way ANOVA followed by a Bonferroni post ad hoc test. All results were analyzed by Prism (GraphPad). Results were considered significant at $p<0.05$. Statistical significance is represented in the figures as follows: *$p< 0.05$, **$p< 0.01$, and ***$p<0.001$.

Results

Our previous studies have shown that the late-stage MOSE-L cells develop a glycolytic phenotype concomitantly with increased invasiveness compared to the early MOSE-E cells[16], suggesting that these changes may be targets for treatment strategies. However, it is unknown as to whether the metabolism of the TICs is different than their precursor cell population, the MOSE-L cells. Since this is critical to eliminate cells that can recapitulate fatal disease, we assessed changes in the metabolism of the TICs.

Differences in glucose and fatty acid oxidation in the TICs compared to their precursor cells. Three methods were employed to assess glucose and fatty acid oxidation. We measured glucose oxidation in a low-glucose medium to assess oxidation of glucose alone in this condition. Next we measured fatty acid oxidation in a glucose-free medium, forcing the cells to rely on this substrate for oxidation. Last, we measured glucose and fatty acid oxidation in tandem to better understand the cell's substrate choice for oxidation. There were no differences in glucose oxidation between the MOSE cells and the TICs when cultured in low-glucose

DMEM with ^{14}C glucose (Figure 1 A). However, there were significant differences seen in the fatty acid oxidation (Figures 1 B-D). Compared to the MOSE-E cells, the MOSE-L cells and TICs had a decrease in CO_2 production derived from ^{14}C-palmitate ($p<0.001$); a decrease in acid soluble metabolites, a product of incomplete β-oxidation (MOSE-L $p<0.05$; TIC $p<0.01$); and a total decrease fatty acid oxidation (CO_2 plus ASMs, $p<0.001$) in glucose-free medium.

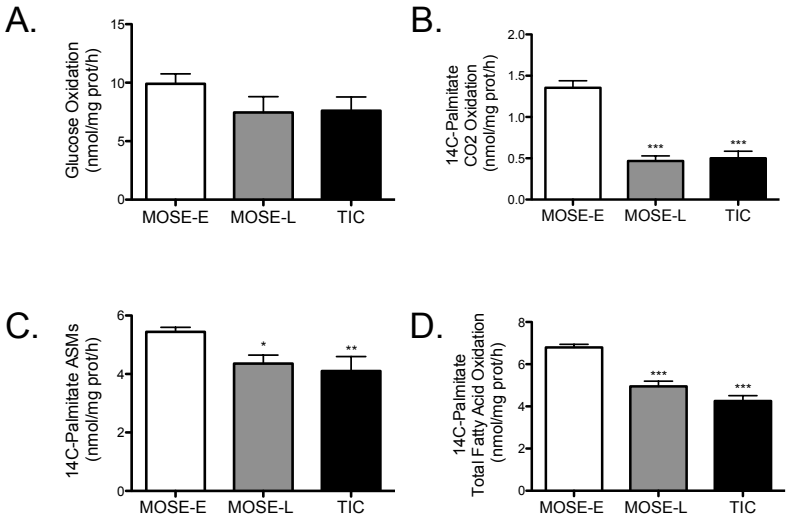

Figure 1. TICs display a decrease in fatty acid oxidation compared to the MOSE-E cells. Cells were incubated in serum-free medium for 2 h, the appropriate substrates added and changes in (A) glucose oxidation in low-glucose DMEM at 3 h, (B) fatty acid oxidation into CO_2 in glucose-free DMEM at 3 h, (C) fatty acid oxidation of incomplete beta-oxidation into acid soluble metabolites (ASMs) in glucose-free DMEM at 3 h, and (D) total fatty acid oxidation as CO_2 plus ASMs. Data are presented as mean ± SEM. Different from MOSE-E, *p≤0.05, **p≤0.01, ***p≤0.001.

More so, when cells were incubated in dual labels ^{14}C-glucose and ^{3}H-palmitate (Figure 2 A-B) in an effort to assess preferential substrate selection, there was a decrease in glucose oxidation ($p<0.01$) and fatty acid oxidation ($p<0.05$) between the MOSE-L and TICs. In addition, there was a decrease in glucose oxidation ($p<0.001$) and fatty acid oxidation ($p<0.001$) between the MOSE-E and TICs. When glucose and fatty acid oxidation were combined, there was a significant decrease in total oxidation in the TICs compared to the MOSE-E ($p<0.001$) and the MOSE-L cells ($P<0.001$) (Figure 2 C). Taken together, the TICs had a greater percentage of

their oxidation attributed to glucose rather than fatty acids as compared to the MOSE-E cells (67.8% versus 51.2%, $p<0.01$) (Figure 2 D). Overall this data suggests that in the presence of both substrates, the TICs appear to be more glycolytic.

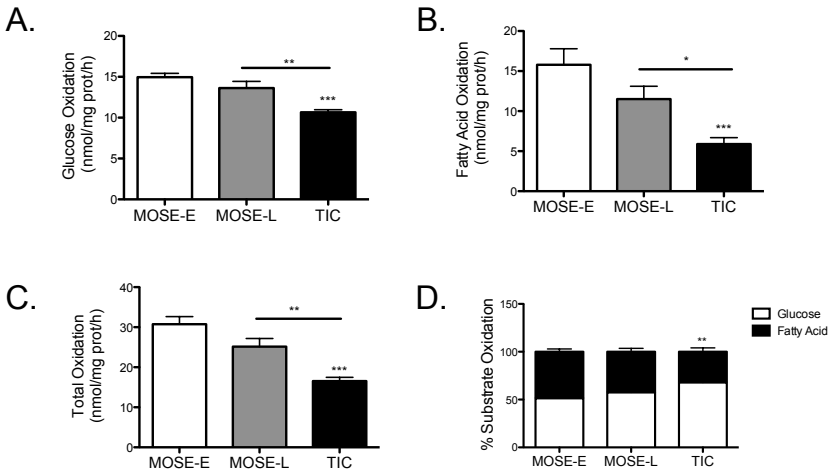

Figure 2. TICs have a decrease in total OxPhos, relying more on glucose as a substrate. Cells were incubated in serum-free medium for 2 h, the substrates were added and changes in (A) glucose oxidation from dual-label experiments with ^{14}C-glucose and ^{3}H-palmitate as competing substrates at 3 h, (B) fatty acid oxidation from dual-label experiments with ^{14}C-glucose and ^{3}H-palmitate as competing substrates at 3 h, (C) total oxidation from either ^{14}C-glucose and ^{3}H-palmitate at 3 h, and (D) percentage of glucose and fatty acids used for oxidation, where the total oxidation are the values from figures E and F, adjusted to 100%. Data are presented as mean ± SEM. Different from MOSE-E, **p≤0.01, ***p≤0.001. Different from MOSE-L, bar with *p≤0.05, **p≤0.01.

De novo fatty acid synthesis and lactate indicate an increase in substrate use with a concomitant increase in glucose and fatty acid transporters. Based on the results of the dual-labeled experiments we next explored whether there were changes in *de novo* fatty acid synthesis and lactate excretion into the medium. There were no differences in fatty acid synthesis from ^{14}C-glucose between the MOSE-L cells and TICs after the 3 h incubation (Figure 3 A). There was a trend toward an increase fatty acid synthesis in the TICs compared to the MOSE-E cells (ANOVA $p<0.067$). With the decrease in oxidation seen in the TICs, we assessed the lactate levels in the medium after the 3 h incubation period with the labeled isotopes. As expected, the

lactate levels were higher in the TICs compared to the MOSE-E ($p< 0.001$) and MOSE-L ($p<0.001$) cells (Figure 3 B) indicating an increase in glycolysis rate.

Given the changes in substrate usage between the cell types, we assessed whether there was a change designated gene targets. Figure 3 C illustrates the changes in mRNA of the five expressed glucose and fatty acid transporters (FAT/CD36 showed high CT values (MOSE-E 36.6; MOSE-L 37.0; TIC 35.6) indicating no expression in these cells). The TICs showed an increase mRNA level in five transporters over the MOSE-E cells (Glut 1 $p<0.01$; Glut 2 $p<0.05$; Glut 4 $p<0.001$; FATP1 $p<0.001$; FABP4 $p<0.001$) and an increase in mRNA level in 3 transporters over the MOSE-L cells (Glut 4 $p<0.05$; FATP1 $p<0.001$; FABP4 $p<0.001$). Additionally, there was a decrease in mRNA expression of Glut 3 ($p<0.01$ compared to the MOSE-E). Together this suggests an overall increased capacity for substrate uptake.

In addition to substrate transporters, known metabolic gene expression alterations commonly seen in cancer were investigated (see Appendix B). Hexokinase II and pyruvate kinase M2 in glycolysis, since these are known to be altered in cancer; pyruvate dehydrogenase subunit b (PDHb) and pyruvate dehydrogenase kinase 1 (PDK1)- the regulator of PDH, since PDH is the master regulator of aerobic versus anaerobic metabolism; uncoupling protein 1 (UCP1), uncoupling protein 3 (UCP3), and carnitine acyl transferase, since the management of reactive oxygen species (ROS) and accumulation of substrates modulate proper mitochondrial function. mRNA changes in TICs compared to the MOSE-E cells were seen in PDHb ($p<0.05$), PDK1 ($p<0.01$) and UCP2 ($p<0.001$), with changes in the TICs compared to the MOSE-L cells seen in PDK1 ($p<0.01$) and UCP2 ($p<0.001$) (Figure 3 C). The increase in PDK1 in the TICs, which decreases PDH activity, is consistent with the glycolytic phenotype observed. Additionally, the increase in PDHb, one subunit of the pyruvate dehydrogenase complex, may be

indicative of the TIC's ability to switch between glycolysis and OxPhos when needed. Future studies will investigate contribution of UCP2 in modulating membrane potential and ROS levels.

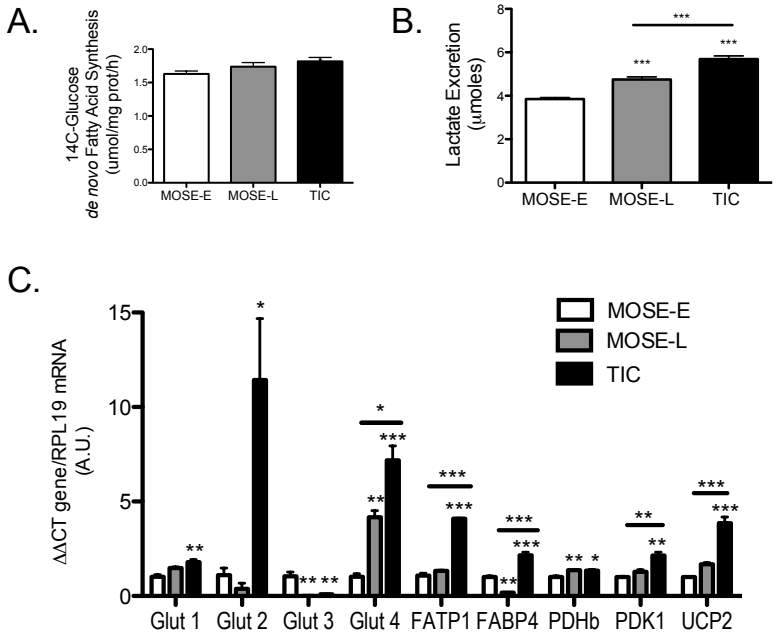

Figure 3. TICs excrete more lactate and have an increased expression of substrate transporters as compared to the MOSE cells. (A) *De novo* fatty acid synthesis from ^{14}C-glucose and (B) non-labeled lactate excretion into the medium from the dual-label substrate experiments; (C) qPCR determination of glucose transporters 1, 2, 3, and 4 (Glut 1, Glut 2, Glut 3, and Glut 4), fatty acid transporter isoform 1 (FATP1), fatty acid binding protein isoform 4 (FABP4), pyruvate dehydrogenase subunit b (PDHb), pyruvate dehydrogenase kinase 1 (PDK1), and uncoupling protein 2 (UCP2). Data are presented as mean ± SEM. Different from MOSE-E, *p≤0.05, **p≤0.01, ***p≤0.001. Different from MOSE-L, bar with *p≤0.05, **p≤0.01,***p≤0.001.

TICs have an increased survival with limited substrates and increased survival with AMPK activation. To better understand how the increased expression of glucose and fatty acid transporters might affect cancer cell survival, we subjected the cells to varying substrates and measured viability. The chosen supplements represented extreme nutrient deficiencies to assess survivability under extreme conditions. All media were supplemented with glutamine due to earlier studies indicating complete cell death without glutamine (data not shown). As shown in Figure 4 A-B, the TICs were able to survive longer in the 2:1 oleate:palmitate medium than

either the MOSE-E or MOSE-L cells ($p<0.001$). MOSE cells and TICs had a 13.5% (MOSE-E), 0.58% (MOSE-L), and 26.1% (TICs) percentage survival in the fatty acid only medium (no glucose DMEM with 2:1 oleate:palmitate) compared to the control medium (HG DMEM 4% FBS + 0.4% BSA) (Figure 4 B). Small differences in survivability were seen in the MOSE-L cells with an increase in survivability in the HG DMEM + 0.4% BSA ($P<0.01$) and HG DMEM + 200uM 2:1 Ol:Pal ($P<0.05$) compared to the HG DMEM 4% FBS + 0.4% BSA. No differences in viability were seen in MOSE-E and TIC cells grown in these substrate mediums.

Due to the differences in substrate survival in a fatty acid only medium between the TICs and MOSE cells, we next sought to examine the impact of a metabolic modulator on cell viability. We targeted adenosine monophosphate kinase (AMPK) due to its central role in moving cells from a state of macromolecule synthesis to an oxidative metabolic state, using the agonist drug AICAR. As seen in Figure 4 C, the TICs had a significantly higher EC_{50} (254.4 μM) over the MOSE-E cells (135.7 μM) and over double the EC_{50} of the MOSE-L cells (103.9 μM). Statistical analysis indicated that each EC_{50} was significantly different for each cell type from the other cell types ($p<0.05$). Overall these results indicate that the TICs were much more resistant to modulation by AMPK.

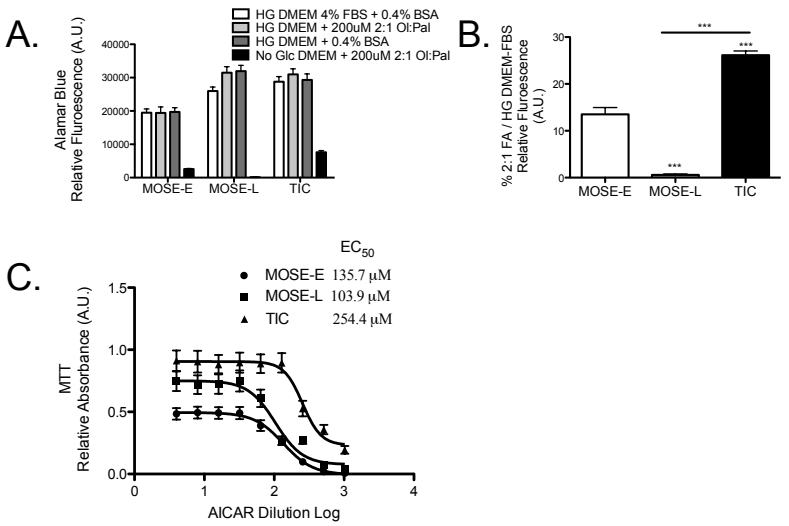

Figure 4. TICs have increased survivability when challenged. (A) Survivability in varying substrate mediums with bar 1 as high glucose DMEM supplemented with 4% FBS and 0.04% BSA, bar 2 as high glucose DMEM supplemented with 200μM 2:1 oleate:palmitate complexed to BSA, bar 3 as high glucose DMEM supplemented with 0.4% BSA, and bar 4 as no glucose DMEM supplemented with 200μM 2:1 oleate:palmitate complexed to BSA, measured via Alamar Blue; (B) the percentage survivability of the cells in no glucose DMEM supplemented with 200μM 2:1 (bar 4) divided by the control high glucose DMEM supplemented with 4% FBS and 0.04% BSA (bar 1); (C) Cytotoxicity of increasing concentrations of AICAR in the determination of the EC_{50} for each cell type via the statistical program GraphPad Prism. Data are presented as mean ± SEM. Different from MOSE- E, ***p≤0.001. Different from MOSE-L, bar with ***p≤0.001.

TICs have an increased FCCP stimulated-OCR and oligomycin stimulated-ECAR compared to differentiated MOSE-L cells. To further investigate the ability of the TICs to alter their metabolism to account for varying extracellular conditions, we used the Seahorse Extracellular Flux Analyzer to measure oxygen consumption rate (OCR) and glycolysis rate indirectly via the extracellular acidification rate (ECAR). FCCP, a mitochondrial uncoupler was used to stimulate maximal OCR. As shown in Figure 5 A-B, MOSE-L cells had a significant decrease in FCCP-stimulated OCR as compared to the MOSE-E ($p<0.001$) and TICs ($p<0.001$), measured as the difference in FCCP-stimulated OCR minus basal OCR, confirming our previous studies[16]. The TICs increased their FCCP stimulated-OCR to the same level as the benign

MOSE-E cells, indicating an ability to up-regulate oxidative phosphorylation (OxPhos) when uncoupled, exhibiting an increased OCR reserve.

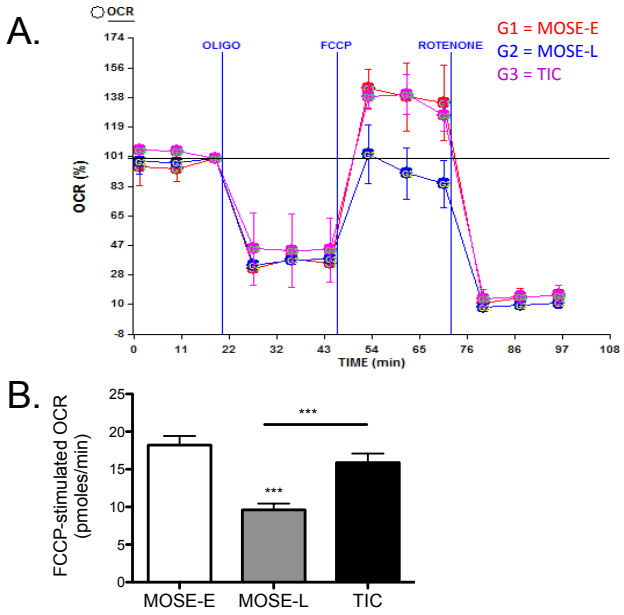

Figure 5. FCCP-stimulated oxygen consumption rate is increased in the TICs compared to the parental MOSE-L. Oxidative capacity rate (OCR) was measured during an uncoupling challenge. Cellular respiration was modified by oligomycin, an ATP synthase blocker, carbonylcyanide-p-trifluoromethoxyphenyl hydrazone (FCCP), an electron transport chain uncoupler followed by rotenone, a complex one inhibitor of the electron transport chain. (A) Image of representative experiment measured over 2 h; (B) Change over base-line in OCR after FCCP treatment. Data are presented as mean ± SEM. Different from MOSE-E, ***p≤0.001. Different from MOSE-L, bar with ***p≤0.001.

Subsequently, the cells were challenged with oligomycin, an ATP Synthase inhibitor to assess glycolytic rate (ECAR). When ATP Synthase is inhibited, ATP production in the ETC is blocked forcing the cells to switch to glycolysis for ATP production. When challenged with oligomycin, the TICs had a much higher oligomycin-stimulated ECAR than the MOSE-E ($p<0.01$) and MOSE-L ($p<0.05$) cells (Figure 6 A-B), measured as the difference in oligomycin-stimulated ECAR minus basal ECAR. This increase in oligomycin-stimulated ECAR suggests that the TICs have a much higher glycolytic reserve and are able to increase flux through this pathway to sustain ATP production when OxPhos is inhibited.

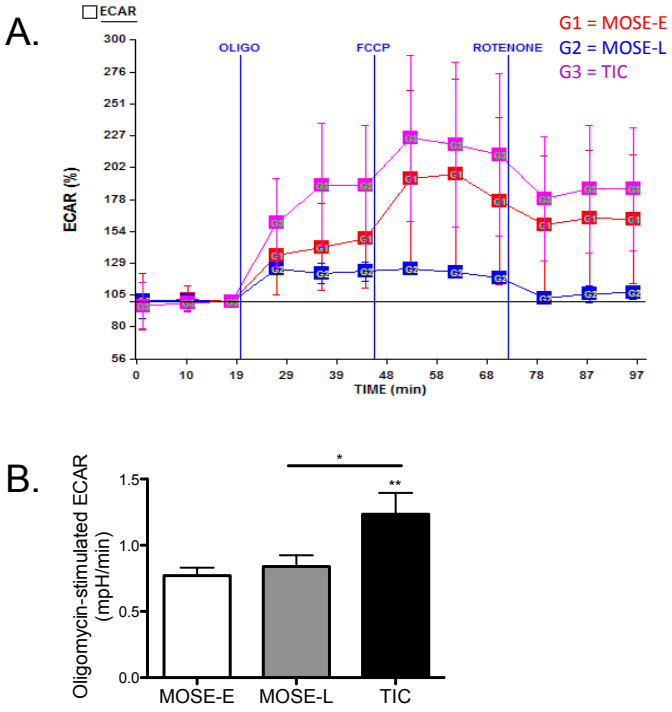

Figure 6. Oligomycin-stimulated ECAR shows an increased glycolytic capacity in the TICs. Extracellular acidification rate (ECAR), an indication of the rate of glycolysis was modified by oligomycin, carbonylcyanide-p-trifluoromethoxyphenyl hydrazone (FCCP), and rotenone (see Fig, 5). (A) Image of representative experiment measured over 2 h; (B) Change in ECAR over baseline after olygomycin treatment. Data are presented as mean ± SEM. Different from MOSE-E **p≤0.01. Different from MOSE-L, bar with *p≤0.05.

Mitochondrial stress test of solid tumors versus tumors found in the ascites indicate that ascites tumors are more glycolytic. TIC cells were originally isolated and purified from the ascites of MOSE-L injected mice possibly indicating enrichment for these tumor-initiating cells in this peritoneal location. To assess whether cells harvested from TIC injected mice might display an altered metabolism depending on their peritoneal location, tumors were harvested from the diaphragm and from the ascites of C57BL/6 mice that had received the TICs three weeks prior. Cells were removed, isolated, and after three passages in culture to remove any extraneous tumor-associated cells, the cells underwent a mitochondrial stress test (Figure 7 A-D). No significant differences in OCR were observed, with a trend towards a decrease in FCCP-

stimulated OCR in the ascites tumor cells (p=0.09). There was a significant increase in basal ECAR, pointing to an increase in glycolytic rate (Figure 7 C). No differences in the oligomycin-stimulated ECAR rate were observed.

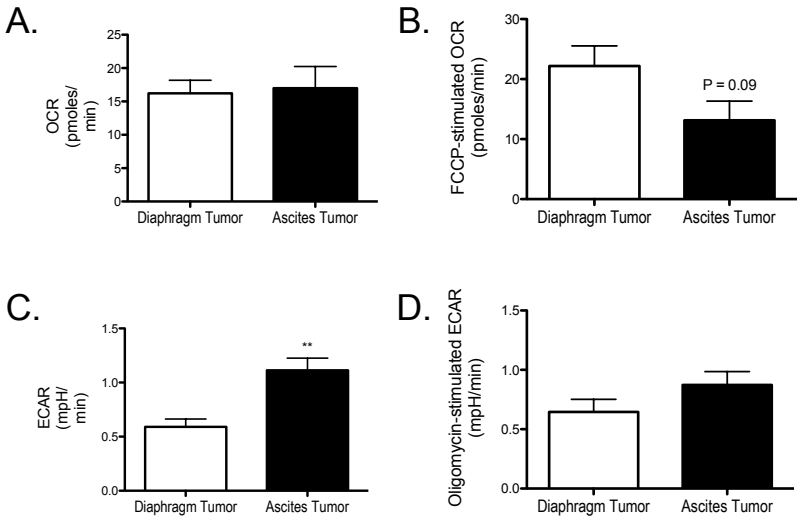

Figure 7. Cells harvested from the ascites are more glycolytic than those harvested from solid tumor. Oxygen consumption rate (OCR) and extracellular acidification rate (ECAR) were modified by oligomycin, carbonylcyanide-p-trifluoromethoxyphenyl hydrazone (FCCP), and rotenone (see Figures 4 and 5) on TICs that were harvested from the ascities of the mouse compared to TICs that were harvested from a solid diaphragm tumor of the mouse. (A) Basal OCR levels, measured over 2 h; (B) Change in OCR over baseline after FCCP treatment; (C) Basal ECAR levels, measured at 2 h; (D) Change in ECAR over baseline after oligomycin treatment. Data are presented as mean ± SEM, **p≤0.01.

Discussion

Due to the altered metabolism of ovarian cancer cells as they progress from benign to highly aggressive[16], the current studies investigated whether ovarian tumor-initiating cells have a unique metabolic phenotype. Here we demonstrate that the TICs are more glycolytic than early- or late-stage MOSE cells, showing a decrease in glucose and fatty acid oxidation, an increase in lactate secretion, and an increase in mRNA expression of PDK1 (Figure 2 A-D, Figure 3 B-C). Although we did not see an increase in *de novo* fatty acid synthesis in the TICs compared to the

MOSE cells using ^{14}C-glucose as the carbon source (Figure 3 A), the contribution of glutamine to metabolism was not assessed and therefore may not reflect the actual number of carbons being incorporated into fatty acids. Other researchers have shown that glutamine can account for approximately 25% of the total fatty acid carbons in glioblastoma tumors[24]. Future studies will investigate the contribution of glutamine to TIC metabolism compared to the MOSE cells, as the contribution of glutamine in ovarian cancer metabolism has not been explored.

Next we showed that the TICs have an increased mRNA expression of Glut 1, Glut 2, Glut 4, FATP1 and FABP4, signifying an increased capacity for substrate uptake and an increased survival in fatty acid only medium (Figure 3 C and Figure 4 A). Additionally, we found that the TICs were metabolically more flexible. They increased their OCR when their mitochondria were uncoupled and increased their ECAR to overcome an ATP Synthase inhibition, and they have increased mRNA expression of PDHb (Figure 3C, Figure 5, Figure 6). The TICs also had a survivability that was double the differentiated MOSE-L cells (EC_{50} of 254.4 μM compared to 103.9 μM) when treated with AICAR (Figure 4 C). Finally, due to the metabolic changes observed between the TICs and MOSE-L cells, we asked the question as to whether the cancer cells found in the ascites had a more glycolytic phenotype compared to those cells which formed solid tumors on the diaphragm. The mitochondrial stress test identified the ascites cancer cells as having a higher basal rate of glycolysis as measured by ECAR in comparison to the diaphragm cancer cells (Figure 7 C), where the TIC's basal ECAR values are similar to the diaphragm tumor. There was also a trend towards a decrease in FCCP-stimulated OCR in the cells from the ascites (Figure 7 B), where the TIC's FCCP-stimulated values are more similar to the cells from the ascites. Although further investigation is needed, these results

suggest that cells in the ascites display a more glycolytic phenotype, which may be due to a higher enrichment of tumor-initiating cells that reside within the ascites.

This increased glycolytic phenotype in the TICs is similar to the glycolytic phenotype of normal stem cells that reside within the body[11, 12]. In addition, others have verified that tumor-initiating cells display an increased glycolytic phenotype in different cancers. In glioblastoma stem cells, a low rate of OxPhos was coupled with a high rate of glycolysis and expression of glycolytic enzymes, indicating a higher reliance on glycolytic flux[25-27]. These results are in contrast to one report showing glioblastoma stem cells as being less glycolytic than their daughter cells, where the researchers identified the cancer stem cells as those having a lower 26S proteasome activity[28]. Besides glioblastomas, colon cancer cells expressing high levels of CD44, a common marker of cancer stem cells, had a high correlation with glycolytic gene expression versus the less invasive CD44 low cells[29].

Increased substrate transporters may be a marker of tumor-initiating cells. Thyroid tumor-initiating cells that were enriched for CD133 positive cells, had an increased expression of stem cell markers as well as GLUT1[30]. In an elegant study by Nieman et al. in 2011, ovarian cancer cells that metastasized to the omentum were able to increase expression of FABP4 on the cancer/adipocyte boundary and increase the uptake of fatty acids and subsequent ATP production through beta-oxidation[31]. Although stem cell markers were not identified in this study, tumors resulting from metastasis to the omentum indicate a population of tumor-initiating cells that can adapt to a secondary environment and thrive. Expression of the other transporters in cancer stem cells has not been reported.

We found that the TICs displayed a more flexible metabolism. Data is lacking describing mitochondrial energy dynamics in cancer stem cells. In iPSCs and hESCs compared to differentiated fibroblasts, it is the differentiated fibroblasts that have a higher FCCP-stimulated OCR over the stem cells[32, 33]. However the differentiated fibroblasts were basally more oxidative than the iPSCs, which is contrary to differentiated cancer cells. In hESCs when ATP Synthase is inhibited with oligomycin, the hESCs have a decrease in oligomycin-stimulated ECAR compared to differentiated fibroblasts. The authors speculate that the hESCs may be near their maximal glycolytic capacity and therefore have a reduced reserve for increased glycolysis[33]. Cancer stem cells may perform similarly to hESCs, but due to the reduced glycolytic reserve capacity of differentiated cancer cells[16], cancer stem cell's glycolytic reserve capacity may be greater, although decreased compared to normal cells.

We investigated the modulation of metabolism by activating adenosine monophosphate–activated protein kinase (AMPK). AMPK is an energy-sensing enzyme that is responsive to increases in the AMP:ATP ratio which produces a conformational change, making it susceptible to phosphorylation and therefore activation by an AMPK kinase. Phosphorylated AMPK works by inhibiting several enzymes including mammalian target of rapamycin (mTOR), acetyl-CoA carboxylase (ACC), fatty acid synthase (FAS), and glycerol phosphate acyltransferase (GPAT), which are key regulators of protein, fatty acid and glycerophospholipid synthesis[34]. Activated AMPK shifts metabolism from energy-consuming pathways to energy-producing pathways[35]. Activation of AMPK may work to decrease cancer growth through reduction in expression of SREBP-1C, which in turn inhibits *de novo* fatty acid synthesis and cholesterol synthesis[34] leading to cytoxicity in ovarian cancer cells[36]. We investigated the survival response to increasing doses of the AMPK agonist AICAR. We chose AICAR due to its ability, through

AMPK modulation, to decrease AKT phosphorylation[37] and inhibit the mTOR pathway through the tuberous sclerosis complex (TSC) inducing ovarian cancer cell death[38]. AKT has been shown to be constitutively active in ovarian cancer cells, sustaining high levels of glycolysis, and giving cancer cells the glycolytic phenotype observed by Warburg in metastatic cancer cells[38]. To our knowledge, there are no other reports looking at AICAR toxicity in tumor-initiating cells compared to their heterogeneous parental cells.

Meformin, another AMPK agonist, is hypothesized to work by blocking complex I in the electron transport chain, thereby raising the AMP:ATP ratio, resulting in AMPK activation[39]. Although both Metformin and AICAR activate AMPK, Metformin does so indirectly. Several groups have shown Metformin to be more effective in killing breast cancer stem cells than parental non-stem cancer cell populations, separating these populations based on the expression of the surface markers $CD44^{+}CD24^{-/low}$ [40, 41]. However this was dependent on these cells having constitutively active NF-κB, for Metformin to be more effective[42]. This indicates that Metformin may work directly by blocking the NF-κB pathway, as Metformin was not effective in reducing the cancer stem cell population in cells secreting low levels of IL-6, a downstream target of NF-κB[42]. In ovarian cancer, Metformin was used to treat cancer stem cells separated by the expression of aldehyde dehydrogenase (ALDH) activity since $ALDH^{+}$ cells can initiate tumors in mice whereas $ALDH^{-}$ cells cannot[43]. Direct comparison of Metformin's effect on the survival ALDH+ cells compared to parental cell lines was not measured and the inflammatory state was not assessed. This evidence suggests that although we show an increased survival of the TICs compared to the parental cell line MOSE-L using AICAR to modulate AMPK, it doesn't necessarily contradict the effects of Metformin in specifically targeting cancer stem cells. This may in part be due to Metformin's ability to block the NF-κB pathway, where AICAR does not.

Future studies will investigate Metformin's affect on the TICs compared to the MOSE-E and MOSE-L cells, as well as the inflammatory state of these cells.

Ovarian cancer stem cells were originally harvested from human ascites[8]. Our TICs were also harvested from the ascites of the parental MOSE-L injected mice. Recent evidence in breast cancer points to a dynamic equilibrium between cancer stem cells and non-stem cancer cells dependent on the inflammatory state or microenvironment, and that this equilibrium is mediated in part by miRNAs[42, 44]. miR-214 (p53), miR-199a (CD44), and miR-200a (ZEB2) have been implicated in the regulation of ovarian cancer stem cells[44]. Future studies will investigate miRNA expression in cancer cells derived from the ascities versus from solid tumor, and compare this expression to their metabolic phenotype.

Conclusion

We demonstrate a distinct metabolic phenotype in the TICs compared to their parent cell population, the MOSE-L. The TICs have a decreased overall OxPhos and a larger contribution of glucose compared to fatty acids for OxPhos than the MOSE-L cells. They also secrete more lactate pointing to an overall increased glycolytic phenotype. When challenged by FCCP or oligomycin, the TICs were able to up-regulate OCR and ECAR, respectively, compared to the MOSE-L cells. This was in conjunction with an increased survivability in the presence of a fatty-acid only medium and also in the presence of AICAR. Together these results indicate that the TICs are more resilient to microenvironmental changes and that they can adapt and survive in these altered microenvironments. Lastly, the microenvironment may drive the glycolytic phenotype where cancer cells harvested from the ascities were basally more glycolytic than those harvested from solid tumors. This insight into the metabolic phenotype of tumor-initiating cells

can be used as the foundation for future treatment therapies to augment cytoreductive surgery and chemotherapy, increasing the survivability of women suffering from ovarian cancer.

Acknowledgments

We would like to thank Dr. Yaru Wu for her assistance in using the Seahorse XF24 extracellular flux analyzer.

Funding

These studies were supported in part by NIH R01 CA118846 (EMS, PCR), and funds provided by the Fralin Life Sciences Institute at Virginia Tech (MWH, EMS and PCR). The funding agencies had no role in the design, performance and analyses of experiments, and writing this report.

Disclosure Statement

The authors have no conflict of interest to disclose.

References

1. Siegel R, Naishadham D, Jemal A. Cancer statistics, 2012. *CA Cancer J Clin.* Jan-Feb 2012;62(1):10-29.
2. Pinsky PF, Zhu C, Skates SJ, et al. Potential effect of the risk of ovarian cancer algorithm (ROCA) on the mortality outcome of the Prostate, Lung, Colorectal and Ovarian (PLCO) trial. *Int J Cancer.* May 1 2013;132(9):2127-2133.
3. Herzog TJ. Recurrent ovarian cancer: how important is it to treat to disease progression? *Clin Cancer Res.* Nov 15 2004;10(22):7439-7449.
4. Abubaker K, Latifi A, Luwor R, et al. Short-term single treatment of chemotherapy results in the enrichment of ovarian cancer stem cell-like cells leading to an increased tumor burden. *Mol Cancer.* Mar 27 2013;12(1):24.
5. Zhan Q, Wang C, Ngai S. Ovarian cancer stem cells: a new target for cancer therapy. *Biomed Res Int.* 2013;2013:916819.
6. Alvero AB, Chen R, Fu HH, et al. Molecular phenotyping of human ovarian cancer stem cells unravels the mechanisms for repair and chemoresistance. *Cell Cycle.* Jan 1 2009;8(1):158-166.
7. Wani AA, Sharma N, Shouche YS, Bapat SA. Nuclear-mitochondrial genomic profiling reveals a pattern of evolution in epithelial ovarian tumor stem cells. *Oncogene.* Oct 12 2006;25(47):6336-6344.
8. Bapat SA, Mali AM, Koppikar CB, Kurrey NK. Stem and progenitor-like cells contribute to the aggressive behavior of human epithelial ovarian cancer. *Cancer Res.* Apr 15 2005;65(8):3025-3029.
9. Warburg O, Wind F, Negelein E. The Metabolism of Tumors in the Body. *J Gen Physiol.* Mar 7 1927;8(6):519-530.
10. Warburg O. On the origin of cancer cells. *Science.* Feb 24 1956;123(3191):309-314.
11. Vacanti NM, Metallo CM. Exploring metabolic pathways that contribute to the stem cell phenotype. *Biochim Biophys Acta.* Feb 2013;1830(2):2361-2369.
12. Rafalski VA, Mancini E, Brunet A. Energy metabolism and energy-sensing pathways in mammalian embryonic and adult stem cell fate. *J Cell Sci.* Dec 1 2012;125(Pt 23):5597-5608.
13. DeBerardinis RJ, Lum JJ, Hatzivassiliou G, Thompson CB. The biology of cancer: metabolic reprogramming fuels cell growth and proliferation. *Cell Metab.* Jan 2008;7(1):11-20.
14. Roberts PC, Mottillo EP, Baxa AC, et al. Sequential molecular and cellular events during neoplastic progression: a mouse syngeneic ovarian cancer model. *Neoplasia.* Oct 2005;7(10):944-956.
15. Creekmore AL, Silkworth WT, Cimini D, Jensen RV, Roberts PC, Schmelz EM. Changes in gene expression and cellular architecture in an ovarian cancer progression model. *Plos One.* 2011;6(3):e17676.
16. Anderson AS, Roberts PC, Frisard MI, et al. Metabolic changes during ovarian cancer progression as targets for sphingosine treatment. *Exp Cell Res.* Mar 19 2013.
17. Szotek PP, Pieretti-Vanmarcke R, Masiakos PT, et al. Ovarian cancer side population defines cells with stem cell-like characteristics and Mullerian Inhibiting Substance responsiveness. *Proc Natl Acad Sci U S A.* Jul 25 2006;103(30):11154-11159.

18. Zhang S, Balch C, Chan MW, et al. Identification and characterization of ovarian cancer-initiating cells from primary human tumors. *Cancer Res.* Jun 1 2008;68(11):4311-4320.
19. Cortright RN, Sandhoff KM, Basilio JL, et al. Skeletal muscle fat oxidation is increased in African-American and white women after 10 days of endurance exercise training. *Obesity (Silver Spring).* Jul 2006;14(7):1201-1210.
20. Dyck DJ, Peters SJ, Glatz J, et al. Functional differences in lipid metabolism in resting skeletal muscle of various fiber types. *Am J Physiol.* Mar 1997;272(3 Pt 1):E340-351.
21. Heilbronn LK, Civitarese AE, Bogacka I, Smith SR, Hulver M, Ravussin E. Glucose tolerance and skeletal muscle gene expression in response to alternate day fasting. *Obes Res.* Mar 2005;13(3):574-581.
22. Hulver MW, Berggren JR, Cortright RN, et al. Skeletal muscle lipid metabolism with obesity. *Am J Physiol Endocrinol Metab.* Apr 2003;284(4):E741-747.
23. Gerencser AA, Neilson A, Choi SW, et al. Quantitative microplate-based respirometry with correction for oxygen diffusion. *Anal Chem.* Aug 15 2009;81(16):6868-6878.
24. DeBerardinis RJ, Mancuso A, Daikhin E, et al. Beyond aerobic glycolysis: transformed cells can engage in glutamine metabolism that exceeds the requirement for protein and nucleotide synthesis. *Proc Natl Acad Sci U S A.* Dec 4 2007;104(49):19345-19350.
25. Yuan S, Wang F, Chen G, et al. Effective elimination of cancer stem cells by a novel drug combination strategy. *Stem Cells.* Jan 2013;31(1):23-34.
26. Goidts V, Bageritz J, Puccio L, et al. RNAi screening in glioma stem-like cells identifies PFKFB4 as a key molecule important for cancer cell survival. *Oncogene.* Jul 5 2012;31(27):3235-3243.
27. Zhou Y, Shingu T, Feng L, et al. Metabolic alterations in highly tumorigenic glioblastoma cells: preference for hypoxia and high dependency on glycolysis. *J Biol Chem.* Sep 16 2011;286(37):32843-32853.
28. Vlashi E, Lagadec C, Vergnes L, et al. Metabolic state of glioma stem cells and nontumorigenic cells. *Proc Natl Acad Sci U S A.* Sep 20 2011;108(38):16062-16067.
29. Ohata H, Ishiguro T, Aihara Y, et al. Induction of the stem-like cell regulator CD44 by Rho kinase inhibition contributes to the maintenance of colon cancer-initiating cells. *Cancer Res.* Oct 1 2012;72(19):5101-5110.
30. Ke CC, Liu RS, Yang AH, et al. CD133-expressing thyroid cancer cells are undifferentiated, radioresistant and survive radioiodide therapy. *Eur J Nucl Med Mol Imaging.* Jan 2013;40(1):61-71.
31. Nieman KM, Kenny HA, Penicka CV, et al. Adipocytes promote ovarian cancer metastasis and provide energy for rapid tumor growth. *Nat Med.* 2011;17(11):1498-1503.
32. Varum S, Rodrigues AS, Moura MB, et al. Energy metabolism in human pluripotent stem cells and their differentiated counterparts. *PLoS One.* 2011;6(6):e20914.
33. Zhang J, Khvorostov I, Hong JS, et al. UCP2 regulates energy metabolism and differentiation potential of human pluripotent stem cells. *EMBO J.* Dec 14 2011;30(24):4860-4873.
34. Luo Z, Saha AK, Xiang X, Ruderman NB. AMPK, the metabolic syndrome and cancer. *Trends Pharmacol Sci.* Feb 2005;26(2):69-76.
35. Chiacchiera F, Simone C. The AMPK-FoxO3A axis as a target for cancer treatment. *Cell Cycle.* Mar 15 2010;9(6):1091-1096.

36. Zhou W, Han WF, Landree LE, et al. Fatty acid synthase inhibition activates AMP-activated protein kinase in SKOV3 human ovarian cancer cells. *Cancer Res.* Apr 1 2007;67(7):2964-2971.
37. Rattan R, Giri S, Singh AK, Singh I. 5-Aminoimidazole-4-carboxamide-1-beta-D-ribofuranoside inhibits cancer cell proliferation in vitro and in vivo via AMP-activated protein kinase. *J Biol Chem.* Nov 25 2005;280(47):39582-39593.
38. Priebe A, Tan L, Wahl H, et al. Glucose deprivation activates AMPK and induces cell death through modulation of Akt in ovarian cancer cells. *Gynecol Oncol.* Aug 2011;122(2):389-395.
39. Aljada A, Mousa SA. Metformin and neoplasia: implications and indications. *Pharmacol Ther.* Jan 2012;133(1):108-115.
40. Hirsch HA, Iliopoulos D, Tsichlis PN, Struhl K. Metformin selectively targets cancer stem cells, and acts together with chemotherapy to block tumor growth and prolong remission. *Cancer Res.* Oct 1 2009;69(19):7507-7511.
41. Cufi S, Corominas-Faja B, Vazquez-Martin A, et al. Metformin-induced preferential killing of breast cancer initiating CD44+CD24-/low cells is sufficient to overcome primary resistance to trastuzumab in HER2+ human breast cancer xenografts. *Oncotarget.* Apr 2012;3(4):395-398.
42. Hirsch HA, Iliopoulos D, Struhl K. Metformin inhibits the inflammatory response associated with cellular transformation and cancer stem cell growth. *Proc Natl Acad Sci U S A.* Jan 15 2013;110(3):972-977.
43. Shank JJ, Yang K, Ghannam J, et al. Metformin targets ovarian cancer stem cells in vitro and in vivo. *Gynecol Oncol.* Nov 2012;127(2):390-397.
44. Kwon MJ, Shin YK. Regulation of ovarian cancer stem cells or tumor-initiating cells. *Int J Mol Sci.* 2013;14(4):6624-6648.

Chapter 7: CONCLUSIONS AND FUTURE DIRECTIONS

Although Otto Warburg cited changes in cancer metabolism as long as ninety years ago, it has been only in the last twenty years that the field of cancer metabolism has expanded. Otto Warburg's initial observations that cancer cells were highly glycolytic has stood the test of time, but his hypothesis that it was due to mitochondrial defects has been proven wrong[1]. Cancer cells are highly glycolytic, but it is because the excessive amount of carbons taken into the cell are shunted out of glycolysis for macromolecular synthesis, leaving lactate as a waste product of this altered metabolism[2]. Cancer cells continue to make ATP through OxPhos for cellular needs, but the rate of carbon entry into the mitochondria is much lower than the carbons secreted as lactate[3]. This new insight into cancer metabolism prompted Hanahan and Weinberg in 2011 to add cancer metabolism to the ten hallmarks of cancer[4]. More recently, the research on metabolic changes as a target for cancer therapy has gained momentum. Although chemotherapy and cytoreduction are the first line of treatment for ovarian cancer[5], often the cancer reoccurs with increased invasiveness[6]. New therapies are needed to augment current therapy and cancer metabolism is a promising target.

In our studies using the MOSE model, we were able to show that as ovarian cancer cells progress from a benign early-stage phenotype (MOSE-E) to an aggressive late-stage phenotype (MOSE-L), there was an increased glycolytic and lipogenic phenotype, thereby validating the use of the MOSE model for studying ovarian cancer metabolism. Metabolic changes occurred throughout the progression of the MOSE cells. Early changes in metabolism included a decrease in glucose oxidation and oxygen consumption rate as the MOSE-E cells transitioned to the MOSE-I. The MOSE-I marked a transitional stage where unexplained decreases in glucose uptake and lactate

excretion as the cells transitioned the more aggressive MOSE-L cells. Increased lipogenesis was later in the progression. Increases in citrate synthase activity but decreases in carbon flux through the TCA cycle were accompanied by increases in de novo fatty acid and cholesterol synthesis in the MOSE-L cells. By characterizing these changes, targets for stage-specific treatments can be designed.

To that end we used a naturally occurring chemotherapeutic agent sphingosine to target metabolism. One of sphingosine's known actions is in blocking the phosphorylation and thereby activity of AKT, a known driver of metabolism[7]. We validated that non-toxic concentrations of sphingosine administered over time to mimic dietary intake, decreased p-AKT protein. Treatment with sphingosine decreased glycolysis rate and pyruvate dehydrogenase activity. Sphingosine also decreased citrate synthase activity and increased carbon flux through the TCA cycle resulting in a decrease in cholesterol synthesis. Here we demonstrate one of sphingosine's affects on decreasing cancer growth and show that the MOSE model is a useful model for the screening of anti-cancer agents and their effects on metabolism.

The MOSE model was expanded with the harvesting of a highly tumorigenic cell line from the ascites of a C57Bl/6 mouse after receiving the MOSE-L cells. These tumor-initiating cells (TICs) were enriched with cancer stem cells, a more chemoresistant population (unpublished results). Characterization of their metabolism indicated that they were basally similar to the MOSE-L cells, but when challenged by changes in their microenvironment, the TICs were able to survive longer than the MOSE-L cells. Additionally they were able to increase oxygen consumption rate when uncoupled and glycolysis rate when ATP synthase was inhibited. This new insight into their metabolism will be the platform for future studies targeting these cells.

Although tracer studies investigated the use of glucose and fatty acids for oxidation and lipid synthesis, the contribution of glutamine to these pathways in the MOSE model is unknown. Therefore future studies should determine the contribution glutamine to the metabolism of these cells. Glutamine becomes particularly important in hypoxia conditions[8]. Current studies are underway looking at the effects of hypoxia on glucose uptake and studies should also include changes in glutamine metabolism as well. The known instigator of glutamine metabolism is the transcription factor c-myc[9]. To better understand the underlying driver of metabolism in these cells it is imperative to understand the oncogenic genotype. The protein level of c-myc in each cell type under normoxic and hypoxic conditions should be assessed.

Human ovarian cancer is classified into subtypes including serous, endometrioid, mucinous, clear cell, transitional cell, and squamous tumors[10]. Understanding the genotype of the MOSE cells will allow the model to better represent the human disease state. For instance, both transitional cell and serous tumors are Wilms Tumor gene product (WT1) positive and overexpress p53[10]. Endometrioid tumors are estrogen receptor (ER) positive and WT1 negative, where mucinous and clear cell tumors are ER and WT1 negative[10]. Further investigation into the genotype of the MOSE model is needed due to each ovarian cancer subtype responding differently to treatment therapies. p53 mutations and over-expression are known hallmarks of serous ovarian cancer and are also a driver of metabolism[10, 11]. Genotyping this gene for each stage of the MOSE model would be applicable for human relevance.

Lastly, continued investigation into the use of Metformin for the treatment of ovarian cancer is warranted. With current research indicating that Metformin is effective in selectively killing cancer stem cells, the use of Metformin in conjunctive with or immediately after chemotherapy should be investigated in cell culture, in mice studies and eventually in clinical studies[12, 13].

Altered cancer metabolism is a realistic target for augmented therapy in the treatment of ovarian cancer. With further research into ovarian cancer metabolism, metabolic targets will be identified and treatments designed, to increase the survival rate of those women suffering with this deadly disease.

References

1. Warburg O. On the origin of cancer cells. *Science.* Feb 24 1956;123(3191):309-314.
2. Lunt SY, Vander Heiden MG. Aerobic glycolysis: meeting the metabolic requirements of cell proliferation. *Annu Rev Cell Dev Biol.* Nov 10 2011;27:441-464.
3. Vander Heiden MG, Cantley LC, Thompson CB. Understanding the Warburg effect: the metabolic requirements of cell proliferation. *Science.* May 22 2009;324(5930):1029-1033.
4. Hanahan D, Weinberg RA. Hallmarks of cancer: the next generation. *Cell.* Mar 4 2011;144(5):646-674.
5. Herzog TJ. Recurrent ovarian cancer: how important is it to treat to disease progression? *Clin Cancer Res.* Nov 15 2004;10(22):7439-7449.
6. Zhan Q, Wang C, Ngai S. Ovarian cancer stem cells: a new target for cancer therapy. *Biomed Res Int.* 2013;2013:916819.
7. Chang HC, Tsai LH, Chuang LY, Hung WC. Role of AKT kinase in sphingosine-induced apoptosis in human hepatoma cells. *J Cell Physiol.* Aug 2001;188(2):188-193.
8. DeBerardinis RJ, Lum JJ, Hatzivassiliou G, Thompson CB. The biology of cancer: metabolic reprogramming fuels cell growth and proliferation. *Cell Metab.* Jan 2008;7(1):11-20.
9. Dang CV. MYC, microRNAs and glutamine addiction in cancers. *Cell Cycle.* Oct 15 2009;8(20):3243-3245.
10. Soslow RA. Histologic subtypes of ovarian carcinoma: an overview. *Int J Gynecol Pathol.* Apr 2008;27(2):161-174.
11. Levine AJ, Puzio-Kuter AM. The control of the metabolic switch in cancers by oncogenes and tumor suppressor genes. *Science.* Dec 3 2010;330(6009):1340-1344.
12. Cufi S, Corominas-Faja B, Vazquez-Martin A, et al. Metformin-induced preferential killing of breast cancer initiating CD44+CD24-/low cells is sufficient to overcome primary resistance to trastuzumab in HER2+ human breast cancer xenografts. *Oncotarget.* Apr 2012;3(4):395-398.
13. Hirsch HA, Iliopoulos D, Tsichlis PN, Struhl K. Metformin selectively targets cancer stem cells, and acts together with chemotherapy to block tumor growth and prolong remission. *Cancer Res.* Oct 1 2009;69(19):7507-7511.

Appendix A: CHANGES IN mRNA LEVELS FOR MOSE PROGRESSION AND MOSE CELLS TREATED WITH So

Gene Name	MOSE-E	MOSE-I	MOSE-L	MOSE-E w/ So	MOSE-I w/ So	MOSE-L w/ So
Glycolysis/ Lactate genes						
Hexokinase 1 (HK1)	1.028 ± .12[a]	1.084 ± .27[a]	0.660 ± .14[b]	1.091 ± .12	0.733 ± .26	0.453 ± .10*
Hexokinase 2 (HK2)	1.014 ± .09[a]	0.835 ± .09[a]	1.168 ± .21[b]	0.643 ± .06	1.118 ± .22	0.907 ± .18
Aldolase C (Aldoc)	1.076 ± .19	0.637 ± .26	1.229 ± .51	0.768 ± .30	0.748 ± .28	2.569 ± .36
Enolase 1 (Eno1)	1.020 ± .10	0.830 ± .06	1.028 ± .13	0.974 ± .08	0.805 ± .04	0.963 ± .10
Enolase 3 (Eno3)	1.004 ± .06	1.917 ± .74	1.380 ± .36	0.828 ± .31	0.717 ± .26	1.209 ± .30
Lactate Dehydrogenase A (Ldha)	1.042 ± .15	0.871 ± .04	1.132 ± .19	0.762 ± .10	1.046 ± .10	1.193 ± .13
Lactate Dehydrogenase B (Ldhb)	1.046 ± .16[a]	0.719 ± .30[a,b]	0.028 ± .00[b]	0.430 ± .18	0.090 ± .03	0.051 ± .01
Pyruvate Kinase M2 (PKM2)	1.013 ± .11	0.984 ± .10	1.113 ± .01	1.131 ± .07	1.071 ± .09	0.965 ± .11
Citrate Synthase (CS)	1.003 ± .05	0.714 ± .13	0.713 ± .17	0.650 ± .02	0.748 ± .14	0.681 ± .05
Pyruvate Oxidation genes						
Pyruvate Dehydrogenase B (Pdhb)	1.002 ± 0.03[a]	0.832 ± 0.21[a,b]	0.732 ± 0.04[b]	0.854 ± 0.06	0.735 ± 0.03	0.902 ± 0.04*
Pyruvate Dehydrogenase Kinase 1 (PDK1)	1.002 ± 0.03[a]	1.183 ± 0.25[a,b]	1.768 ± 0.21[b]	0.986 ± 0.22	1.206 ± 0.34	1.967 ± 0.29
Pyruvate Dehydrogenase Kinase 4 (PDK4)	1.045 ± 0.13[a,b]	1.630 ± 0.43[a]	0.290 ± 0.10[b]	0.391 ± 0.12*	0.341 ± 0.14*	0.333 ± 0.15
dihydrolipoamide S-acetyltransferase (Dlat)	1.010 ± 0.10	0.783 ± 0.09	1.067 ± 0.15	1.133 ± 0.13	0.934 ± 0.06	0.940 ± 0.08
Beta Oxidation gene						
3-Hydroxyacyl-Coenzyme A Dehydrogenase (β-Had)	1.016 ± 0.08	1.353 ± 0.30	1.135 ± 0.15	1.109 ± 0.14	0.868 ± 0.06	0.925 ± 0.09
Transport genes						
Glucose Transporter 1 (Glut1)	1.022 ± 0.14	0.632 ± 0.14	0.740 ± 0.09	0.836 ± 0.19	0.456 ± 0.10	0.980 ± 0.18
Monocarboxylate Transporter 1 (Slc16a1)	1.035 ± 0.19	0.568 ± 0.04	0.914 ± 0.05	0.934 ± 0.17	0.515 ± 0.05	0.786 ± 0.21
Monocarboxylate Transporter 4 (Slc16a3)	1.115 ± 0.24	0.668 ± 0.16	1.624 ± 0.49	0.793 ± 0.14	2.770 ± 1.17*	3.963 ± 0.20*
Carnitine Acyl-carnitine Translocase (Slc25a20)	1.079 ± 0.18	0.589 ± 0.06	0.780 ± 0.14	0.934 ± 0.06	0.622 ± 0.05	0.592 ± 0.05
FA Synthesis/ Cholesterol Synthesis genes						
Acetyl CoA Carboxylase A (Acaca)	1.115 ± 0.32	0.678 ± 0.07	1.758 ± 0.50	0.924 ± 0.06	0.962 ± 0.33	1.067 ± 0.35
Acetyl CoA Carboxylase B (Acacb)	1.155 ± 0.29	2.881 ± 0.55	2.493 ± 0.49	1.747 ± 0.39	2.695 ± 0.99	1.631 ± 0.27
ATP-Citrate Lyase (ACLY)	1.023 ± 0.16	0.889 ± 0.05	1.070 ± 0.07	1.056 ± 0.05	0.961 ± 0.07	0.834 ± 0.15
HMG CoA Reductase (HMGCR)	1.020 ± 0.14	1.022 ± 0.02	1.294 ± 0.09	1.075 ± 0.08	0.928 ± 0.10	0.641 ± 0.05*
Lipin 1 (Lipin1b)	1.126 ± 0.38	0.565 ± 0.17	0.557 ± 0.19	1.032 ± 0.30	0.337 ± 0.09	0.955 ± 0.52
TCA Cycle/ Enzymes leaving the TCA genes						
Malic Enzyme (Me1)	1.021 ± 0.15	0.923 ± 0.08	0.748 ± 0.21	0.939 ± 0.26	0.701 ± 0.12	0.658 ± 0.11
Pyruvate Carboxylase (PCX)	1.032 ± 0.18	1.043 ± 0.25	0.711 ± 0.06	0.921 ± 0.26	1.110 ± 0.12	0.801 ± 0.17
Malate Dehydrogenase (Mdh1)	1.051 ± 0.24	1.226 ± 0.15	0.723 ± 0.19	0.630 ± 0.16	0.659 ± 0.22	0.604 ± 0.20
NADPH-dependent oxidoreductase gene						
aldo-keto reductase family 1, member E1 (Akr1e1)	1.000 ± 0.02	0.638 ± 0.17	0.744 ± 0.28	0.545 ± 0.07*	0.486 ± 0.11	0.670 ± 0.09
Immune System genes						
TLR-2	1.023 ± 0.09[a]	0.430 ± 0.06[a]	3.727 ± 1.01[b]			3.806 ± 0.52
TLR-4	1.033 ± 0.19[a]	0.203 ± 0.02[b]	0.225 ± 0.01[b]			0.244 ± 0.08
Mitochondrial genes						
Mitofusion 2 (MFN2)	1.018 ± 0.05	0.940 ± 0.09	0.837 ± 0.08	0.977 ± 0.06	0.857 ± 0.06	1.022 ± 0.12
Mitofilin (IMMT)	1.015 ± 0.05[a]	0.434 ± 0.06[b]	0.831 ± 0.10[a]	0.718 ± 0.09*	0.692 ± 0.08	0.640 ± 0.07
Optic Atrophy 1 (OPA1)	1.106 ± 0.10[a]	1.836 ± 0.20[b]	1.828 ± 0.15[b]	1.438 ± 0.10*	1.355 ± 0.12*	1.398 ± 0.19
Cytochrome C Oxidase subunit 6c (Cox6c)	1.037 ± 0.08[a]	0.859 ± 0.12[a]	1.926 ± 0.20[b]	1.080 ± 0.14	1.462 ± 0.15*	1.582 ± 0.11
Ubiquinol Cytochrome C Reducatase (Uqcrc)	1.056 ± 0.08[a]	0.331 ± 0.06[b]	0.696 ± 0.08[c]	0.946 ± 0.10	0.657 ± 0.10*	0.753 ± 0.07
Dynamin-1-like Protein (DRP1)	1.005 ± 0.03	0.944 ± 0.12	0.915 ± 0.03	1.083 ± 0.04	1.113 ± 0.06	0.840 ± 0.03
ATP Synthase	1.057 ± 0.16[a]	2.587 ± 0.32[b]	1.354 ± 0.04[a]			
NADH Dehydrogenase	1.013 ± 0.11	0.903 ± 0.18	0.785 ± 0.05			

Appendix A. qPCR data analyzed using the ΔΔCT method indicating fold-change over the MOSE-E cells, where different letters denote statistical significance ($p<0.05$) and the same letters are not statistically different for the MOSE-E, MOSE-I and MOSE-L cells. An * denotes a significant difference ($p<0.05$) in the So treated cells compared to the untreated counterpart of the same cell type. Data is presented as mean ± SEM.

Appendix B: CHANGES IN mRNA LEVELS FOR MOSE-E AND MOSE-L COMPARED TO THE TICS

Gene Name	MOSE-E	MOSE-L	TIC
Transport genes			
Glut 1	1.015 ± 0.12^{a}	$1.477 \pm 0.06^{a,b}$	1.796 ± 0.14^{b}
Glut 2	1.111 ± 0.38^{a}	$0.384 \pm 0.29^{a,b}$	11.430 ± 3.20^{b}
Glut 3	1.045 ± 0.22^{a}	0.008 ± 0.00^{b}	0.097 ± 0.01^{b}
Glut 4	1.024 ± 0.15^{a}	4.175 ± 0.34^{b}	7.182 ± 0.76^{c}
FATP1	1.079 ± 0.13^{a}	1.332 ± 0.03^{a}	4.095 ± 0.03^{b}
FABP4	1.004 ± 0.06^{a}	0.179 ± 0.01^{b}	2.155 ± 0.17^{c}
Glycolysis genes			
Pyruvate Kinase M2 (PKM2)	1.005 ± 0.07	0.714 ± 0.06	0.857 ± 0.10
Hexokinase II (HKII)	1.056 ± 0.26	0.910 ± 0.03	0.630 ± 0.08
Pyruvate Oxidation genes			
Pyruvate Dehydrogenase b (PDHb)	1.004 ± 0.06^{a}	1.367 ± 0.04^{b}	1.345 ± 0.07^{b}
Pyruvate Kinase 1 (PDK1)	1.002 ± 0.04^{a}	$1.284 \pm 0.11^{a,b}$	2.149 ± 0.16^{b}
Mitochondrial genes			
Uncoupling protein 2 (UCP2)	1.000 ± 0.02^{a}	1.684 ± 0.08^{b}	3.853 ± 0.33^{c}
Uncoupling protein 3 (UCP3)	1.066 ± 0.26	4.083 ± 0.41	16.66 ± 8.10
Carnitine Acetyl Transferase (CrAT)	1.007 ± 0.08	0.786 ± 0.03	1.134 ± 0.13

Appendix B. qPCR data analyzed using the ΔΔCT method indicating fold-change over the MOSE-E cells, where different letters denote statistical significance ($p<0.05$) and the same letters are not statistically different for the MOSE-E, MOSE-L and TIC cells. Data is presented as mean ± SEM.